2006

The role of physical scheme interactions on warm season rainfall forecasts

Isidora Jankov
Iowa State University

The role of physical scheme interactions on warm season rainfall forecasts

by

Isidora Jankov

A dissertation submitted to the graduate faculty
in partial fulfillment of the requirements for the degree of
DOCTOR OF PHILOSOPHY

Major: Meteorology

Program of Study Committee:
William A. Gallus, Jr., Major Professor
William J. Gutowski
Raymond W. Arritt
Mike T.-C. Chen
Xiaoqing Wu
Steven E. Koch

Iowa State University
Ames, Iowa
2006

Graduate College

Iowa State University

This is to certify that the doctoral dissertation of

Isidora Jankov

has met the dissertation requirements of Iowa State University

Signature was redacted for privacy.

Major Professor

Signature was redacted for privacy.

For the Major Program

TABLE OF CONTENTS

1. GENERAL INTRODUCTION

1.1 Introduction

Mesoscale Convective Systems (MCSs) represent the major source of warm-season precipitation for the agriculturally important American Midwest (Fritsch et al. 1986), and dangerous flash flooding is often associated with these systems (Doswell et al.1996). Accurate forecasts of MCS rainfall would help to mitigate these events. The accurate forecast of these events requires correct predictions of the occurrence, timing, and location of the systems, and the potentially even greater challenge of forecasting rainfall amount.

Favorable conditions for Mesoscale Convective Complex (MCC), described by Maddox (1980), or more general MCS development are frequently associated with identifiable synoptic scale patterns such as: a quasi-stationary thermal boundary associated with rather weak synoptic-scale features (typical for warm season) or an intense, fast moving low pressure system associated with an upper level trough to the west and strong southerly low level jet. The low level jet (LLJ) promotes development of a MCC in three main ways: by enhancing the convective instability with the moisture advection from the Golf of Mexico, by destabilizing the temperature profiles with the temperature advection and by convergence (lifting) due to overrunning the frontal zone or due to a convergence at the nose of the LLJ (Maddox 1983, Cotton et al. 1989). The initial state of an MCC also coincides with a maximum of 700 mb warm advection and a maximum in 700-400 mb mixing ratio. The low and mid level warm advection destabilizes the temperature profile supporting the release of conditional instability, and the low and mid level moisture sources helps in maintaining the convection. The mature stage of an MCC life cycle is characterized with a decrease in a

surface level equivalent potential temperature due to convective downdrafts, which results in a strong temperature inversion that decouples the MCC from the surface. At this stage convective elements are driven by the boundary layer convergence while the moisture source is from the levels just above the boundary layer.

In models for numerical weather prediction, larger-scale forcing associated with the MCC's (MCS's) initiation and development are generally well resolved especially in the case of stronger forcing (fronts associated with a strong low pressure system; Jankov and Gallus 2003a). On the other hand, equally important mesoscale features, which are possibly acting as the main source for convective forcing (i. e. outflow boundaries), are often poorly resolved in the models (Kain and Fritsch 1993; Stensrud and Fritsch 1994) or improperly analyzed with observations. The importance of these smaller scale forcing mechanisms in warm season MCS events results in precipitation skill scores remaining much lower in the warm season than in the cold season (e.g. Olson et al. 1995).

The forecasting of MCS rainfall is further complicated by the fact that numerical simulation of sub-grid processes, such as convective precipitation and planetary boundary layer (PBL) evolution, involves multiple, semi-empirical parameterizations. More precisely, current grid spacing in operational numerical models is still too coarse to explicitly simulate convection, requiring use of a convective parameterization (Stensrud and Fritsch 1994). It has been found that convective parameterizations influence strongly the simulated precipitation patterns (Wang and Seaman 1997, Jankov and Gallus 2003b), and affect the response of a model to changes in grid spacing (Gallus 1999) or soil moisture (Gallus and Segal 2000). Each convective scheme has to address the issues of how the environment modifies convection (dynamic control), how the convection modifies the environment

(feedback), and calculation of cloud thermodynamical properties needed for both dynamic and feedback (Grell et al. 1991). Various convective schemes deal with these three parts of convection differently. The most commonly used schemes for operational and experimental purposes and also schemes that are going to be used in the present study are Betts-Miller-Janjic (Betts 1986, Betts and Miller 1986, Janjic 1994) and Kain-Fritsch convective schemes.

The Betts-Miller-Janjic (BMJ) parameterization is a member of the moist-adjustment parameterizations family. The scheme first locates the most unstable parcel (parcel with the highest θ_e) within the lowest 200 mb. If this parcel is found, it is lifted to its Lifting Condensation Level (LCL) with this height determining the cloud base. From the LCL the parcel is lifted moist adiabaticaly until its Equilibrium Level (EL) is reached. The cloud top is defined as the highest level where the parcel is still buoyant and it is typically just below the EL. If the parcel is not buoyant at all, the scheme moves to the next grid column. If the cloud is less than 200 mb deep the scheme switches to the shallow convection, otherwise the scheme checks if there is the potential for deep convection. The next step is in creation of a reference temperature and water vapor profile. The reference temperature profile is based on Betts-Miller (1986) set of observations and it is created by connecting the cloud bottom and the environmental freezing level with a line with 90% slope of the corresponding moist adiabate, and connecting the environmental freezing level and the cloud top with a straight line (Fig. 1). When a reference temperature is established a reference specific humidity is calculated using a subsaturation profile. The subsaturation differs depending on the amount of precipitation generated by the scheme in previous time steps (Janjic, 1994). When the model profiles of temperature and specific humidity are established the next step compares them with the reference profiles and checks if the conservation of

enthalpy, ($C_pT + L_vq$ where C_p is the heat capacity of air at constant pressure and is the latent heat of vaporization) is satisfied. Conservation of enthalpy ensures that the latent heat released through convection is proportional to the removal of water vapor.

$$\int_{p_b}^{p_t} C_p \Delta T dp = -\int_{p_b}^{p_t} L_v \Delta q dp$$

where $\Delta T = (T_{ref} - T_{model}), \Delta q = (q_{ref} - q_{model})$

This criteria is usually not satisfied in the first step, then the profiles are adjusted within the scheme until the conservation is satisfied. A more thorough overview about the BMJ scheme is provided in Baldwin et al. (2002). The scheme structure favors activation in cases with significant amounts of moisture in low and mid levels and positive Convective Available Potential Energy (CAPE).

In the case of Kain-Fritsch (KF) convective parameterization (Kain and Fritsch 1993) it is assumed that convection removes CAPE with vertical reorganization of mass in a grid element. The CAPE calculation is performed using the traditional, undiluted parcel ascent method. The convective updrafts and downdrafts are represented with one-dimensional entraining-detraining plume model. A unique characteristic of this plume model is that it modifies the exchange of mass between the cloud and the environment (entrainment and detrainment) based on buoyancy characteristics of different mixtures of clear and cloudy air. The scheme computes buoyancy variations of different mixtures of clear and cloudy air produced through turbulent mixing. Mixtures that remain positively buoyant in each model layer continue to rise with updraft, while the mixtures that lose their positive buoyancy, due to evaporative cooling effects, detrain into the environment. The KF scheme trigger function is derived from checking the parcel for buoyancy at the calculated LCL starting with the

lowest 50 mb layer and repeating the same procedure up to the 600-700 mb layer. The buoyancy criterion is satisfied if $T_{LCL} + dT > T_{ENV}$, where T_{LCL} is the parcel temperature at the LCL, T_{ENV} is the environmental temperature and dT is a temperature perturbation added to the parcel based on an assumption that convective development can be supported with a background upward motion. The perturbation formula is $dT = k(w_g - c(z))^{1/3}$, where k is a unit number with $Ks^{1/3}cm^{-1/3}$ dimensions, w_g is the mean grid-resolved vertical velocity at the LCL ($cm\ s^{-1}$), and c(z) is a threshold vertical velocity defined as $w_0(Z_{LCL}/2000)$ for $Z_{LCL} \leq 2000$ m (Z_{LCL} is the height of the LCL above the ground, and $w_0 = 2\ cm\ s^{-1}$) and w_0 for $Z_{LCL} > 2000$ m. If a buoyant parcel is found, the scheme estimates the thermodynamic path to cloud top. This means that surface convergence with the induced vertical motion may have a big impact on the KF convective parameterization. For example, in a case with a capping inversion suppressing convection and rather low relative humidity above the inversion, there may be a good chance for the KF scheme to activate. Finally, the closure assumption used by the KF convective parameterization is that the scheme will rearrange mass in the column until 90% of the CAPE is removed.

Further more, convective scheme performance is highly influenced by the choice of the PBL scheme. In general, PBL schemes are responsible for simulations of physical and chemical processes in the atmosphere (interactions between clouds and radiation, nocturnal transport and vertical mixing) which highly affect performance of convective schemes. More specifically, various PBL schemes can differently affect lower troposphere temperature and moisture profiles which further interact with other schemes including convective scheme (e.g., Bright and Mullen 2002; Wisse and Vila-Guerau de Arellano 2004). Due to differences

in convective schemes' designs, various convective schemes favor activation under different environmental conditions. For example, it has been found that the Eta PBL (often referred to as Mellor-Yamada-Janjic 2.5; Janjic 2001) scheme tends to simulate a PBL which is too moist and too shallow (Bright and Mullen 2002, Jankov et al. 2006). As previously discussed the BMJ convective scheme's design favors activation in cases with significant amounts of moisture in low and mid levels and positive Convective Available Potential Energy (CAPE). Therefore, when Eta PBL scheme is used its tendency to simulate PBLs that are too moist favors more frequent activation of the Betts-Miller-Janjic scheme. This would lead to a substantial amount of rainfall being produced by deep convection at the expense of grid-resolved precipitation. Moreover, the amount and spatial distribution of grid-resolved precipitation would possibly depend on the choice of microphysical scheme, which then introduces an additional level of complexity in terms of interactions between physical schemes. In general, different combinations of physical schemes and their interactions results in a large diversity of rainfall simulations, as well as an increase in uncertainty and bias associated with each physical parameterization. Knowledge of the nature of the influence that different physical schemes as well as their interactions have on simulated rainfall might be exceptionally useful in an experiment design or design of an ensemble for rainfall forecasting.

Problems in improving deterministic rainfall forecasts, have prompted recent use of ensemble forecasting techniques. At first, ensembles were designed based on perturbed initial conditions and the ensemble mean values were found to estimate the verifying state (usually large-scale circulations) better than the forecast from a single ensemble member (Molteni et al. 1996; Hamill and Colucci 1997). In addition, the ensemble dispersion gives an estimate of

the forecast uncertainty (Tracton and Kalnay, 1993). This is very important because neglecting uncertainty during the forecast processes reduces quality and value (Murphy, 1993). Earlier studies tended to concentrate more on predictability of larger scale features and model fields such as geopotential heights and temperature (Lorenz 1982; Dalcher and Kalnay, 1987; Molteni and Palmer, 1993; Molteni et al. 1996; Buizza 1997), while recent studies are more focused on smaller scale features and investigation of the predictability of other meteorological fields, such us precipitation. Du et al. (1997) in their investigation of the impact of errors in initial conditions on quantitative precipitation forecasts showed higher improvement over climatology of probabilistic quantitave precipitation forecast than the improvement obtained with a single run with doubled resolution. However, results from previous studies, based on data obtained from the experimental NCEP Short Range Ensemble Forecast (SREF) program, indicated that ensembles generally have insufficient dispersion. This means that solutions produced by an ensemble are not sufficient to adequately represent the reality.

Insufficient ensemble dispersion may be a consequence of the assumption that errors primarily results from uncertainties in the initial conditions, but errors results from model error as well. An approach to address this issue is to vary model physics or to combine forecasts from different models. Stensrud et al. (2000) discussed both significance of variations in model physics as well as model variability in ensemble forecasting. Alhamed (2001) showed that model diversity as an ensemble system yields forecasts with greater spread containing more possible solutions.

The main objective of the present study is help optimize a mixed physics ensemble (model runs with different physical options) for warm season MCS rainfall forecasting by

evaluating the impact that various physical schemes as well as their interactions have on rainfall forecasts. In addition, the work investigates how the impact of the physical schemes and their interaction changes when different initial conditions are used. For this purpose, high resolution (12-km grid spacing, 34 vertical levels) simulations from the Weather Research and Forecasting (WRF) model of 8 International H_2O Project (IHOP; Weckwerth et al. 2004) events were examined. For each event a matrix of 18 WRF model configurations was created by varying the convective parameterization scheme, the PBL scheme, and microphysical schemes. The same matrix of 18 different model configurations was used in testing sensitivity to the parameterizations in runs using 40 km NCEP Eta model GRIB data as initial and boundary conditions to the sensitivity in runs using a LAPS 'hot' start for initialization.

1.2 Thesis organization

The evaluation of the impact that various physical schemes and their interactions have on simulated rainfall was a subject of a journal paper with the title 'The impact of different WRF model physical parameterizations and their interactions on warm season MCS rainfall' presented in Chapter 2. This paper has been published in the American Meteorological Society journal *Weather and Forecasting* in 2005. The investigation of how this impact changes when different initial conditions are used was a subject of a journal paper with the title 'Influence of initial conditions on the WRF model QPF response to physical parameterization changes' presented in Chapter 3. This paper has been submitted for publication in *Weather and Forecasting*. An extended analysis of PBL schemes sensitivity

and some preliminary results are presented in Chapter 4. Concluding remarks and discussion are presented in Chapter 5.

1.2 References

Baldwin, M. E., J.S. Kain, and M. P. Kay, 2002: Properties of the convection scheme in NCEP's Eta model that affect forecast sounding interpretation. *Wea. Forecasting*, **17**, 1063-1079.

Betts, A. K., 1986: A new convective adjustment scheme. Part I: Observational and theoretical basis. *Quart. J.Roy. Meteor.* Soc., **112**, 677-692.

Bright, D. R., and S. L. Mullen, 2002: The sensitivity of the numerical simulation of the southwest monsoon boundary layer to the choice of PBL turbulence scheme in MM5. *Wea. Forecasting*, **17**, 99-114.

Buizza, R., 1997: Potential forecast skill of ensemble prediction and spread and skill distribution of the ECMWF ensemble prediction system. *Mon. Wea. Rev.*, **125**, 99-119.

Cotton, W. R., M.-S. Lin, R. L. McAnelly and C. J. Tremback, 1989: A composite model of mesoscale convective complexes. *Mon. Wea. Rev.*, **117**, 765-783.

Dalcher, A., and E. Kalnay, 1987: Error growth and predictability in operational ECMWF forecasts. *Tellus*, **39A**, 474-491.

Doswell, C. A., III, H. E. Brooks, and R. A. Maddox, 1996: Flash flood forecasting: An ingredients-based methodology. *Wea. Forecasting*, **11**, 560-581.

Du, J., S. L. Mullen, and F. Sanders, 1997: Short-range ensemble forecasting of quantitative precipitation. *Mon. Wea. Rev.*, **125**, 2427-2459.

Fritsch, J. M., R. J. Kane, and C. R. Chelius, 1986: The contribution of mesoscale convective weather systems to the warm-season precipitation in the United States. *J. Climate Appl. Meteor.*, **25**, 1333-1345.

Gallus, W. A., Jr., 1999: Eta simulations of three extreme precipitation events: Impact of resolution and choice of convective parameterization. *Wea. Forecasting*, **14**, 405-426.

-------, and M. Segal, 2000: Sensitivity of forecast rainfall in a Texas convective system to soil moisture and convective scheme. *Wea. Forecasting*, **15**, 509–526.

Grell, G.A., Y.H. Kuo, and R. Pasch, 1991: Semi-prognostic tests of cumulus parameterization schemes in the middle latitudes. *Mon. Wea. Rev.*, **119**, 5-31.

Hamill, T. M., and S. J. Colucci, 1997: Verification of Eta-RSM short-range ensemble forecasts. *Mon. Wea. Rev.*, **125**, 1312-1327.

Janjic Z., 2001: Nonsingular Implementation of the Mellor-Yamada Level 2.5 Scheme in the NCEP Meso Model. NCEP Office Note No. 437, 61pp.

--------, 1994: The step-mountain Eta coordinate model: Further developments of the convection closure schemes. *Mon. Wea. Rev.*, **122**, 927-945.

Jankov, I., and W. A., Jr. Gallus, 2004a: MCS Rainfall forecast accuracy as a function of large-scale forcing. *Wea. Forecasting*, **19**, 428-439.

--------, and -------., 2004b: Contrast between good and bad forecasts of warm season MCS rainfall. *J. Hydrol.*, **288**, 122-152.

--------,--------, M. Segal, B. Shaw, and S. E. Koch, 2005: The impact of different WRF model physical parameterizations and their interactions on warm season MCS rainfall. *Wea. Forecasting* (in press).

Johns, H. R., 1993: Meteorological conditions associated with bow echo development on convective systems. *Wea. Forecasting*, **8**, 294-299.

Kain, J. S., and J. M. Fritsch, 1993: The role of the convective "trigger function" in numerical prediction of mesoscale convective systems. *Meteor. Atmos. Phys.*, **49**, 93-106.

Lorenz, E. N., 1982: Atmospheric predictability experiments with a large numerical model. *Tellus*, **34**, 505-513.

Maddox, R. A., 1983: Large-scale meteorological conditions associated with midlatitude mesoscale convective complexes. *Mon. Wea. Rev.*, **111**, 1475-1493.

Maddox, R. A., 1980: Mesoscale convective complexes. *Bull. Amer. Meteor. Soc.*. **61**, 1374-1387.

Molteni, F., R. Buizza, T. N. Palmer, and T. Petroliagis, 1996: The ECMWF ensemble prediction system: Methodology and validation. *Quart. J. Roy. Meteor. Soc.*, **122**, 73-119.

-------, F., and T. N. Palmer, 1993: Predictability and finite-time instability of the northern winter circulation. *Quart. J. Roy. Meteor. Soc.*, **77**, 2637-2649.

Murphy, J. M., 1993: What is a good forecast? An essay on the nature of goodness in weather forecasting. *Wea. Forecasting*, **8**, 281-293.

Olson, David A., Norman W. Junker, Brian Korty, 1995: Evaluation of 33 Years of Quantitative Precipitation Forecasting at the NMC. *Wea. Forecasting*, **10**, 498–511.

Stensrud, D. J., and J. M. Fritsch, 1994:Mesoscale convective systems in weakly forced large scale environments. Part III: Numerical simulations and implications for operational forecasting. *Mon. Wea. Rev.*, **122**, 2084-2104.

----------, D. J., J.-W., Bao, and T. T., Warner, 2000: Using initial conditions and model physics perturbations in short-range ensembles simulations of mesoscale convective systems. *Mon. Wea. Rev.*, **128**, 2077-2107.

Tracton, M. S., and E. Kalnay, 1993: Operational ensemble prediction at the National Meteorological Center: Practical aspects. *Wea. Forecasting*, **8**, 379-398.

Weisman, M. L., 1990: The genesis of bow echoes: A rear-inflow induced meso-convective structure. Cooperative thesis No. 125, The Pennsylvania State University and National Center for Atmospheric Research. NCAR/CT-125, 149 pp. [Available from the Department of Meteorology, The Pennsylvania State University, University Park, PA 16802].

--------, M. L., W. C. Skamarock, and J. B. Klemp, 1997: The resolution dependence of explicitly modeled convective systems. *Mon. Wea. Rev.*, **125**, 527-548.

Wang, W., and N. L. Seaman, 1997: A comparison study of convective schemes in a mesoscale model. *Mon. Wea. Rev.*, **125**, 252–278.

Weckwerth, T. M., D. B. Parsons, S. E. Koch, J. A. Moore, M. A. LeMone, B. B. Demoz, C. Flamant, B. Geerts, J. Wang, and W. F. FeTSz, 2004: An overview of the International H_2O Project (IHOP_2002) and some preliminary highlights. *Bull. Amer. Meteor. Soc.*, **85**, 253-277.

Wisse, J. S. P., and J. Vila-Guerau de Arellano, 2004: Analysis of the role of the planetary boundary layer schemes during a severe convective storm. *Annales Geophysicae*, **22**, 1861-1874.

List of Figures

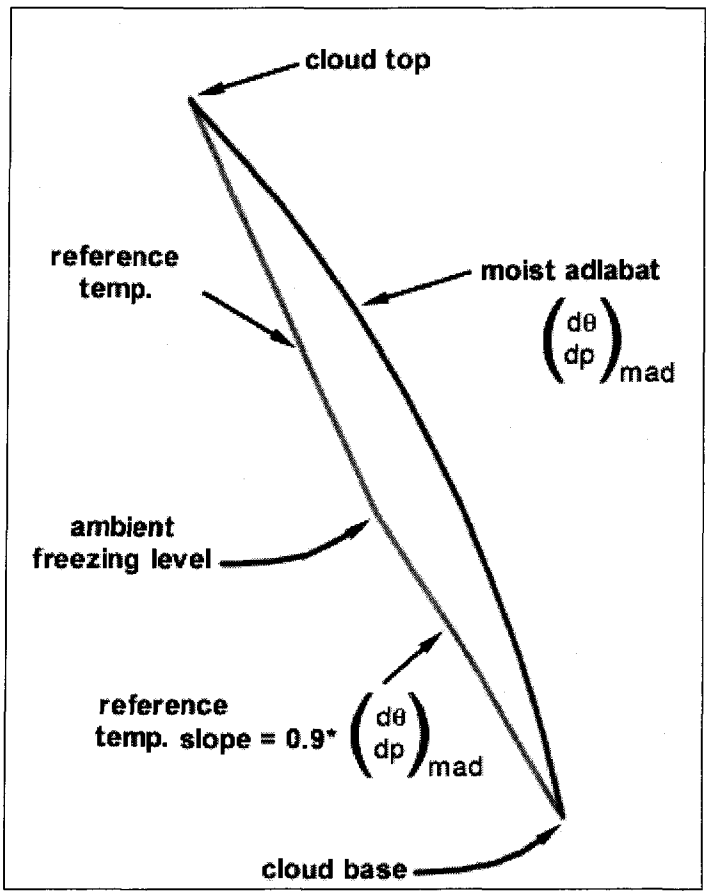

Figure 1. Illustration of the reference temperature profile creation for Betts-Miller-Janjic convective parameterization.

2. THE IMPACT OF DIFFERENT WRF MODEL PHYSICAL PARAMETERIZATIONS AND THEIR INTERACTIONS ON WARM SEASON MCS RAINFALL

Majority of the material presented in this chapter has been published in

Weather and Forecasting

Isidora Jankov, William A. Gallus, Jr., Moti Segal, Brent Shaw, and Steven E. Koch

2. 1 Abstract

In recent years, a mixed physics ensemble approach has been investigated as a method to better predict Mesoscale Convective System (MCS) rainfall. For both mixed physics ensemble design and interpretation, knowledge of the general impact of various physical schemes and their interactions on warm season MCS rainfall forecasts would be useful. Adopting the newly emerging Weather Research and Forecasting (WRF) model for this purpose would further emphasize such benefits. To pursue this goal, a matrix of 18 WRF model configurations, created using different physical scheme combinations, was run with 12 km grid spacing for 8 International H_2O Project (IHOP) MCS cases. For each case, 3 different treatments of convection, 3 different microphysical schemes and 2 different planetary boundary layer schemes were used. Sensitivity to physics changes was determined through the use of Correspondence Ratio and Squared Correlation Coefficient. The factor separation method also was used to quantify in detail the impacts of the variation of two different physical schemes and their interaction on the simulated rainfall.

Skill score measures averaged over all 8 cases for all 18 configurations indicated that no one configuration was obviously best at all times and thresholds. The greatest variability in forecasts was found to come from changes in the choice of convective scheme, although notable impacts also occurred from changes in the microphysics and planetary boundary layer (PBL) schemes. Specifically, changes in convective treatment notably impacted the forecast of system average rain rate, while forecasts of total domain rain volume were influenced by choices of microphysics and convective treatment. The impact of interactions (synergy) of different physical schemes, although occasionally of comparable magnitude to the impacts from changing one scheme alone (compared to a control run), varied greatly among cases and over time, and was typically not statistically significant.

2.2 Introduction

Considering that warm season rainfall is among the most poorly forecasted of meteorological varaibles (e. g. Doswell et al. 1996, Fritsch and Carbone 2004), numerous efforts have been undertaken to try to improve the forecasts. Stensrud and Fritsch (1994) and Stensrud et al. (1999b) showed that proper initialization of mesoscale features such as cold pools would likely be needed to improve convective system rainfall forecasts; however Gallus and Segal (2001) found that several techniques to improve mesoscale initialization, including a technique to ensure depiction of cold pools, did not consistently improve rainfall skill scores significantly. Wang and Seaman (1997) and Gallus (1999), among others, have also shown that the choice of convective scheme strongly influences the simulated rainfall patterns. The convective scheme also affects the response of a model to changes in grid

spacing (Gallus 1999) or soil moisture (Gallus and Segal 2000). With such extreme sensitivity to this one parameterization alone, and objective measures showing that no one scheme is better consistently than any other (e.g., Gallus and Segal 2001), the path to improved deterministic forecasts of warm season rainfall appears to be difficult.

Because of the problems in improving deterministic rainfall forecasts, ensemble forecasting techniques have been increasingly used in recent years. At first, ensembles were designed based on perturbed initial conditions, and the ensemble mean values were found to estimate the verifying state (usually large-scale circulations) better than the forecast from a single ensemble member (Molteni et al. 1996; Hamill and Colucci 1997). Similar results using multi-model analyses for initial conditions were found for 2-m temperature and 10-m wind forecasts by Grimit and Mass (2002). Ensembles also are advantageous because they supply probabilistic forecast information which may be of more value to users than a single deterministic forecast (Murphy 1993), and the ensemble dispersion gives an estimate of forecast uncertainty (Tracton and Kalnay 1993).

One of the first studies to investigate ensemble prediction of rainfall was Du et al. (1997), which found in an investigation of errors in initial conditions on cold season synoptic-scale quantitative precipitation forecasts (QPF) that greater improvement over climatology was present in the probabilistic forecast than in a single run using doubled horizontal grid resolution. However, results from other studies using data from the experimental NCEP Short Range Ensemble Forecast (SREF) program indicate that these ensembles, which were built using only initial perturbations, generally have insufficient dispersion (Hamill and Colucci 1998; Stensrud et al. 1999a). It should be noted that a goal of

increasing ensemble spread is not always an advantage but overall probably helpful for warm season rainfall forecasts which are usually characterized by low skill.

Insufficient ensemble dispersion may be a consequence of the original assumption that errors primarily result from uncertainties in the initial conditions. It is likely that the insufficient dispersion problem is more severe in a short-range forecast because initialization perturbations require time to grow and may not be capable of providing consistent dispersion in the short range (Stensrud et al. 2000). In the warm season when forcing and flow are weaker, the growth of the perturbations may be even slower. Due to the fact that errors result from any bias present in a model, an ensemble utilizing variations in both dynamics/numerics and model physics should result in higher spread. Alhamed et al. (2000) showed that model diversity in an ensemble system yields forecasts with greater spread containing more possible solutions. Stensrud et al. (2000) discussed significance of both variations in model physics as well as initial conditions in ensemble forecasting. Based on studies like these, NCEP changed the SREF system in 2004 (Du et al. 2004) to introduce physics uncertainty (through the use of varied convective parameterizations) in addition to initial condition uncertainty.

In the case of a mixed physics ensemble approach to MCS rainfall forecasting, knowledge of the nature of the impact of different physical schemes on rainfall would be exceptionally useful. As discussed earlier, numerous studies have shown the large impact the convective scheme has on rainfall forecasts. The choice of planetary boundary layer (PBL) scheme can substantially affect temperature and moisture profiles in the lower troposphere, which could interact with other schemes such as the convective parameterization to influence simulation of precipitation (e.g., Bright and Mullen 2002; Wisse and Vila-Guerau de Arellano 2004). However, the impact of different PBL schemes and microphysical schemes

on warm season rainfall fields and the interactions of all three of these physical process schemes have received little attention. Our study will use the WRF model to explore these issues. The model selection is of particular merit due to the fact that the emerging WRF community model will be used increasingly for ensemble forecasting in the near future (Bernardet et al. 2004). The main objective of the present study is to investigate the general impact that various physical schemes as well as their interactions have on warm season MCS rainfall forecasts. For this purpose, high resolution (12-km grid spacing, 34 vertical levels) simulations from the WRF model of 8 IHOP (Weckwerth et al. 2004) events were examined. For each event a matrix of 18 WRF model configurations was created by varying the convective parameterization scheme, the PBL scheme, and microphysical schemes. The various methodologies used in the present study are discussed in section 2, results in section 3, with concluding discussion and summary in the final section.

2.3 Methodology

A matrix of 18 WRF variants created using different combinations of physical schemes was run for 8 IHOP convective cases. The IHOP domain covered a roughly 1500x1500 km region centered over the south-central United States. The cases were purposely selected to represent a range of different synoptic settings in which significant rainfall, primarily from MCSs, was observed and/or forecasted in the IHOP domain over the central United States.

For the majority of cases the MCS systems dominated the rainfall field and were captured in the interior of the domain. Satellite-surface composites with analyzed surface

pressure and surface data plotted for all 8 events at their initial time (May 16, 2002 initialized at 06 UTC, May 23, 2002 initialized at 12 UTC, May 24, 2002 initialized at 18 UTC, June 02, 2002 initialized at 12 UTC, June 04, 2002 initialized at 00 UTC, June 13, 2002 initialized at 00 UTC, June 15, 2002 initialized at 06 UTC and June 19, 2002 initialized at 12 UTC) are presented in Figure 1. Satellite-surface composite image for May 16, 2002 at 06 UTC indicates a primary surface low over the southeastern Canada and its associated cold front northeast-southwest oriented over the central part of the domain (Fig, 1a). With time the cold front moved from west to east and its southwestern part altered to a stationary front. During the whole integration period this case was characterized with convection on both sides of the cold/stationary front. At its initial time the May 23, 2002 case was characterized with a cold northeast-southwest oriented front over the western part of the domain associated with a surface low located in northern Minnesota (Fig. 1b). With time the whole system moved east. During the first half of the integration period the convective activity was confined ahead of the front while at later times some post frontal activity was present too. Similarly to the May 23 of 2002 case, the May 24, 2002 case was also characterized with active convections on both sides of a cold front oriented northeast-southwest over the southern part of the domain (Fig. 1c). For the June 02, 2002 case satellite-surface composite at its initial time (Fig. 1d) indicated ongoing precipitation associated with a stationary front west-east oriented over the central part of the domain. At the same time a dry line was located along the eastern Colorado and New Mexico borders. The dry line with its movement (both forward and backward) and strong convective activity associated with it was the main feature during the 24-hour forecast period. The June 04, 2002 event at its initial time was characterized with a surface low over southern Iowa and its associated fronts (Fig. 1e). The major rainfall for this

event was due to the postfrontal elevated convection. At its initial time, the June 13 of 2002 case was characterized with a northeast-southwest oriented stationary front over the central part of the domain (Fig. 1f). During the 24-hour forecast period while moving southeast the stationary front was altered to a cold and back to a stationary front. The entire forecast period was characterized with the intense, mainly elevated convection which moved along, ahead, and behind the frontal zone. The June 15, 2002 event at its initial time was characterized with a strong ongoing convection over the northwestern Texas (Fig. 1g). Strong convection persisted throughout the 24-hour integration period and was mainly associated with the return flow and a strong low level jet. June 19, 2002 event was characterized with a passage of a cold front from west and a dry line located close to the western Texas boundary. Both the cold front passage and the dry line activity were associated with intense convection. The satellite-surface composite for this event at its initial time is presented in Fig. 1h.

For each of these 8 events, three different treatments of convection were used: the Kain-Fritsch (KF) scheme (Kain and Fritsch 1993), the Betts-Miller-Janjic (BMJ) scheme (Betts 1986, Betts and Miller 1986, Janjic 1994), and the use of no convective scheme. For elaborations on differences between KF and BMJ see Jankov and Gallus (2004). For each of these 3 choices, 3 different microphysical schemes were used: Lin et al. (1983), NCEP-5 class (Hong et al. 1998), and Ferrier et al. (2002). Within these 9 possible configurations, two different PBL schemes were used: MRF (Troen and Mahrt 1986) and Eta (Janjic 1994). It is important to note that our exploration of impacts and interactions between all possible combinations of physical schemes is slightly affected (only 4 out of 17 possible interactions were neglected) by our choice of the 'control run'. To explore all interactions using one 'control run' would involve synergism among three different processes, greatly complicating

interpretation. In the present study, the 'control run', chosen to match the real-time model configuration adopted by NOAA's Forecast System Laboratory (FSL) during the IHOP experiment, used the KF convective scheme, MRF PBL scheme and NCEP class-5 microphysical scheme. The abbreviations for runs using different combinations of the physical schemes are found in Table 1. For the rainfall validation, observed 6-hour accumulated precipitation fields from the NCEP Stage IV (Baldwin and Mitchell 1997) analysis were used.

All runs were initialized with a diabatic Local Analysis and Prediction System (LAPS) 'hot' start initialization (Jian et al. 2003). This technique is based on a three-dimensional analysis of cloud attributes (i. e., coverage and type), which proceeds with a method of estimating mixing ratios, precipitable water, and cloud vertical motions. By using a variational adjustment procedure (involving dynamic balancing and a mass conservation constraint), horizontal wind fields and the mass field are adjusted to produce divergence consistent with the cloud updraft properties (depth, magnitude, and shape of the updraft profiles). This approach was developed for grid spacings that resolve saturated updrafts and compensating subsidence, but it is still used quasi-operationally for much coarser resolutions (Δx>10 km).

As a measure of forecast accuracy, Equitable Threat Score (ETS; Schaefer 1990) and bias were calculated, where:

$$\mathrm{ETS} = \frac{(\mathrm{CFA} - \mathrm{CHA})}{(\mathrm{F} + \mathrm{O} - \mathrm{CFA} - \mathrm{CHA})}, \qquad (1)$$

$$CHA = O\frac{F}{V}, \qquad (2)$$

and

$$bias = \frac{F}{O}. \qquad (3)$$

In the above equations, each variable indicates the number of grid points at which: (i) rainfall was correctly forecasted to exceed the specified threshold (CFA), (ii) rainfall was forecasted to exceed the threshold (F), (iii) rainfall was observed to exceed the threshold (O), and (iv) a correct forecast would occur by chance (CHA), where V is the total number of evaluated grid points.

Correspondence Ratio (Stensrud and Wandishin 2000) was computed when two of three model physical schemes were held fixed and the third was varied. Correspondence Ratio (CR), defined as the ratio of the area of the intersection (I) of all individual field values to the area of union (U) of the same field values, is a useful measure of the sensitivity to physical scheme changes, and is written

$$CR = \frac{I}{U}, \qquad (4)$$

where I and U are defined using threshold values of rainfall.

The same approach that was used for the CR calculation was repeated in the calculation of the Squared Correlation Coefficient (r^2),

$$r^2 = \left[\frac{\sum_{i=1}^{N} (x_i - \bar{x})(y_i - \bar{y})}{\sqrt{\sum_{i=1}^{N} (x_i - \bar{x})^2 \sum_{i=1}^{N} (y_i - \bar{y})^2}} \right]^2, \qquad (5)$$

where the standard statistical notation was used.

In order to quantify the impact of varying two different model physical schemes on the simulated rainfall field, the factor separation methodology formulated by Stein and Alpert (1993) was adopted. Based on this methodology:

$$f_{xy} - f_0 = (f_x - f_0) + (f_y - f_0) + \hat{f}_{xy}, \qquad (6)$$

where f_0 represents the control run simulated rainfall amount, f_{xy} represents the rainfall amount simulated by a run with changes in both physical schemes of interest (two physical schemes changed compared to the control run), f_x stands for the rainfall amount produced by a run that has one of the two physical schemes of interest changed (as compared to the control run), f_y represents the rainfall amounts simulated by a run with another physical scheme of interest changed (as compared to the control run), and $\hat{f}_{xy}$ stands for a synergistic term [$\hat{f}_{xy} = f_{xy} - (f_x + f_y) + f_0$] reflecting, in the present study, the rainfall amount associated with the non-linear interaction between two physical schemes. This term may be thought of as the difference between the actual rainfall occurring in the run in which two schemes have been changed and the rainfall expected by adding the impacts of each individual change. Assuming a continuum of physical schemes, Eq. 6 is then equivalent to Taylor's series second order expansion in two variables. The first two terms in the right hand side (RHS) of

Eq. 6 represent the contribution of the first order derivatives, while the third term (synergistic term) is a mixed second order derivative (the non-mixed second order derivatives are zero). In essence, if the synergistic term is equal to zero, no interaction occurs between the two changed physical schemes.

The notation presented in Table 1 will be used to indicate different model configurations with physical schemes that are changed from the control one (KF-MRF-MPN) presented in bold face throughout the manuscript.

2.4 Results

2.4.1 Sensitivity of rainfall forecast skill to physical scheme changes

ETSs for all eight cases for all model versions, during the first six forecast hours valid for four different thresholds (0.01 in., 0.1 in., 0.5 in. and 1. in.; the thresholds are stated in inches as commonly used, 1 inch=25.4 mm) are presented in Table 2. Relatively "good" ("bad") forecasts [ETS one or more standard deviation above (below) the median for each 6 hourly time period] are indicated. One out of eight cases exhibited relatively "good" forecast skill for lower thresholds, while a different case had relatively "good" forecast skill for heavier thresholds. The same analysis but for the 12-18 hour forecast period indicated generally lower scores than at earlier times but once again higher scores for lighter amounts than heavier amounts (Table 3). It should also be noted that a "good" or "bad" forecast in the 00-06 h forecast period did not necessarily mean a "good" or "bad" forecast at later times. Bias analyses (not shown) indicated that for light amounts, both convective schemes had a

substantial high bias (roughly 2.0) during the first 12 hours of the forecast, while at later times biases slightly decreased (~1.6). The worst overestimate occurred during the 06-12 h period. No specific trends in bias were noted for heavier thresholds.

ETS and bias averaged over all 8 cases for all 18 configurations indicated that no one configuration was obviously best at all times and thresholds (Tables 4 and 5). However, it should be pointed out that during the 00-06 forecast period, for lighter thresholds the highest ETSs were clustered among NC runs, possibly due to the positive impact of the 'hot' start initialization. For the heavier thresholds these same model configurations tended to have the lowest ETSs (Table 4). Based on subjective analyses, these low ETS values were sometimes related to a displacement error, while at other times it is possible the NC runs were still undergoing 'spin-up' of strong enough vertical motions to produce heavier rainfall. With regard to bias, once again **NC** runs appeared to have an advantage as compared to runs that included convective parameterizations. Runs using convective schemes were usually characterized by large biases, especially in the case of **BMJ** runs for light rainfall. This reflects the **BMJ** tendency to often notably overpredict areas of light precipitation (Jankov and Gallus 2004). Later in time, during the 12-18h forecast period (Table 5), the highest ETS values accompanied by bias values near 1.0 were clustered among **NC**-MRF runs. This is interesting since 'spin up' problems are typically no longer present by this time in a forecast and the 'hot' start might not be expected to be helpful at this time.

Over the four time periods, and for six different rainfall thresholds, the highest ETSs by a particular physics scheme occurred: 7 times for MPN, 11 times for **MPL**, 5 times for **MPF**, 10 times for MRF, 13 times for **ETA**, 12 times for KF, 8 for **NC**, and 4 times for

BMJ. It should be noted that differences in ETSs were usually small. Hereafter, discussion will be limited to only two rainfall thresholds, 0.01 in. and 0.5 in.

2.4.2 Sensitivity of rainfall forecast spatial patterns to physical schemes changes

To objectively test the sensitivity of the rainfall forecast pattern to physics changes, CR was calculated using Eq. 4 (neglecting outliers). Based on the CR definition, it is natural to expect CR to decrease as the number of evaluated runs increases. Because the present study investigated three different convective treatments and three different microphysical schemes, but only two different PBL schemes, CR was calculated as an average value of all possible couplets when two of three model physical schemes were held fixed and the third varied (e. g., PBL scheme and convective scheme held constant while microphysics varied between two different schemes). Additionally, it should be noted that CR primarily provides information about the spatial variability among the evaluated runs. To determine the variability in terms of rainfall amounts, CR was analyzed for two thresholds (0.01 in. and 0.5 in.). Fig. 2a shows values of CR for changes in microphysical, PBL, and convective schemes at both thresholds. It can be seen that the sensitivity to the choice of convective treatment dominated during the whole 24-hour forecast period. For light rainfall, sensitivity to convective treatment was the highest (lowest CR) among all physics options during the first 6 hours of the forecast, becoming at later times more similar to (though still higher than) the sensitivities to the other two physical process schemes. Sensitivity to PBL scheme choice increased with time, while no pronounced trend was present with respect to choice of microphysical scheme. For heavier rainfall, the CR for the set of different convective

schemes was highest in the first 6 hours and much lower at later times. At all times sensitivity to changes in the convective scheme exceeded that of the two other physical schemes. The sensitivity to PBL scheme was generally comparable to, or a little larger than, that of microphysical scheme, with changes in both causing more spread (lower CR) for heavier amounts, especially at later times. However, for rainfall amounts in excess of 0.5 in., sensitivity increased rapidly with time for all physics (microphysics, PBL, and convection), a trend not generally observed for the lighter rainfall amounts.

The lowest values of r^2 (largest differences in forecasts) for both thresholds during the whole forecast period also occurred when the convective treatment was changed (Fig. 2b). The r^2 values after hour 6 when PBL schemes were varied were lower than when microphysics were varied, and the differences increased with time. The largest differences between the impact of changes in convective treatment and changes in other schemes occurred during the two earliest forecast periods. These results and the results from previous studies related to impacts of resolution and choice of convective scheme on MCS rainfall (Wang and Seaman 1997, Gallus 1999), imply that in order to achieve a large spread of solutions in a 6 or 12 h forecast with models having horizontal grid spacing of 10 km or more, it is important to vary the convective treatment.

A subjective analysis of rainfall fields for all cases and all model configurations was performed as well. The subjective analysis agreed well with the objective analysis features discussed above, suggesting the greatest variability in the forecasts came from changes in the choice of convective scheme. However, noticeable impacts from changes in the microphysical or PBL schemes were occasionally observed in some events. Figure 3

illustrates an example of the simulated rainfall fields in the domain of integration for the June 19, 2002 case initialized at 12 UTC for the 06-12 h forecast period and for four different model configurations: KF-MRF-MPN ('control run'; Fig. 3a), KF-MRF-**MPL** (Fig. 3b), **NC**-MRF-MPN (Fig. 3c), and **BMJ**-MRF-MPN (Fig. 3d). Specific features of Fig. 3 are discussed later in the text. Because rainfall extrema near the edges of the model domain (e. g., Figs. 3a and b) may reflect the influence of lateral boundaries, grid points near the boundaries were excluded in the computation of parameters discussed in this study.

2.4.3 Sensitivity of system average rain rate and domain total rain volume to physical scheme changes

Factor separation methodology (analysis of the three terms on the RHS of Eq. 6) was used as an additional evaluation of sensitivity to changes in the physical schemes. These terms, expressed as a fraction of the control run rainfall amount shown in Table 6, are presented in Tables 7 and 8. Two different rainfall measures were evaluated for this analysis. First, the RHS terms of Eq. 6 were computed using averages over all 8 cases for each 6 hr forecast period for 18 different model configurations (physical schemes were varied) at the number of points where rainfall exceeded specified thresholds. Essentially, this expresses system average rain rate (hereafter rain rate) or intensity, where the system is defined to be those points having rainfall above a specified threshold. In addition to system average rain rates, the same terms in Eq. 6 were computed over the entire domain, yielding a domain total rain volume (hereafter rain volume). The use of both measures better characterizes the QPF, since two runs could have the same total rain volume with one achieving it through light rainfall over a large area and the other through heavy rainfall in a small area.

As part of the investigation of changes in rain rate and rain volume due to variations in physical schemes, statistical significance testing was performed. In order to perform rigorous hypothesis testing, Hamill's (1999) resampling methodology was used. This procedure was strictly followed and repeated 1000 times for both a separate treatment of each 6-hourly forecast period and for all 6-hour periods combined. Combining all forecast periods together helped to increase the small sample size to better evaluate statistical significance. However, this technique to enlarge sample size was only valid when statistical stationarity was present and was not appropriate for cases in which variables were characterized by strong temporal variability. The synergistic term computed values often exhibited such variability and for these parameters each 6-hour period had to be examined separately. With only a few exceptions (to be noted later) the synergistic interactions were not statistically significant. For some parameters where the impacts of changes in schemes or synergistic interactions were large but no statistical significance was found, the small sample size is likely a problem, and future studies should examine the interactions with a larger independent dataset (Nichols 2001). In these situations the lack of statistical significance does not necessarily imply that these physical schemes and their interactions have no impact on precipitation simulations. Due to the already extensive size of the present experiment (18 model configurations for 8 different cases resulting in 144 model runs) it was not possible to substantially expand the dataset. The discussion to follow will emphasize statistically significant results, although non-significant trends occasionally will be noted when they are supported by the results of other studies addressing differences in behavior between physical schemes.

To facilitate a comparison of different model configuration results with the 'control run' and observations, rain rate and rain volume for both are included in Table 6. For the 0.01 in. threshold the control run has a roughly 30% larger areal coverage than observed for the first 6 forecast hours. During the next 6-hour period the control run areal coverage is similar to the observed, while at later times it is smaller, by as much as ~40% in the 18-24 h period. Control rain rates are 10-20% smaller than the observed for all 6 hour forecast periods. For the 0.5 in. threshold, the control areal coverage is much smaller than the observed at all times, while the rain rate is generally larger except for the 12-18 h forecast period. For both thresholds the control rain volume is always smaller than the observed, particularly for the 0.5 in. threshold, where the forecast is an order of magnitude less than that observed during the 18-24 h period.

*2.4.3a Change from MRF to **ETA** combined with changes in microphysical schemes*

Factor separation evaluation of changes from MRF to ETA and from MPN to both MPL and MPF are presented in Table 7. The switch from MRF to ETA (run f_1) for the 0.01 in. threshold always increased the areal coverage. This result is consistent with a subjective analyses performed within the present study which indicated that the ETA PBL scheme tends to generate boundary layers that are more moist than MRF, a result agreeing with Bright and Mullen's (2002) findings. On the other hand, this change did not significantly impact rain rate and rain volume. For the 0.5 in. threshold, the change in the PBL scheme had even more limited impact.

Changes in microphysics (runs f_2 and f_3 in Table 7) at all times produced an increase in the areal coverage for both the 0.01 in. and the 0.5 in. thresholds, especially when MPN (run f_0) was replaced with MPL (run f_2). This increase in areal coverage for the 0.01 in. threshold was accompanied by an increase in rain rate. For the 0.5 in. threshold increases in rain rate were usually small and significant only in the case of MPL. Both of the above changes in microphysics, in runs using KF and MRF, resulted in the largest positive impact (compared to all other tested physical schemes changes) on rain volume at all times. Increases were often twice as large for the 0.5 in. threshold than the 0.01 in. threshold and exceeded 100% for the 0.5 in. threshold for both f_2 and f_3 in the last 6-hour period. These results (supported by subjective analyses) imply that both MPL and MPF produce larger areas of heavier rainfall amounts as compared to runs using MPN. In addition, runs that use MPL often produced limited areas of excessive rainfall amounts (e. g., Fig. 3b). These results are strictly valid only when KF is used, but information found in upcoming table extends these results to simulations using other convective treatments.

The expressions $\hat{f}_{12}/f_0$ and $\hat{f}_{13}/f_0$ in Table 7 indicate values of the synergistic term normalized by the control run value. For rain rate, synergistic terms were statistically insignificant, implying that the impact on rain rate of the microphysics used is not affected by the PBL scheme used.

Regarding rain volume, the synergistic terms ($\hat{f}_{12}/f_0$ and $\hat{f}_{13}/f_0$) for the 0.01 in. threshold were statistically insignificant with an exception for MPL microphysics during the last 6h forecast period. For the 0.5 in. threshold, these schemes' interactions were large and negative after the 00-06h forecast, especially for MPL in the last 6 hours. Thus it appears the

use of ETA limits the impacts of changes in the microphysical scheme. A subjective analysis of the total and convective part of the rainfall indicated that greater moisture in the boundary layer causes more frequent triggering of the convective scheme, leading to more of the rainfall produced by deep convection at the expense of the grid-resolved component, possibly explaining the negative values of the synergistic terms.

*2.4.3b Change from MRF to **ETA** combined with changes in convective treatment*

Factor separation evaluation of the impact from changes of KF to NC (run f_4) and form KF to BMJ (run f_5) is presented in Table 8. The largest positive impact on rain rate, compared to impacts produced by changing all other physical schemes, for both the 0.01 and 0.5 in. thresholds, was due to a switch from KF to NC. Although areal coverage decreased, changes were not statistically significant. Fig. 3c is an example of a case in which during the early forecast periods areal coverage in the NC runs was considerably smaller but with heavier intensities as compared to runs that used KF and BMJ (Figs. 3a and 3d). It should be noted that in the present study NC often had a higher ETS than runs with a convective scheme, especially at earlier times. This result differs from Gallus and Segal (2001) who found in the simulation of warm season cases with a 10 km version of the Eta model that the run using no convective scheme performed significantly worse than runs using the BMJ or KF schemes. This implies that initialization using the LAPS diabatic analysis (as done here but not in Gallus and Segal 2001) likely helped the NC runs to perform better than they would have otherwise. Rain volume was not significantly impacted by a change from KF to NC.

Previous studies by Gallus and Segal (2001) and Jankov and Gallus (2004) have indicated that Eta model runs using the BMJ scheme usually produce much wider areas of lighter rainfall amounts compared to runs using KF. In the present study, when KF was replaced by BMJ (f_5 run), the subjective analysis identified the same trend (e. g., Figs. 3a and 3d). For the light threshold at all times a considerable increase in areal coverage occurred (Table 8) when KF was replaced with BMJ. In addition, rain rate and volume typically also decreased but these changes were not statistically significant. For the 0.5 in. threshold the change from KF to BMJ did not impact areal coverage or rain rate significantly, but rain volume did decrease markedly. Synergistic terms ($\hat{f}_{15}$) for both rain rate and volume were statistically insignificant, implying the PBL scheme does not strongly influence the sensitivity to convective scheme in our sample of 8 cases. This finding was also true for synergistic terms relating to changes from KF to NC and from MRF to ETA ($\hat{f}_{14}$).

*2.4.3c Change from KF to **NC** or **BMJ** combined with changes in microphysical schemes*

Rain volume synergistic terms related to a switch to **NC** and change in microphysics to **MPL** or **MPF** ($\hat{f}_{24}$ and $\hat{f}_{34}$ in Table 8) likewise were not statistically significant. Because results with the KF scheme (Table 7) showed a large impact on rain volume when microphysical scheme was varied, one might expect even larger impacts when no convective scheme was used since all of the rainfall is produced by the microphysical scheme. However, the variability and statistical insignificance of these synergistic terms indicates that a complex interaction occurs between KF and the microphysics such that the use of no

convective scheme does not necessarily result in more sensitivity to the choice of microphysics.

The rain rate-related synergistic terms associated with a switch to **BMJ** and change in microphysics to **MPL** and **MPF** were almost always negative (not shown), agreeing with the well-known characteristic of **BMJ** to generate large areas of light rainfall while substantially drying the atmosphere so that grid-resolved precipitation is often small. Rain volume-related synergistic terms were generally large and negative especially for the heavier threshold at later times implying that the **BMJ** and KF schemes exert very different impacts on grid-resolved precipitation processes. Because **BMJ** generally reduced the microphysical scheme contribution to precipitation, the large positive impact of switching microphysical schemes that existed when KF or **NC** was used was markedly reduced although still present [e. g., the 180% increase in rain volume that occurred in the 18-24h period in KF runs where MPN was switched to **MPL** (Table 7) decreased to a 49% increase (not shown)].

2.5 Sensitivity of simulated systems' morphology to physical scheme changes

For each of the 8 events and for all 18 available model configurations simulated systems morphologies were evaluated and compared to the observed morphologies in order to investigate if and how they might be affected by physical schemes changes. For this purpose 6-hour model accumulations and 6-hour Stage IV data accumulations were evaluated. It should be mentioned that for these classifications radar images are commonly used but due to the rather coarse 12 km model output, and the lack of model estimates of reflectivity in the output files Stage IV accumulations were used.

The morphology types used in the classification were chosen to match those used by Grams at al. (2006). These different morphology types included continuous linear (CL), continuous nonlinear (CNL), and discontinuous areal (DA). Linear systems were sub-classified as having trailing stratiform (TS), leading stratiform (LS) and parallel stratiform (PS). In the present study a system was classified as a CNL if the model 6-hour accumulation or Stage IV 6-hour accumulation contained a continuous stratiform area with embedded cells that covered at least 100 km x 100 km. The same criterion was valid for the DA type, except for the stratiform region which had to be discontinuous. For the system classification 1:3 aspect ratio was used. In other words, a system was classified as TS if the model 6-hour accumulation (Stage IV 6-hour accumulation) was at least 50 km wide and 150 km long with lighter rainfall amounts consistently to the rear of heavier ones. Similarly a system was classified as LS if the lighter amounts were in front.

The morphology classification results are presented in Table 9. Specific morphology category was assigned to the event if it persisted throughout the whole integration period or throughout longer period than others. If two different morphology categories were equally present over the forecast period (i. e. CNL type was present for the first 12 forecast hours and then TS type was present during the second half of the forecast period) it was indicated in Table 9.

Table 9 shows that over all the majority of the simulated and observed morphologies were classified as CNL. On the other hand, it can be seen that use of different convective treatments frequently resulted in different types of simulated morphologies. For all available cases runs using BMJ scheme were classified as CNL for at least a part of the 24 h forecast period. In 4 out of 8 cases besides being classified as the CNL the simulations were classified

as the CLs and its TS sub-category. In the case of runs using the KF scheme, in addition to the CNL category 6-hourly accumulations were also classified as CLs with theirs TS and PS subcategories, and occasionally as DAs. The NC runs were also most frequently classified as CNLs but also as DAs. For only 2 out of 8 cases and for specific parts of the forecast period the NC simulations were classified as CLs and their TS subcategory. For this limited sample of cases changes in PBL and microphysical schemes rarely impacted simulated morphologies and only in the case of the KF and NC runs. In the case of KF runs different PBL and microphysical schemes occasionally resulted in different sub-category of CL systems (i. e. TSs as opposed to PSs) while in the case of the NC runs, different PBL and microphysics schemes resulted in an omission of a specific morphology for the part of the forecast period (i. e. for the May 24, 2002 case NC-ETA-LIN run was classified as CNL while all other NC runs where classified as DAs for the first part of the forecast period and then as CNLs for the rest of the period). A comparison between morphologies simulated with runs using different configurations and observations showed that most of the model configurations correctly depicted morphologies for at least part of the forecast period.

2.6 Summary and concluding remarks

The main goal of the present study was to note and quantify general trends in the impact of various physical schemes and their interactions on warm season MCS rainfall forecasts. Knowledge of how different physical schemes or their combinations influence rainfall forecasts may be of major importance in designing and interpreting mixed physics ensembles. To pursue this goal, a matrix of 18 WRF model configurations, with 12–km grid

spacing, was created using different physical scheme combinations for 8 IHOP MCS cases. For each case, three different treatments of convection were used (KF, **BMJ** and the use of no convective scheme), with 3 different microphysical schemes (MPN, **MPL**, and **MPF**) and two different PBL schemes (MRF and **ETA**). All runs were initialized with a diabatic Local Analysis and Prediction System (LAPS) 'hot' start initialization (Jian et al. 2003). Also, it should be noted that for the majority of cases the MCS systems dominated the rainfall field and were captured in the interior of the domain.

An analysis of ETS and bias indicated that no single model configuration was clearly better than the rest. The best configuration varied both with time and rainfall threshold. Objective testing of sensitivity to physical scheme changes was performed by evaluating Correspondence Ratio and Squared Correlation Coefficient values. Both objective measures were computed for sets of two model runs in which two of three model physical schemes were held fixed and the third varied (e. g., the PBL and the convective schemes held fixed while microphysical scheme varied). Both Correspondence Ratio and correlation coefficient indicated that the highest sensitivity is to the choice of convective treatment, with less sensitivity to the PBL scheme, and the least to microphysics. In addition, correspondence ratio for light rainfall indicated that sensitivity was highest during the first 6 hours, while it was highest at later times for heavier rainfall.

Additional testing of sensitivity of rain rate and rain volume to physics changes was performed using the factor separation method (Stein and Alpert 1993). This method was used to quantify the impacts of the variation of two different physical schemes as compared to a 'control run' (KF-MRF-MPN; chosen to match the real-time model configuration used by NOAA's FSL during the IHOP experiment) and their interaction (synergy) on the simulated

rainfall. Statistical significance of the obtained results was tested by following a resampling method suggested by Hamill (1999). A change from KF to **NC** significantly increased system rain rate. A change from KF to **BMJ** significantly increased areal coverage of lighter rainfall while lowering system rain rates (though not significantly) compared to KF runs. In general, changes in convective treatment were found to have the largest impact on rain rate when KF was replaced with **NC** no matter what microphysical and PBL schemes were used. Regarding rain volume, the microphysical scheme choice exerted the largest impact in **NC** runs and least impact in **BMJ** runs, as would be expected by the amount of grid-resolved precipitation likely to occur in each.

The impact of interactions (synergy) of different physical schemes, though occasionally of comparable magnitude to that occurring from a change in one scheme alone, was found to vary greatly and typically not to be statistically significant (in our limited sample of 8 cases). One exception was for the interaction of **ETA** with **MPL** or **MPF** which did significantly reduce the rain volume increase that had been noted for the heavier threshold when the microphysics were switched from MPN. These results suggest that most of the significant trends noted for a switch in one physical process scheme (e.g., increase in rain rate when KF is switched to **NC**) remain consistent even when other physical process schemes are changed. A switch from MPN to either **MPL** or **MPF** increased rain volume markedly no matter what convective and PBL schemes were used. A switch from KF to **BMJ** decreased rain volume, especially for heavier amounts, regardless of what microphysics and PBL schemes were used.

In conclusion, the results imply that if an ensemble designed for MCS rainfall prediction lacks sufficient spread, model runs with different convective schemes should be

included as an efficient way to increase spread substantially. On the other hand, if rain volume is a desired quantity (e. g., hydrological purposes), model runs with **MPL** and **MPF** microphysical schemes may require different bias correction or weighting in an ensemble compared to runs using MPN.

Finally, an analysis of systems' morphologies from runs using different physical schemes revealed the CNL as the most frequently simulated category. In addition, results showed that use of different convective treatments occasionally resulted in different types of simulated morphologies. Changes in PBL and microphysical schemes impacted simulated morphology in very limited number of cases and only in the case of KF and NC runs.

Future work will focus on more detailed case analyses in order to relate the explicit interaction of physics schemes to the larger scale environment. These detailed case analyses along with the more general findings from the present study will be used to design and later interpret results from a mixed physics ensemble.

Acknowledgments

The authors would like to thank three anonymous reviewers for their comments which helped to improve the manuscript. In addition Linda Wharton at NOAA's Forecast Systems Laboratory and Eric Aligo and Daryl Herzmann at Iowa State University assisted with the computational work. This research was funded by NSF Grant 0226059 and by a NOAA grant from the U.S. Weather Research Program administered through the Forecast Systems Laboratory. Support was also provided by the Iowa Agriculture and Home Economics Experiment Station Project 3803.

2.7 References

Alhamed, A., S. Lakshmivarahan, and D. J. Stensrud, 2001: Cluster analysis of multimodel ensemble data from SAMEX. *Mon. Wea. Rev.*, **130**, 226-251.

Baldwin, M. E., and K.E. Mitchell, 1997: The NCEP hourly multi-sensor U.S. precipitation analysis for operations and GCIP research. Preprints, *13th Conf. on Hydrology*, Long Beach, CA, Amer. Meteor. Soc., 54-55.

Bernardet, L.R., L. Nance, H.-Y. Chuang, A. Loughe, and S.E. Koch, 2004: Verification statistics for the NCEP WRF pre-implementation test. Part 1: Deterministic verification of ensemble members. Preprints, *5th Joint WRF/14th MM5 User's Workshop*, Boulder, CO, Amer. Meteor. Soc., 229-232.

Betts, A. K., 1986: A new convective adjustment scheme. Part I: Observational and theoretical basis. *Quart. J. Roy. Meteor.* Soc., **112**, 677-692.

--------, and M. J. Miller, 1986: A new convective adjustment scheme. Part II: Single column tests using GATE wave, BOMEX, ATEX and arctic air-mass data sets. *Quart. J. Roy. Meteor. Soc.*, **112**, 693-709.

Bright, D. R., and S. L. Mullen, 2002: The sensitivity of the numerical simulation of the southwest monsoon boundary layer to the choice of PBL turbulence scheme in MM5. *Wea. Forecasting*, **17**, 99-114.

Doswell, C. A., III, H. E. Brooks, and R. A. Maddox, 1996: Flash flood forecasting: An ingredients-based methodology. *Wea. Forecasting*, **11**, 560-581.

Du, J., S. L. Mullen, and F. Sanders, 1997: Short-range ensemble forecasting of quantitative rainfall. *Mon. Wea. Rev.*, **125**, 2427-2459.

-------, J. McQueen, G. DiMego, T. Black, H, Juang, E. Rogers, B. Ferrier, B. Zhou, Z. Toth and M. S, Tracton, 2004: The NOAA/NWS/NCEP short-range ensemble forecast (SREF) system: evaluation of an initial condition vs. multi-model physics ensemble approach. Preprints, 16^{th} *Conf. on Numerical Weather Prediction*, Seattle, Washington, Amer. Meteor. Soc., CD-ROM, 21.3.

Ferrier, B. S., Y. Jin, Y. Lin, T. Black, E. Rogers, and G. DiMego, 2002: Implementation of a new grid-scale cloud and rainfall scheme in the NCEP Eta model. Preprints, *15th Conf. On Numerical Weather Prediction*, San Antonio, TX, Amer. Meteor. Soc., 280-283.

Fritsch, J. M., and R. E. Carbone, 2004: Improving quantitative precipitation forecasts in the warm season. *Bull. Amer. Meteor. Soc.*, **85**, 955-965.

Gallus, W. A., Jr., 1999: Eta simulations of three extreme rainfall events: Impact of resolution and choice of convective scheme. *Wea. Forecasting*, **14**, 405-426.

-------, and M. Segal, 2000: Sensitivity of forecast rainfall in a Texas convective system to soil moisture and convective scheme. *Wea. Forecasting*, **15**, 509–526.

-------, and -------, 2001: Impact of improved initialization of mesoscale features on convective system rainfall in 10-km Eta simulations. *Wea. Forecasting*, **16**, 680-696.

Grams, J. S., W. A. Gallus, Jr., L. S. Wharton, S. E. Koch, A. Loughe, and E. E. Ebert, 2004: The use of a modified Ebert-McBride technique to evaluate Eta QPF as a function of covective system morphology during IHOP. *Wea. Forecasting*, (submitted).

Grimit, E. P., and C. F. Mass, 2002: Initial results of a mesoscale short-range ensemble forecasting system over the Pacific Northwest. *Wea. Forecasting*, **17**, 192-205.

Hamill, T. M., 1999: Hypothesis test for evaluating numerical precipitation forecasts. *Wea. Forecasting*, **14**, 155-167.

-------, and S. J. Colucci, 1997: Verification of Eta-RSM short-range ensemble forecasts. *Mon. Wea. Rev.*, **125**, 1312-1327.

--------, and --------, 1998: Evaluation of Eta-RSM ensemble probabilistic rainfall forecasts. *Mon. Wea. Rev.*, **126**, 711-724.

Hong, S.-Y., H.-M. H. Juang, and Q. Zhao,1998: Implementation of prognostic cloud scheme for a regional spectral model. *Mon. Wea. Rev.*, **126**, 2621-2639.

Janjic, Z. I., 1994: The step-mountain Eta coordinate model: Further developments of the convection closure schemes. *Mon. Wea. Rev.*, **122**, 927-945.

Jankov, I., and W. A. Gallus Jr., 2004: Contrast between good and bad forecasts of warm season MCS rainfall. *J. Hydrol.*, **288**, 122-152.

Jian, G.-J., S.-L. Shieh, and J.A. McGinley, 2003: Precipitation simulation associated with Typhoon Sinlaku (2002) in Taiwan area using the LAPS diabatic initialization for MM5. *Terrestrial, Atmospheric, and Oceanic Sciences,* **14**, 261-288.

Kain, J. S., and J. M. Fritsch, 1993: The role of the convective "trigger function" in numerical prediction of mesoscale convective systems. *Meteor. Atmos. Phys.,* **49**, 93-106.

Lin, Y.-L., R. D. Farley, and H. D. Orville, 1983: Bulk scheme of the snow field in a cloud model. *J. Climate Appl. Meteor.,* **22**, 1065-1092.

MoTSeni, R. Buizza, T. N. Palmer, and T. Petroliagis, 1996: The ECMWF ensemble prediction system: Methodology and validation. *Quart. J. Roy. Meteor. Soc.*, **122**, 73-119.

Murphy, J. M., 1993: What is a good forecast? An essay on the nature of goodness in weather forecasting. *Wea. Forecasting*, **8**, 281-293.

Nicholls, N., 2001: The insignificance of significance testing. *Bull. Amer. Meteor.* Soc., **82**, 981-986.

Schaefer, J. T., 1990: The critical success index as an indicator of warning skill. *Wea. Forecasting*, **5**, 570-575.

Stein, U., and P. Alpert, 1993: Factor separation in numerical simulations. *J. Atmos. Sci.*, **50**, 2107-2115.

Stensrud, D. J., and J. M. Fritsch, 1994: Mesoscale convective systems in weakly forced large scale environments. Part III: Numerical simulations and implications for operational forecasting. *Mon. Wea. Rev.*, **122**, 2084-2104.

--------, and M.S. Wandishin, 2000: The correspondence ratio in forecast evaluation. *Wea. Forecasting*, **15**, 593-602.

--------, H. E. Brooks, J. Du, M. S. Tracton, and E. Rogers, 1999a: Using ensembles for short-range forecasting. *Mon. Wea. Rev.*, **127**, 433-446.

-------, G. S. Manikin, E. Rogers, and K. E. Mitchell, 1999b: Importance of cold pools to NCEP mesoscale Eta Model forecasts, *Wea. Forecasting*, **15**, 650-670.

--------, J.-W. Bao and T. T. Warner, 2000: Using initial condition and model physics perturbations in short-range ensemble simulations of mesoscale convective systems. *Mon. Wea. Rev.*, **128**, 2077-2107.

Tracton, M. S., and E. Kalnay, 1993: Operational ensemble prediction at the National Meteorological Center: Practical aspects. *Wea. Forecasting*, **8**, 379-398.

Troen, I., and L. Mahrt, 1986: A simple model of the atmospheric boundary layer: Sensitivity to surface evaporation. *Bound.-Layer Meteor.*, **47**, 129-148.

Wang, W., and N. L. Seaman, 1997: A comparison study of convective schemes in a mesoscale model. *Mon. Wea. Rev.*, **125**, 252–278.

Weckwerth, T. M., D. B. Parsons, S. E. Koch, J. A. Moore, M. A. LeMone, B. B. Demoz, C. Flamant, B. Geerts, J. Wang, and W. F. FeTSz, 2004: An overview of the International H_2O Project (IHOP_2002) and some preliminary highlights. *Bull. Amer. Meteor. Soc.*, **85**, 253-277.

Wisse, J. S. P., and J. Vila-Guerau de Arellano, 2004: Analysis of the role of the planetary boundary layer schemes during a severe convective storm. *Annales Geophysicae*, **22**, 1861-1874.

List of Figures

Figure 1. Satellite-surface composites with analyzed surface pressure and surface data plotted for a) May 16, 2002 at 06 UTC, b) May 23, 2002 at 12 UTC, c) May 24, 2002 at 18 UTC, d) June 02, 2002 at 12 UTC, e) June 04, 2002 at 00 UTC, f) June 13, 2002 at 00 UTC, g) June 15, 2002 at 06 UTC and h) June 19, 2002 at 12 UTC.

Figure 2. Values of a) Correspondence Ratio (CR) and b) Squared Correlation Coefficient (r^2) for changes in microphysical (mp), PBL (pbl), and convective schemes (cs). Results are presented for the two thresholds indicated on the abscissa (0.01 in. and 0.5 in.) and for the four 6-hourly periods ending at the times indicated in the legend.

Figure 3. Accumulated rainfall in the simulated domain for the 06-12 h forecast period for the June 19, 2002 run initialized at 12 UTC for different model runs: a) KF-MRF-MPN ('control run'), b) KF-MRF-**MPL**, c) **NC**-MRF-MPN and d) **BMJ**-MRF-MPN. Contours are shown for 1 mm, 10 mm, 50 mm, and 100 mm.

List of Tables

Table 7. Time series of percentage changes in system rain rate and domain rain volume (averaged for all 8 cases) due to physics changes (f_1 represents rainfall in the run where PBL scheme is changed from MRF to **ETA**, f_2 represents rainfall in the run in which microphysics is changed from MPN to **MPL,** and f_3 represents rainfall in the run where microphysics is changed from MPN to **MPF**) averaged over points where rainfall exceeded specified thresholds (0.01 in. and 0.5 in.). f_0 represents rainfall in the control run (KF-MRF-MPN). Values presented in bold-italic, bold and italic face indicate results that are statistically significant at the 95%, 90% and 80% confidence level, respectively, when the test sample consists of all 6-hourly periods combined. $\hat{f}_{12}$ and $\hat{f}_{23}$ represent corresponding synergistic terms. A_1, A_2, and A_3 stand for the areal coverage for runs with physical scheme changed. All values are expressed as a percentage relative to the 'control run' rain rate, rain volume, and areal coverage, which are presented in Table 6.

Table 8. As in Table 7 except for f_4 and f_5, where f_4 stands for rainfall in the run where no convective scheme (**NC**) is used and f_5 stands for rainfall in the run where the **BMJ** scheme is used.

Table 9. Observed and simulated systems' morphologies for 8 events and 18 different model configurations. CA, DA, SL, PS, TS, and LS stand for continuous areal, discontinuous areal, squall line, squall line with parallel stratiform region, squall line with trailing stratiform region, and squall line with leading stratiform region, respectively.

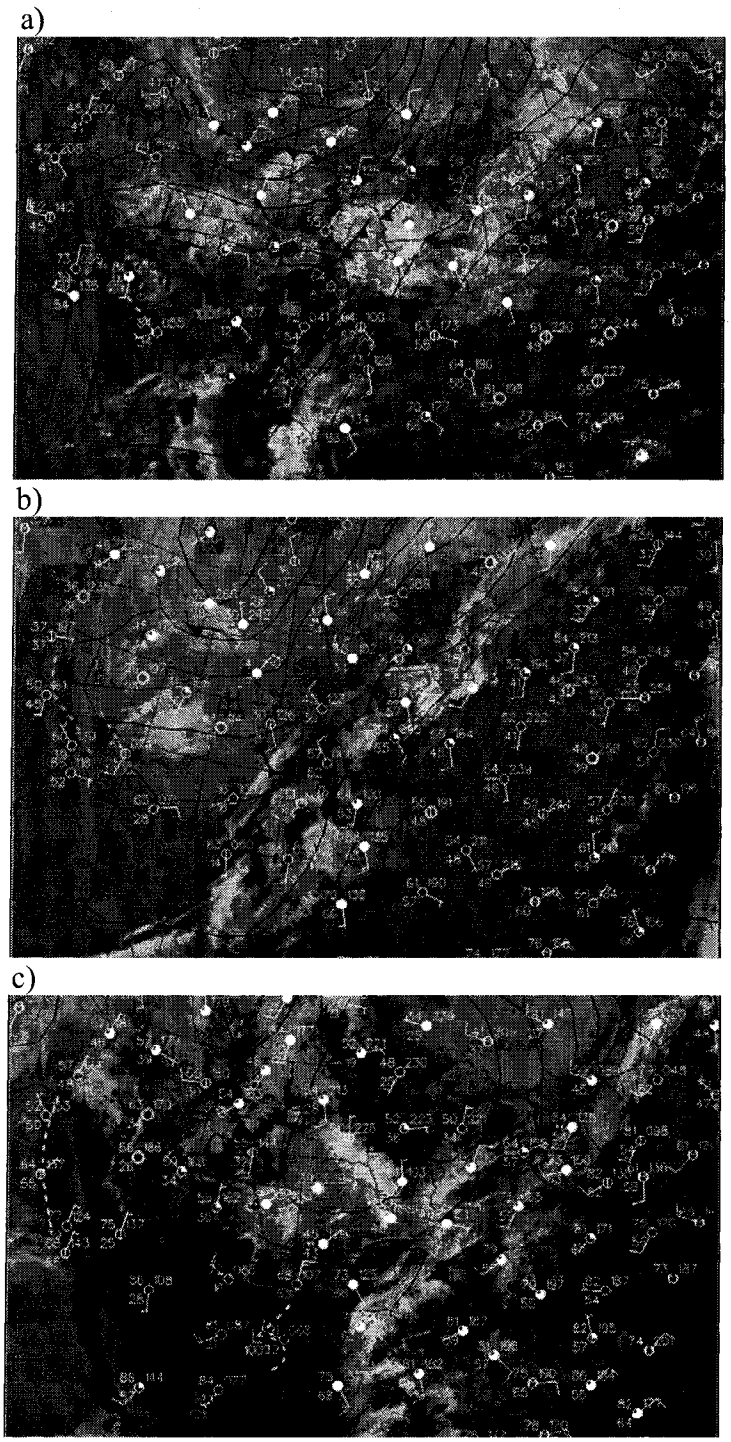

Figure 1. Satellite-surface composites with analyzed surface pressure and surface data plotted for a) May 16, 2002 at 06 UTC, b) May 23, 2002 at 12 UTC, c) May 24, 2002 at 18 UTC, d) June 02, 2002 at 12 UTC, e) June 04, 2002 at 00 UTC, f) June 13, 2002 at 00 UTC, g) June 15, 2002 at 06 UTC and h) June 19, 2002 at 12 UTC.

d)

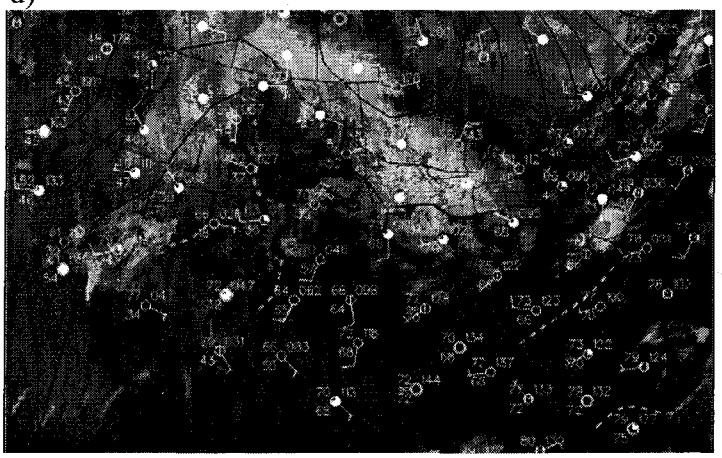

e)

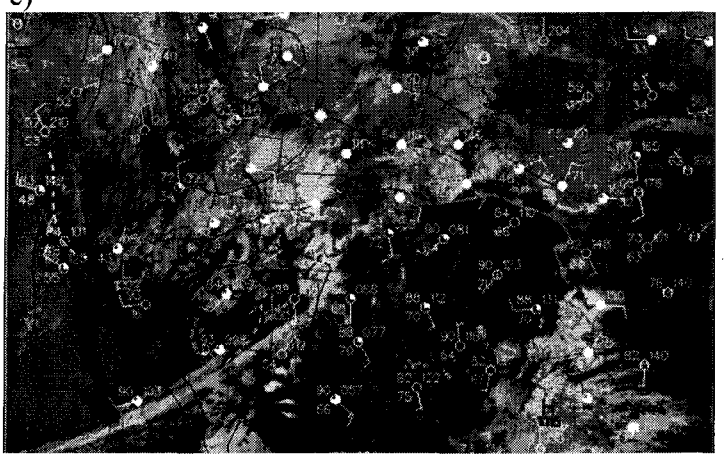

f)

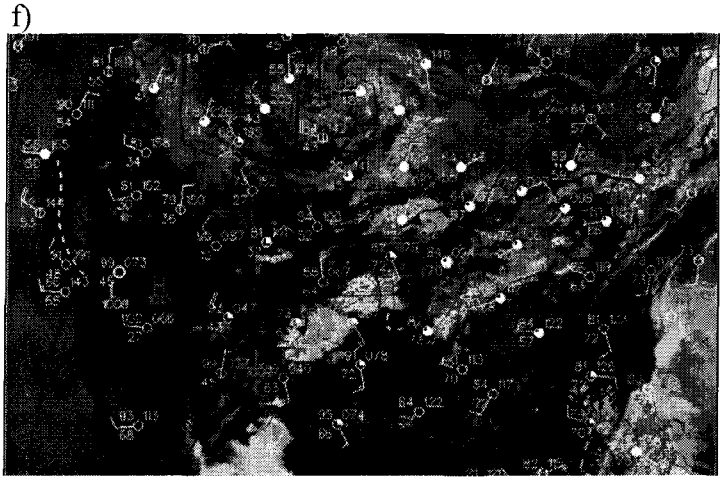

Figure 1. Continued

g)

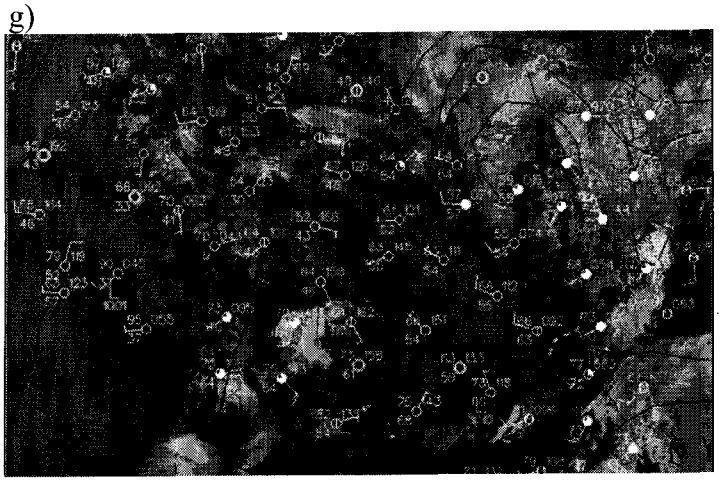

h)

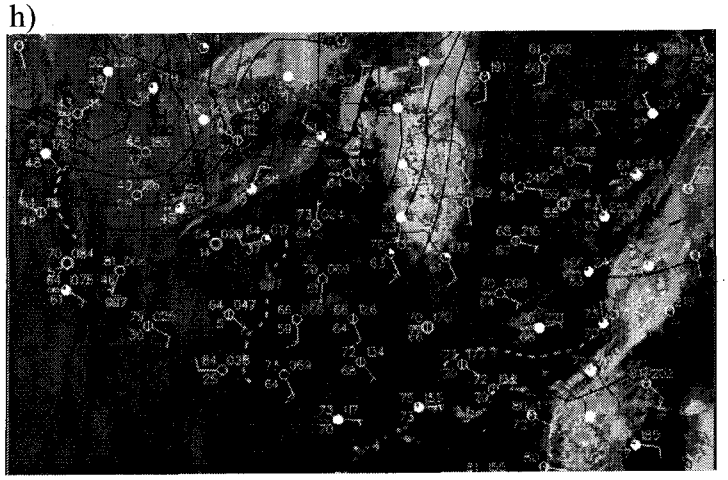

Figure 1. Continued

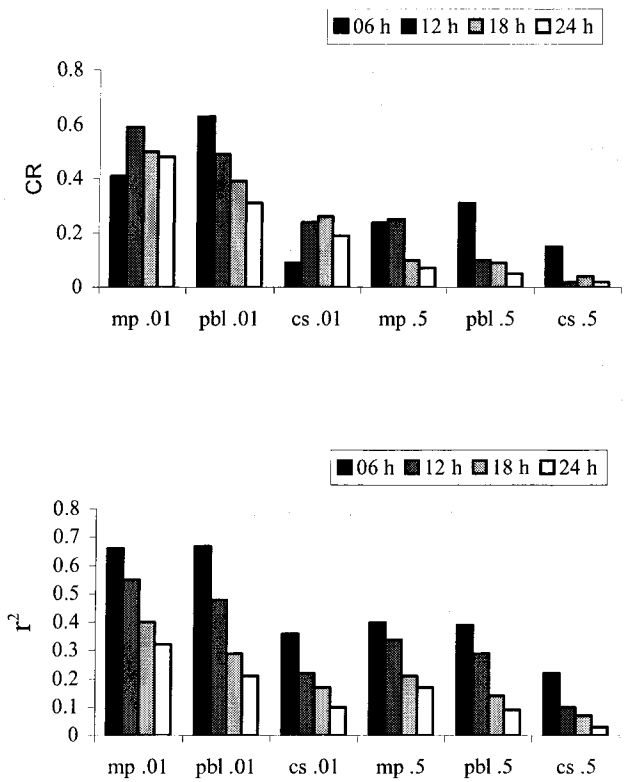

Figure 2. Values of a) Correspondence Ratio (CR) and b) Squared Correlation Coefficient (r^2) for changes in microphysical (mp), PBL (pbl), and convective schemes (cs). Results are presented for the two thresholds indicated on the abscissa (0.01 in. and 0.5 in.) and for the four 6-hourly periods ending at the times indicated in the legend.

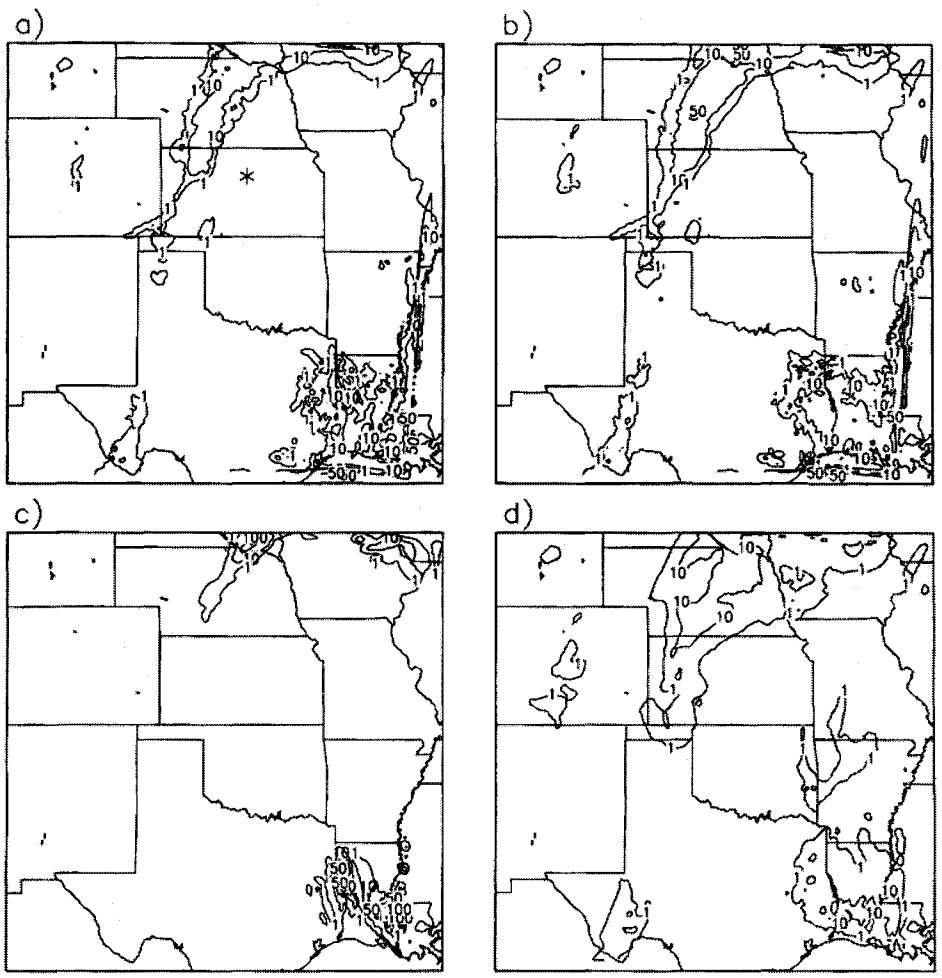

Figure 3. Accumulated rainfall in the simulated domain for the 06-12 h forecast period for the June 19, 2002 run initialized at 12 UTC for different model runs: a) KF-MRF-MPN ('control run'), b) KF-MRF-**MPL**, c) **NC**-MRF-MPN, and d) **BMJ**-MRF-MPN. Contours are shown for 1 mm, 10 mm, 50 mm, and 100 mm.

Table 1. Notation used for different physical schemes in the present study.

Physical scheme	Notation
Betts-Miller-Janjic convection	BMJ
Kain-Fritsch convection	KF
Run without a convection	NC
ETA PBL	ETA
MRF PBL	MRF
Lin et al. microphysics	MPL
NCEP-5 microphysics	MPN
Ferrier microphysics	MPF

Table 2. ETS values for four rainfall thresholds for 8 IHOP cases for the 00-06 h forecast period, with relatively "good" forecasts in bold face and relatively "bad" forecasts in italic (see Section 3a for definition of "good" and "bad").

Case	Threshold (in.)			
	0.01	**0.10**	**0.50**	**1.0**
May 16, 06Z	0.355	0.212	*-0.003*	*0.000*
May 23, 12Z	0.176	0.115	*0.000*	*0.000*
May 24, 18Z	0.209	0.130	0.039	*0.003*
June 02, 12Z	**0.407**	**0.280**	*0.000*	*0.000*
June 04, 00Z	0.332	0.265	0.134	0.078
June 13, 00Z	0.251	0.268	**0.236**	**0.157**
June 15, 06Z	*0.090*	*0.041*	*0.004*	*0.000*
June 19, 12Z	0.353	0.235	**0.150**	0.068
Average ETS	0.272	0.193	0.070	0.038

Table 3. As in Table 2 except for the 12-18 h forecast period.

Case	Threshold (in.)			
	0.01	**0.10**	**0.50**	**1.0**
May 16, 06Z	*0.028*	*0.018*	*-0.001*	*0.000*
May 23, 12Z	**0.328**	**0.295**	*-0.001*	*-0.002*
May 24, 18Z	**0.273**	**0.261**	0.040	*0.000*
June 02, 12Z	*0.007*	*-0.007*	*-0.001*	*0.000*
June 04, 00Z	0.203	0.165	**0.152**	**0.056**
June 13, 00Z	0.188	0.117	0.031	0.000
June 15, 06Z	0.184	0.214	**0.259**	**0.060**
June19, 12Z	0.171	0.169	**0.147**	**0.074**
Average ETS	0.173	0.154	0.078	0.023

Table 4. ETS and bias (in parentheses) values averaged over the 8 IHOP cases for different physical scheme combinations for the 00-06 h forecast period for four different rainfall thresholds. The notation presented in Table 1 is used to indicate different model configurations with physical schemes that are changed from the 'control run' (KF-MRF-MPN) presented in bold face. Bold face ETS values indicate best single value for each threshold.

Run	Threshold (in.)			
	0.01	**0.10**	**0.50**	**1.0**
KF-MRF-MPN	0.265 (1.6)	0.211 (1.8)	0.067 (1.1)	0.041 (0.4)
KF-**ETA**-**MPL**	0.235 (2.4)	0.187 (2.6)	0.077 (1.8)	0.055 (0.8)
KF-**ETA**-MPN	0.242 (2.0)	0.201 (2.1)	0.066 (1.2)	0.033 (0.4)
KF-**ETA**-**MPF**	0.272 (1.8)	0.205 (2.1)	0.090 (2.2)	**0.063** (1.2)
KF-MRF-**MPL**	0.255 (2.1)	0.196 (2.6)	0.073 (1.8)	0.059 (1.2)
KF-MRF-**MPF**	0.276 (1.8)	0.206 (2.1)	0.075 (1.4)	0.038 (0.5)
NC-**ETA**-**MPL**	**0.349** (1.0)	**0.247** (1.3)	0.086 (1.9)	0.044 (1.2)
NC-**ETA**-MPN	0.327 (0.8)	0.215 (1.8)	0.048 (0.9)	0.022 (0.5)
NC-**ETA**-**MPF**	0.298 (1.1)	0.203 (1.4)	0.055 (0.8)	0.041 (0.5)
NC-MRF-**MPL**	0.308 (1.1)	0.201 (1.5)	0.066 (1.0)	0.039 (0.8)
NC-MRF-MPN	0.304 (0.7)	0.191 (0.7)	0.057 (0.3)	0.029 (0.4)
NC-MRF-**MPF**	0.311 (1.1)	0.208 (1.4)	0.057 (1.0)	0.032 (1.0)
BMJ-**ETA**-**MPL**	0.246 (2.1)	0.167 (2.6)	**0.100** (1.0)	0.053 (0.6)
BMJ-**ETA**-MPN	0.249 (2.2)	0.182 (2.6)	0.070 (0.8)	0.026 (0.5)
BMJ-**ETA**-**MPF**	0.249 (2.4)	0.177 (2.8)	0.079 (1.1)	0.029 (0.8)
BMJ-MRF-**MPL**	0.249 (2.4)	0.179 (2.8)	0.099 (0.7)	0.054 (0.5)
BMJ-MRF-**MPN**	0.249 (2.1)	0.178 (2.5)	**0.100** (0.7)	0.046 (0.3)
BMJ-MRF-**MPF**	0.252 (2.5)	0.180 (2.7)	0.074 (1.0)	0.038 (0.4)

Table 5. As in Table 4 except for the 12-18h period.

Run	Threshold (in.)			
	0.01	**0.10**	**0.50**	**1.0**
KF-MRF-MPN	0.169 (1.3)	0.155 (1.7)	0.091 (1.0)	0.027 (0.8)
KF-**ETA**-**MPL**	0.160 (2.1)	0.145 (1.9)	0.102 (1.4)	0.029 (1.4)
KF-**ETA**-MPN	0.168 (1.8)	0.157 (1.6)	0.089 (1.3)	0.018 (0.9)
KF-**ETA**-**MPF**	0.133 (2.0)	0.122 (1.8)	0.105 (1.0)	0.027 (1.0)
KF-MRF-**MPL**	0.177 (1.7)	0.146 (1.7)	0.103 (2.5)	**0.047** (1.6)
KF-MRF-**MPF**	0.172 (1.5)	0.141 (1.5)	0.085 (2.6)	0.023 (1.3)
NC-**ETA**-**MPL**	0.156 (1.4)	0.152 (1.0)	0.079 (1.9)	0.016 (1.4)
NC-**ETA**-MPN	0.156 (1.3)	0.152 (1.0)	0.079 (0.9)	0.016 (1.1)
NC-**ETA**-**MPF**	0.164 (1.4)	0.151 (1.1)	0.057 (2.3)	0.014 (1.5)
NC-MRF-**MPL**	**0.239 (1.1)**	**0.213 (1.0)**	0.113 (1.5)	0.043 (1.4)
NC-MRF-MPN	0.211 (0.8)	0.195 (0.8)	**0.118 (0.7)**	0.040 (0.5)
NC-MRF-**MPF**	0.181 (1.1)	0.159 (1.2)	0.077 (1.1)	0.034 (0.9)
BMJ-**ETA**-**MPL**	0.167 (2.1)	0.141 (2.8)	0.064 (1.4)	0.020 (0.5)
BMJ-**ETA**-MPN	0.162 (2.2)	0.148 (2.7)	0.065 (1.2)	0.014 (0.4)
BMJ-**ETA**-**MPF**	0.160 (2.1)	0.145 (2.6)	0.053 (1.0)	0.020 (0.3)
BMJ-MRF-**MPL**	0.176 (2.0)	0.148 (1.6)	0.065 (1.4)	0.022 (0.6)
BMJ-MRF-MPN	0.168 (1.8)	0.145 (1.5)	0.043 (1.4)	0.009 (0.2)
BMJ-MRF-**MPF**	0.160 (2.0)	0.126 (1.5)	0.061 (1.6)	0.015 (0.5)

Table 6. Observed and control run areal coverage, rain rate and rain volume. Areal coverage for observations and the 'control run' is expressed as number of grid points where rainfall amount exceeded specified thresholds

Threshold (in.)	Parameters	Forecast period (h)			
		00-06	06-12	12-18	18-24
	System rain rate characteristics				
0.01	Observed areal coverage (pts.)	2072	2625	2657	3015
	Observed rain rate (in.)	0.18	0.22	0.22	0.23
	Control areal coverage (pts.)	2638	2683	2291	1750
	Control rain rate (in.)	0.15	0.20	0.19	0.20
0.5	Observed areal coverage (pts.)	227	353	370	510
	Observed rain rate (in.)	0.81	0.75	0.93	0.88
	Control areal coverage (pts.)	159	235	202	163
	Control rain rate (in.)	0.89	0.87	0.82	0.90
	Domain rain volume characteristics				
0.01	Observed rain volume $x10^9$ (m^3)	1.58	2.26	2.26	2.77
	Control rain volume $x10^9$ (m^3)	1.52	1.97	1.64	1.28
0.5	Observed rain volume $x10^9$ (m^3)	0.77	1.16	1.28	1.67
	Control rain volume $x10^9$ (m^3)	0.51	0.74	0.59	0.18

Table 7. Time series of percentage changes in system rain rate and domain rain volume (averaged for all 8 cases) due to physics changes (f_1 represents rainfall in the run where PBL scheme is changed from MRF to **ETA**, f_2 represents rainfall in the run where microphysics is changed from MPN to **MPL**, and f_3 represents rainfall in the run where microphysics is changed from MPN to **MPF**) averaged over points where rainfall exceeded specified thresholds (0.01 in. and 0.5 in.). f_0 represents rainfall in the control run (KF-MRF-MPN). Values presented in bold-italic, bold and italic face indicate results that are statistically significant at the 95%, 90% and 80% confidence level, respectively, when the test sample consists of all 6-hourly periods combined. $\hat{f}_{12}$ and $\hat{f}_{23}$ represent corresponding synergistic terms. A_1, A_2, and A_3 stand for the areal coverage for runs with physical scheme changed. All values are expressed as a percentage relative to the 'control run' rain rate, rain volume, and areal coverage which are presented in Table 6.

Threshold (in.)	Parameters	Forecast period (h)			
		00-06	06-12	12-18	18-24
	System rain rate characteristics				
0.01	$(f_1 - f_0)/f_0$ (%)	-10	-6	-6	-12
	$(A_1\text{-}A_0)/A_0$ (%)	***26***	***22***	***29***	***35***
	$(f_2 - f_0)/f_0$ (%)	*5*	*16*	*16*	*39*
	$(A_2\text{-}A_0)/A_0$ (%)	***27***	***13***	***26***	***22***
	$(f_3 - f_0)/f_0$ (%)	**10**	**14**	**12**	**22**
	$(A_3\text{-}A_0)/A_0$ (%)	*13*	*7*	*13*	*19*
	$\hat{f}_{12}/f_0$ (%)	5	-8	0	-8
	$\hat{f}_{13}/f_0$ (%)	10	-4	-10	-8
0.5	$(f_1 - f_0)/f_0$ (%)	0	2	-2	-8
	$(A_1\text{-}A_0)/A_0$ (%)	6	21	26	25
	$(f_2 - f_0)/f_0$ (%)	*2*	*0*	*8*	*25*
	$(A_2\text{-}A_0)/A_0$ (%)	***56***	***42***	***81***	***92***
	$(f_3 - f_0)/f_0$ (%)	-2	1	1	11
	$(A_3\text{-}A_0)/A_0$ (%)	***38***	***51***	***53***	***80***
	$\hat{f}_{12}/f_0$ (%)	0	-17	9	-4
	$\hat{f}_{13}/f_0$ (%)	-2	0	13	-3
	Domain rain volume characteristics				
0.01	$(f_1 - f_0)/f_0$ (%)	16	15	14	20
	$(f_2 - f_0)/f_0$ (%)	***37***	***32***	***53***	***94***
	$(f_3 - f_0)/f_0$ (%)	***26***	***22***	***22***	***46***
	$\hat{f}_{12}/f_0$ (%)	-5	-9	-1	**-69**
	$\hat{f}_{13}/f_0$ (%)	11	-7	-1	-3
0.5	$(f_1 - f_0)/f_0$ (%)	7	25	-4	16
	$(f_2 - f_0)/f_0$ (%)	***59***	***72***	***94***	***180***
	$(f_3 - f_0)/f_0$ (%)	***37***	***54***	***41***	***101***
	$\hat{f}_{12}/f_0$ (%)	0	*-25*	*-20*	*-83*
	$\hat{f}_{13}/f_0$ (%)	14	*-15*	*-39*	*-27*

Table 8. As in Table 7 except for f_4 and f_5, where f_4 stands for rainfall in the run where no convective scheme (**NC**) is used and f_5 stands for rainfall in the run where the **BMJ** scheme is used.

Threshold (in.)	Parameters	Forecast period (h) 00-06	06-12	12-18	18-24
	System rain rate characteristics				
0.01	$(f_4 - f_0)/f_0$ (%)	***52***	***55***	***37***	***10***
	$(A_4\text{-}A_0)/A_0$ (%)	-53	-52	-52	-46
	$(f_5 - f_0)/f_0$ (%)	-25	-37	-27	-45
	$(A_5\text{-}A_0)/A_0$ (%)	***33***	***39***	***15***	***17***
	$\hat{f}_{14}/f_0$ (%)	8	-6	-18	18
	$\hat{f}_{15}/f_0$ (%)	12	6	2	12
	$\hat{f}_{24}/f_0$ (%)	12	24	8	73
	$\hat{f}_{34}/f_0$ (%)	-25	-24	-14	16
0.5	$(f_4 - f_0)/f_0$ (%)	***3***	***45***	***21***	***11***
	$(A_4\text{-}A_0)/A_0$ (%)	-12	-8	-13	-34
	$(f_5 - f_0)/f_0$ (%)	8	19	-19	-29
	$(A_5\text{-}A_0)/A_0$ (%)	-55	-74	-64	-88
	$\hat{f}_{14}/f_0$ (%)	10	-16	0.0	19
	$\hat{f}_{15}/f_0$ (%)	-5	-13	-3	25
	$\hat{f}_{34}/f_0$ (%)	8	-22	2	25
	$\hat{f}_{34}/f_0$ (%)	-24	-36	-16	-11
	Domain rain volume characteristics				
0.01	$(f_4 - f_0)/f_0$ (%)	-15	-13	-20	-19
	$(f_5 - f_0)/f_0$ (%)	2	-12	-25	-36
	$\hat{f}_{14}/f_0$ (%)	-5	14	-4	4
	$\hat{f}_{15}/f_0$ (%)	-8	-8	-17	-10
	$\hat{f}_{24}/f_0$ (%)	-8	24	-18	8
	$\hat{f}_{34}/f_0$ (%)	-7	10	-5	-1
0.5	$(f_4 - f_0)/f_0$ (%)	32	56	24	1
	$(f_5 - f_0)/f_0$ (%)	*-50*	*-68*	*-69*	*-91*
	$\hat{f}_{14}/f_0$ (%)	16	10	1	35
	$\hat{f}_{15}/f_0$ (%)	9	-17	-5	1
	$\hat{f}_{24}/f_0$ (%)	18	49	-8	72
	$\hat{f}_{34}/f_0$ (%)	-21	-23	-25	-6

Table 9. Observed and simulated systems' morphologies for 8 events and 18 different model configurations. CL, CNL, DA, TS, LS, and PS stand for continuous linear, continuous nonlinear, discontinuous areal, region, squall line with trailing stratiform region, squall line with leading stratiform region, and squall line with parallel stratiform, respectively.

Cases/Conf.	051602	052302	052402	060202	060402	061302	061502	061902
OBSERV.	CNL	CNL	CNL	CNL	CNL/CL	CNL	CNL	CNL/CL
BMJ-ETA-MPF	CNL	CNL/CL	CNL	DA/CNL	CNL/TS	CNL	CNL	CL
BMJ-ETA-MPL	CNL	CNL/SL	CNL	DA/CNL	CNL/TS	CNL/TS	CNL	CL
BMJ-ETA-MPN	CNL	CNL/SL	CNL	CNL	CNL/TS	CNL/TS	CNL	CL
BMJ-MRF-MPF	CNL	CNL/SL	CNL	CNL	CNL/SL	CNL	CNL	CL
BMJ-MRF-MPL	CNL	CNL/CL	CNL	CNL	CNL/TS	CNL/TS	CNL	CNL
BMJ-MRF-MPN	CNL	CNL/CL	CNL	CNL	CNL/TS	CNL	CNL	CNL
KF-ETA-MPF	CNL/TS	DA/CL	CL	CNL	CNL/SL	CNL	CNL	SL/DA
KF-ETA-MPL	CNL/TS	DA/CL	CL	CNL	CNL/TS	CNL	CNL	SL
KF-ETA-MPN	CNL/TS	DA/CL	CL	CNL	CNL	CNL	CNL	SL
KF-MRF-MPF	CNL/TS	DA/CL	CNL	CNL	CNL/TS	CNL	CNL	SL
KF-MRF-MPL	CNL/TS	DA/CL	CNL	CNL	CNL/PS	CNL/SL	CNL	SL/CNL
KF-MRF-MPN	CNL	DA/CL	CNL	CNL/DA	CNL/PS	CNL	CNL	CL/CNL
NC-ETA-MPF	CNL	CNL	DA/CNL	CNL	CNL/TS	CNL/DA	CNL	CL/DA
NC-ETA-MPL	CNL	CNL	CNL	CNL	CNL/TS	CNL/DA	CNL/DA	CL/DA
NC-ETA-MPN	CNL	CNL	DA/CNL	CNL	CNL	CNL	CNL	CNL/DA
NC-MRF-MPF	CNL	CNL	DA/CNL	CNL	CNL/TS	CNL	CNL/DA	CL/DA
NC-MRF-MPL	CNL	CNL	DA/CNL	CNL	CNL/TS	CNL/DA	CNL/DA	CL
NC-MRF-MPN	CNL	CNL	DA/CNL	CNL	CNL/TS	CNL	CNL	CNL

3. INFLUENCE OF INITIAL CONDITIONS ON THE WRF-ARW MODEL QPF RESPONSE TO PHYSICAL PARAMETERIZATION CHANGES

A paper submitted to *Weather and Forecasting*

Isidora Jankov, William A. Gallus, Jr., Moti Segal, and Steven E. Koch

3.1 Abstract

To assist in optimizing a mixed physics ensemble for warm season Mesoscale Convective System (MCS) rainfall forecasting, the impact of various physical schemes as well as their interactions on rainfall when different initializations were used has been investigated. For this purpose, high-resolution Weather Research and Forecasting (WRF) model simulations of 8 International H_2O Project (IHOP) events were performed. For each case, 3 different treatments of convection, 3 different microphysical schemes and 2 different planetary boundary layer (PBL) schemes were used. All cases were initialized with both Local Analyses and Prediction System (LAPS) 'hot' start analyses and 40 km Eta model analyses. In order to evaluate the impacts of the variation of two different physical schemes and their interaction on the simulated rainfall under the two different initial conditions the factor separation method was used.

The sensitivity to the use of various physical schemes and their interactions was found to be dependent on the initialization data set. Runs initialized with Eta analyses appeared to be influenced by the use of the Betts-Miller-Janjic (BMJ) scheme in that model's assimilation system, which tended to reduce the WRF's sensitivity to changes in microphysical scheme compared to that present when LAPS analyses were used for

initialization. In addition, differences in initialized thermodynamics resulted in changes in sensitivity to PBL and convective schemes. With both initialization data sets, the greatest sensitivity to simulated rain rate was due to changes in the convective scheme. However, for rain volume, substantial sensitivity was present due to both changes in physical parameterizations and initial data sets.

3. 2 Introduction

To assist in optimizing a mixed physics ensemble for warm season MCS rainfall forecasting, Jankov et al. (2005) evaluated the impact that various physical schemes as well as their interactions had on rainfall forecasts skill in high resolution (12-km grid spacing WRF model with ARW dynamic core; 34 vertical levels) simulations of 8 IHOP (Weckwerth et al. 2004) events. All runs were initialized with a diabatic Local Analyses and Prediction System (LAPS) 'hot' start initialization (Jian et al. 2003). Jankov et al. (2005) found that no single model configuration was clearly better than the rest. In terms of skill measures the best configuration varied both with the prediction time and rainfall threshold. In addition, results implied that if an ensemble designed for MCS rainfall prediction lacks sufficient spread, model runs with different convective schemes should be included as the most efficient way to increase spread substantially. On the other hand, for hydrological purposes when rain volume is a desired quantity, model runs with Ferrier et al. (2002) and Lin et al. (1983) microphysical schemes may require different bias correction or weighting in an ensemble compared to runs using NCEP-5 class microphysics (Hong et al. 1998).

The present study provides an extension to issues presented in Jankov et al. (2005). It adopts the same approach with the same matrix of 18 different model configurations but compares the sensitivity to the parameterizations in runs using 40 km NCEP Eta model GRIB data as initial and boundary conditions to the sensitivity in runs using a LAPS 'hot' start for initialization. The main focus of the present study is to investigate if and how the impact of the physical schemes and their interaction changes when different initial conditions are used. Such an evaluation has a two-fold merit: i) further exploring the WRF-ARW model's prediction performance; and ii) providing an additional insight relevant to the ensemble prediction of convection under varied physical schemes and initial conditions. In order to perform this evaluation some of the results from Jankov et al. (2005) will be used in the present study. Methodologies used in this paper are described in section 2, results in section 3, with concluding summary and discussion in the final section.

3.3 Methodology

As in Jankov et al. (2005), the WRF-ARW model (with 12-km grid spacing) was used for simulations of 8 IHOP convective cases with 18 different combinations of physical schemes. The integration domain covered a roughly 1500x1500 km region centered over the south-central United States. For each case, three different treatments of convection were used: the Kain-Fritsch (KF) scheme (Kain and Fritsch 1993), the BMJ scheme (Betts 1986, Betts and Miller 1986, Janjic 1994), and the use of no convective scheme. For an elaboration on performance differences between the KF and BMJ schemes, see Jankov and Gallus (2004). For each of these 3 convection treatments, 3 different microphysical schemes were

used: Lin et al. (1983), NCEP-5 class (Hong et al. 1998), and Ferrier et al. (2002). Within these 9 possible configurations, two different PBL schemes were used: MRF (Troen and Mahrt 1986) and Eta (often referred to as Mellor-Yamada-Janjic 2.5; Janjic 2001). The 'control run', as in Jankov et al. (2005), was chosen to match the real-time model configuration adopted by NOAA's Forecast System Laboratory (FSL) during the IHOP experiment. It used the KF convective scheme, MRF PBL scheme and NCEP-5 class microphysical scheme. The abbreviations used in this study for runs with different combinations of physical schemes and the initialization data sets are found in Table 1. A t otal of 288 WRF-ARW simulations were considered in the present study. For rainfall validation, observed 6 h accumulated rainfall from the NCEP Stage IV analysis (Baldwin and Mitchell 1997) was used.

All new runs were initialized with 40 km NCEP Eta model GRIB data, and integrated for 24 hours. Comparisons are made with the Jankov et al. (2005) results which used the diabatic LAPS 'hot' start initialization (Jian et al. 2003). The LAPS 'hot' start technique is based on a three-dimensional analysis of cloud attributes (i. e., coverage and type), which proceeds with a method of estimating mixing ratios, precipitable water, and cloud vertical motions. By using a variational adjustment procedure (involving dynamic balancing and a mass conservation constraint), horizontal wind fields and the mass field are adjusted to produce divergence consistent with the cloud updraft properties (depth, magnitude, and shape of the updraft profiles).

As a measure of forecast accuracy, Equitable Threat Score (ETS; Schaefer 1990) and bias were calculated. A quantification of an impact of varying two different model physical

schemes on the simulated rainfall field was performed by using the factor separation methodology formulated by Stein and Alpert (1993). Based on this methodology:

$$f_{xy} - f_0 = (f_x - f_0) + (f_y - f_0) + \hat{f}_{xy}, \qquad (1)$$

where f_0 represents the control run simulated rainfall amount, f_{xy} represents the rainfall amount simulated by a run with changes in both physical schemes of interest (two physical schemes changed compared to the control run), f_x stands for the rainfall amount produced by a run that has one of the two physical schemes of interest changed (as compared to the control run), f_y represents the rainfall amounts simulated by a run with another physical scheme of interest changed (as compared to the control run), and $\hat{f}_{xy}$ stands for a synergistic term [$\hat{f}_{xy} = f_{xy} - (f_x + f_y) + f_0$] reflecting the rainfall amount contributed by the non-linear interaction between the two physical schemes. This term may be thought of as the difference between the actual rainfall occurring in the run in which two schemes have been changed and the rainfall expected by adding the impacts of each individual change. When the synergistic term is equal to zero, no rainfall is attributed to the interaction of the two changed physical schemes.

The factor separation method was applied for an analysis of two different rainfall measures: system average rain rate (hereafter rain rate), and domain total rain volume (hereafter rain volume). The use of both measures characterizes the QPF better, since two runs could have the same total rain volume with one achieving it through light rainfall over a large area and the other through heavy rainfall in a small area. As part of the evaluation of changes in rain rate and rain volume due to variations in physical schemes, statistical significance testing was performed. For the rigorous hypothesis testing, Hamill's (1999)

resampling methodology was used. This procedure was strictly followed and repeated 1000 times for both a separate treatment of each 6-hourly forecast period and for all 6-hour periods combined. Combining all forecast periods together helped to increase the small sample size to better evaluate statistical significance. This technique to enlarge sample size was only valid when statistical stationarity was present and was not appropriate for cases in which variables were characterized by strong temporal variability. In the present study discussion will be focused on statistically significant results. The notation presented in Table 1 will be used to indicate different model configurations with physical schemes that are changed from the control configuration, (KF-MRF-MPN) presented in bold face throughout the manuscript.

3. 4 Results

3.4.1 Sensitivity of rainfall forecast skill to physical scheme changes under different initial conditions

ETSs and bias values averaged for all 8 cases for all 18 model configurations indicated that no one configuration was obviously best at all times for all thresholds with both initializations (see Appendix for more details). Figure 1 illustrates ETS and bias averaged for the 6 configurations of KF, **BMJ** and **NC** runs for both initializations, during the 00-06 h forecast period. It can be seen that for lighter thresholds the highest ETSs (Fig. 1a), accompanied by a slight positive bias error (Fig. 1b), were associated with **NC** runs initialized with LAPS analyses. These high ETSs might be explained by the impact of the 'hot' start initialization. This initialization incorporates the ongoing precipitation in the model, and in that way the spin-up effect and precipitation delay that is often associated with runs without convective parameterizations are minimized. For runs using convective schemes

errors related to the schemes are still present resulting in a lower skill compared to **NC** runs. For the heavier thresholds, **NC** runs tended to have the lowest ETSs. A subjective analysis showed that the low ETS values associated with **NC** runs were very frequently related to a displacement error. The low ETSs are also consistent with the fact that the **NC** runs always had lower bias values compared to runs using convective schemes.

For runs initialized with Eta analyses, the highest ETSs for lighter and moderate thresholds were found for the **BMJ** runs (Fig. 1c). These high ETSs might be related to the fact that the Eta's assimilation system (EDAS) uses the **BMJ** scheme. Thus, the initialized thermodynamics may favor activation of the **BMJ** scheme during the early forecast hours. In addition, the **BMJ** scheme has a tendency to generate large areas of light rainfall (Jankov and Gallus 2004), yielding a high bias (Fig. 1d) which is usually associated with higher ETSs (Mason, 1989).

Later, during the 12-18h forecast period (Fig. 2), for lighter thresholds, the highest ETSs were generally associated with **NC** runs initialized with LAPS analyses and with **BMJ** runs initialized with Eta analyses. In the case of **NC** runs, bias values were about 1 while in the case of **BMJ** runs they were higher, and around 2. At this time for heavier thresholds **NC** runs had the highest ETSs and as would be expected, biases had increased compared to earlier times and were now comparable to runs using the KF convective scheme.

Figures 3 and 4 illustrate differences in ETS and bias for runs when: i) initial conditions were changed and the model configuration was kept the same, and ii) for runs initialized with the two initial conditions when the model control configuration was changed (i. e., KF changed to **BMJ** and **NC**; MRF to **ETA**; MPN to both **MPL** and **MPF**), for two different thresholds (0.01 in. and 0.5 in.), during the 00-06 h and 12-18 h forecast periods.

Thus, for example, the notation IC-BMJ indicates differences between ETSs and biases averaged for the 6 model configurations using the **BMJ** scheme for the two different initial conditions, while PP-BMJ indicates differences in ETSs and biases between averages of the 6 model configurations using the **BMJ** scheme and the model control configuration and then averaged for both initial conditions. It can be seen that differences in ETS (Figs. 3a and 4a) and bias (Figs. 3b and 4b) due to changes in initial conditions and changes in the model configuration were generally comparable with an exception for the 0.01 in. threshold during the 00-06 h forecast period, when ETS was more influenced by changes in initial conditions.

For the 0.01 in. threshold during the early forecast period, runs initialized with LAPS analyses had higher ETSs (usually statistically significant) compared to runs initialized with Eta analyses (Fig. 3a). These higher ETSs were associated with higher biases (Fig. 3b). For the 0.5 in. threshold, ETSs were generally lower (with much lower biases) for runs initialized with LAPS analyses with an exception for runs using **ETA** and **MPL**.

Regarding ETS changes when the model configuration was changed, during the 00-06 h forecast period for the 0.01 in. threshold, a statistically significant impact occurred only for a change from KF to **NC** (Fig 3a). With regard to changes in bias, they were larger as compared to changes due to use of different initial conditions. For the heavier threshold the largest impacts on ETS were associated with changes from KF to both **BMJ** and **NC**.

During the 12-18 h forecast period, nearly all runs initialized with LAPS analyses were characterized by higher ETSs and biases compared to runs initialized with Eta analyses (Fig. 4). Statistically significant changes in ETS values due to a change in initial conditions occurred at the 0.01 in. threshold for runs using **NC** and **MPL**, and at the 0.5 in. threshold for **BMJ** and **MPL** runs.

With regard to ETS changes due to varying model configurations, statistically significant impacts only occurred for **BMJ** runs at the 0.01 in. threshold. Changes in bias were comparable to those associated with changes in initial conditions for both thresholds. The overall comparable magnitudes of changes in ETS and bias from changes in physics and initial conditions imply that ensemble spread might be effectively increased by the use of variations in both (Stensrud et al. 2000, Grimit and Mass 2002).

3.4.2 Sensitivity of system average rain rate and domain total rain volume to physical scheme changes under different initial conditions

3.4.2a Quantitative results

The factor separation methodology was used to evaluate sensitivity of both rain rate (Table 2) and rain volume (Table 3) to changes in the physical schemes when two different initializations were used. The tables show the change in rainfall due to individual changes in physical schemes, as expressed by $(f_x - f_0)$ or $(f_y - f_0)$, and due to synergistic interactions between two physical schemes, as expressed by $\hat{f}_{xy}$, (see Eq. 1).

Only results that are statistically significant are presented. Table 2 shows the impact on rain rate for runs initialized with both LAPS and Eta analyses for two different thresholds (0.01 in. and 0.5 in.). It was found that for runs initialized with LAPS analyses, the largest positive impact on rain rate, associated with a statistically significant decrease in areal coverage, for the lighter threshold was due to a change from KF to **NC** (Jankov et al. 2005). Changes in microphysics (from MPN to both **MPL** and **MPF**) also resulted in a statistically

significant increase of rain rate but with lower levels of confidence. For the heavier threshold, only the change from MPN to **MPL** had a statistically significant impact (increase) on rain rate. None of the synergistic interactions between physical schemes had a statistically significant impact on rain rate for both thresholds.

Runs initialized with Eta analyses behaved similarly to those initialized with LAPS analyses for the 0.01 in. threshold, with the largest increase in rain rate due to changes in convective treatment from KF to both **BMJ** and **NC,** and less of a positive impact due to changes in microphysics. For the 0.5 in. threshold, the largest impact (negative) on rain rate, associated with a statistically significant increase in areal coverage (not shown), was due to a change from KF to **BMJ**. This might be expected as a consequence of the **BMJ** scheme tendency to underpredict heavier amounts. In addition, changes in microphysics increased rain rate (statistically significant with a lower level of confidence).

In contrast to runs initialized with LAPS analyses, runs initialized with Eta analyses differed in the magnitude of the synergistic interactions among different schemes, with several having a statistically significant impact on simulated rain rate. For the 0.01 in. threshold a synergistic interaction between **MPL** and **NC** resulted in a notable increase in rain rate with a 95% level of confidence. Specifically, both changes from MPN to **MPL** and from KF to **NC** increased the rain rate, and the synergistic interaction between **MPL** and **NC** had the same positive impact. On the other hand, the synergistic interaction between **MPF** and **NC** significantly decreased simulated rain rate but with a lower level of confidence (80%-90%). Changes from both MPN to **MPF** and from KF to **NC** increased the rain rate while the synergistic interaction between **MPF** and **NC** resulted in a decrease.

A similar trend occurred for the heavier 0.5 in. threshold for the interaction between **ETA** and **MPF** except that the confidence level was higher (95%). In addition, the interaction between **MPL** and **NC** was statistically significant, but in contrast to the 0.1 in. threshold, the synergy contribution was positive like these of the individual changes. If the goal is not only to increase the ensemble spread by using different physical schemes but also to improve the accuracy of the simulated rainfall, information about the synergistic effect may be used as a calibration tool. Specifically, knowing how particular physical schemes and their interactions impact the simulated rainfall quantitatively may determine the choice of physical schemes used in an ensemble.

Table 3 presents the factor separation results for rain volume. For runs initialized with LAPS analyses at both light and heavier thresholds, the largest positive impact was due to changes in microphysics. In addition, for the 0.5 in. threshold, a change from KF to **BMJ** decreased rain volume. On the other hand, for runs initialized with Eta analyses, for the 0.1 in. threshold, only a change in PBL scheme produced a statistically significant positive impact. For the 0.5 in. threshold, both a change from KF to **NC** and from KF to **BMJ** reduced the rain volume notably. A change from MPN to **MPL** and from MRF to **ETA** both resulted in an increase in rain volume but with a lower level of statistical confidence.

In both Table 2 and 3, the change from KF to **BMJ** appeared to significantly impact simulated rainfall when 40 km Eta analyses were used, but not when LAPS analyses were used. On the other hand a change from KF to **NC** had a significant impact on simulated rainfall for both initializations. This once again may imply that the **BMJ** scheme used in

EDAS influences the initial conditions in such a way that when a different convective scheme is used in the model, the impact on simulated rainfall is particularly large.

Finally, using Eq. 1, but with $(f_x - f_0)$ representing a change in physical scheme and $(f_y - f_0)$ representing a change in initial conditions, synergistic terms for both rain rate and rain volume were calculated (not shown). The synergistic term magnitudes appeared to be small for all physics variations for both thresholds and at all times. In addition, the majority of the synergistic terms were negative. The only exceptions were in the case of rain rate, when the change from LAPS analyses to Eta analyses was combined with changes from KF to both **BMJ** (for both thresholds) and to **NC** (only for the lighter threshold).

3.4.2b Illustrative results

Results previously presented indicated a larger sensitivity to changes in microphysics for runs initialized with LAPS analyses compared to those initialized with Eta analyses. This might be explained by the fact that the 40 km Eta analysis is generated by the EDAS that uses the **BMJ** convective scheme, which has a tendency to generate large areas of light rainfall while substantially drying the atmosphere and reducing the grid-resolved component of precipitation (e. g., Gallus 1999). Thus, runs initialized with 40 km Eta analyses may be too dry initially for microphysical schemes to activate in areas where precipitation is likely to be observed, and the role of microphysics is restricted until later forecast times when the influence of initial conditions has diminished. Support for this argument is provided in Figure 5 which shows the total, and grid resolved rainfall components for the first forecast hour on

June 13, 2002 for the **BMJ-ETA-MPF** model run initialized with both Eta and LAPS analyses. The total rainfall field from the run initialized with the Eta analysis (Fig. 5a) was characterized by a much lighter and broader rainfall area compared to the run initialized with a LAPS analysis (Fig. 5b). More importantly, Fig. 5c implies that most of the rainfall simulated during the first forecast hour by the run initialized with the Eta analysis came from the parameterized convective precipitation component. In the case of the run initialized with a LAPS analysis, a notable part of the total simulated rainfall (Fig. 5b) was resolved on the grid (Fig. 5d). Figure 6 shows the same fields as Fig. 5 except for the 17-18 h forecast period. It can be seen that later in the forecast, as the influence of the initial conditions diminished, the grid-resolved component of rainfall for the run initialized with the Eta analysis (Fig. 6c) became more substantial, but was still smaller than it was in the run initialized with the LAPS analysis (Fig. 6d).

As an additional issue it was found that early in the forecast, for runs initialized with LAPS analyses, the change in PBL scheme did not notably affect the rainfall forecast, while for runs initialized with Eta analyses, rainfall was considerably altered. This might be related to the fact that the EDAS uses the **BMJ** scheme, whose structure favors activation in cases with significant amounts of moisture in low and mid levels and positive convective available potential energy (CAPE), and the fact that the LAPS 'hot' start analysis is a dynamically balanced initialization. In other words, favorable conditions for convective scheme activation associated with the Eta analyses result in an early triggering of convection, which then induces differences in evolution of thermodynamic profiles for runs using various PBL schemes. These differences are especially noticeable for runs initialized with the Eta analyses and they are illustrated in the following.

Figure 7 presents temporal variations of thermodynamic profiles at the grid point (34N, 100W), indicated by a '*' in Fig. 5a, for **BMJ**-MRF-**MPF** (dashed lines) and **BMJ**-**ETA**-**MPF** (solid lines) model runs initialized at 00Z for June 13, 2002. The two model configurations differ only in their PBL schemes (MRF vs. **ETA**). It can be seen that at this location both initializations were characterized by nearly neutral elevated mixed layers, and the Eta analysis (Fig. 7a) was slightly less stable compared to the LAPS analysis (Fig. 7b). The Eta profile was characterized by a large value of surface CAPE (~ 3500 Jkg^{-1}) and a negligible convective inhibition (CIN ~ 1 Jkg^{-1}), while in the case of the LAPS analysis, surface CAPE was much smaller (~ 1300 Jkg^{-1}) and the CIN was much larger (~105 Jkg^{-1}). Consequently, in the run initialized with the Eta analysis the BMJ scheme activated (Fig. 7c) and produced light rainfall during the first 2 forecast hours. The profiles from runs that used different PBL schemes started to evolve differently. On the other hand, at this time, profiles from runs initialized with the LAPS analysis using different PBL schemes remained identical (Fig. 7d). Two hours later, in runs initialized with the Eta analysis (Fig. 7e), both profiles were characterized by a distinctive 'onion' shape, but they differed notably in other ways. The profile from the run that used the MRF scheme (dashed lines) was characterized by a drier and more stable boundary layer. At the same time, in runs initiated with the LAPS analysis (Fig. 7f) the convective scheme had now activated and the profiles began to differ. Even at 06 UTC, differences between profiles from runs that used different PBL schemes and were initialized with the Eta analysis (Fig. 7g) were larger than difference in profiles from runs initialized with the LAPS analysis (Fig. 7h). This type of behavior among runs using different PBL schemes initialized with different initializations was frequently observed.

3.4.3 Mixed-physics and mixed-initial condition ensemble skill

Results from the factor separation method indicated that for both initializations, changes in convective treatment affected the rain rate the most. Rain volume appeared to be influenced the most by changes in microphysics in the case of runs initialized with LAPS analyses and by changes in convective treatment for runs initialized with 40 km Eta analyses. This information was used in designing four different ensembles evaluated below.

Table 4 provides the areas under Relative Operating Characteristic (ROC) curves (Mason and Graham, 1999) for an 18-member ensemble, 9-member ensemble (including 3 different convective treatments, **ETA** PBL, and 3 different microphysics), and two 6-member ensembles (one including 3 different convective treatments, 2 different PBL schemes and **MPF**, and another including the **BMJ** scheme, 2 different PBL schemes and 3 different microphysics), for the 0.01 in. and 0.5 in. thresholds for the two different initializations during four 6-hourly forecast periods. Areas under the ROC curves are a measure of probabilistic forecast skill, with values greater than 0.5 implying the potential for a skillful forecast and values near 0.7 implying a useful forecast (Buizza et al. 1999). It should be noted that due to differences in bias among runs initialized with different analyses, magnitudes of areas under ROC curves for ensembles using different initial conditions should be interpreted with caution. An increase in bias has been shown to lead to an increase in probability of detection (Baldwin and Kain, 2004) and most likely a smaller increase in probability of false detection, resulting in higher values of areas under ROC curves for ensembles with higher biases.

Because the trapezoidal approach was used for calculation of the areas under the ROC curves, ensembles with more members would likely earn higher values (more probability thresholds exist). Despite this, Table 4 shows larger values for the 9-member ensemble than the 18-member one for both initializations and both thresholds. In addition, values associated with the two 6-member ensembles were generally similar to values from the full 18-member ensemble for both initializations. These results further support findings indicated by the factor separation method (identifying convective and microphysical treatments as those affecting simulated MCS rainfall the most) in design of ensembles.

Areas under ROC curves were also computed for ensembles which combined various physical schemes and different initial conditions (not shown). It was found that runs initialized with Eta analyses using different convective treatments combined with runs initialized with LAPS analyses using various microphysics tended to have the largest scores, but the scores were lower than scores from ensembles initialized with the LAPS analyses presented in Table 4. This might be explained by the bias differences among the ensemble members.

In addition, rank histograms were created for ensembles listed in Table 4 for both initial conditions. Because histograms related to different initial conditions showed the same general trend, only those associated with Eta initial conditions will be presented. Figure 8 shows these for the 00-06 h and Figure 9 for the 12-18 h forecast periods. During the 00-06 h forecast period, the histogram for the full 18-member ensemble (Fig. 8a) indicates that the ensemble members were too wet compared to the observations. The same trend was present in histograms related to the two 6-member ensembles (Figs. 8b and 6c), especially in the case of the ensemble using the **BMJ** scheme (Fig. 8c). More precisely, this trend was present for

all ensembles involving different convective treatments combined with different PBL schemes except when **NC** runs were the only ones used. When only **NC** runs were used, the rank histogram had a 'U' shape indicating insufficient spread (not shown). Additionally, ranked histograms were created using physical schemes from the two 6-member ensembles but combining different initial conditions (not shown). The tendency of the ensemble members being too wet was reduced, although still present. This may imply that use of increased number of initial conditions in an ensemble designed for rainfall forecast might reduce bias related to light rainfall at earlier times.

On the other hand, the histogram for the 9-member ensemble which combined different convective treatments and different microphysical schemes (Fig. 8d) showed reasonable spread. Later in time (Fig. 9a-d) all histograms indicate a reasonable spread.

3. 5 Summary and discussion

General trends in the impact of various physical schemes and their interactions on warm season MCS rainfall forecasts were evaluated under different initial conditions. A matrix of 18 WRF-ARW model configurations with 12–km grid spacing was created using different physical scheme combinations for 8 IHOP MCS cases. For each case, three different treatments of convection were used, with 3 different microphysical schemes and two different PBL schemes. The runs were initialized with both a diabatic LAPS 'hot' start initialization (Jian et al. 2003) and 40 km Eta GRIB files.

ETS and bias analyses of the 288 WRF-ARW model simulations considered in the present study indicated that for both initializations no single model configuration was clearly

best for the entire simulation period and for all thresholds. Differences in ETS and bias for runs initialized with different initial conditions but using the same model configuration, as well as ETS and bias changes for runs initialized with the two different initial conditions but with changes in model configuration were often statistically significant implying that both variations in physics and initial conditions may be applied to increase the spread of an ensemble used for MCS rainfall forecasting.

The factor separation method (Stein and Alpert 1993) was used to quantify the impacts of the variation of two different physical schemes compared to a 'control run' (KF-MRF-MPN) and their interaction (synergy) on the simulated rainfall. For both initializations, changes in convective treatment affected the rain rate the most. For runs initialized with LAPS analyses, rain volume was affected the most by changes in microphysics, while for runs initialized with 40 km Eta analyses, rain volume was influenced most by choice of convective treatment. Information about the interactions among different physical schemes obtained through the synergistic term analysis should be useful in an ensemble calibration procedure.

Rank histograms and areas under ROC curves were examined for ensembles using these various model configurations and different initial conditions. Findings supported results from the factor separation methodology which identified convective and microphysical treatments as those with the largest impact on simulated MCS rainfall.

In conclusion, it appears that sensitivity of the WRF-ARW model rainfall forecasts to the use of varied physical schemes and their interactions is dependent on the initialization data set or procedure. If an ensemble designed for MCS rainfall prediction lacks sufficient spread, model runs with different convective schemes should be included. If rain volume is a

desired quantity (e. g., hydrological purposes), and initialization uses the LAPS analyses, runs with **MPL** and **MPF** microphysical schemes may require different bias correction or weighting in an ensemble compared to runs using MPN. In contrast, when the Eta analysis is used for initialization, runs with these different microphysical schemes may not need such different weighting, but runs with **NC** and **BMJ** would require different weighting as compared to KF runs. Knowledge of which physical schemes exert the greatest impact on rainfall forecasts can allow for design of ensembles that maximize skill while minimizing the number of members needed.

Acknowledgments

The authors would like to thank Daryl Herzmann at Iowa State University for his assistance with the computational work. This research was funded by NSF Grant 0226059, by a NOAA grant from the U.S. Weather Research Program administered through the Forecast Systems Laboratory, and by Iowa Agriculture and Home Economics Experiment Station Project 3803.

Appendix

ETSs and bias values averaged for all 8 cases for all 18 model configurations, for the 00-06 h (Table A1) and 12-18 h (Table A2) forecast periods computed for four different thresholds (0.01 in., 0.1 in., 0.5 in. and 1. in) and for both initializations indicated generally lower scores at later times. Scores were always higher for lighter than heavier thresholds. In addition, ETS and bias analyses indicated that no one configuration was obviously best at all times for all thresholds with both initializations.

3. 6 References

Baldwin, M. E., and J. S. Kain, 2004: Examining the sensitivity of various performance measures. Preprints, *17th Conf. On Probability and Statistics in the Atmospheric Sciences*, Seattle, Washington, Amer. Meteor. Soc., CD-ROM, 2.9.

-------., and K. E. Mitchell, 1997: The NCEP hourly multi-sensor U.S. precipitation analysis for operations and GCIP research. Preprints, *13th Conf. on Hydrology*, Long Beach, CA, Amer. Meteor. Soc., 54-55.

Betts, A. K., 1986: A new convective adjustment scheme. Part I: Observational and theoretical basis. *Quart. J. Roy. Meteor.* Soc., **112**, 677-692.

--------, and M. J. Miller, 1986: A new convective adjustment scheme. Part II: Single column tests using GATE wave, BOMEX, ATEX and arctic air-mass data sets. *Quart. J. Roy. Meteor. Soc.*, **112**, 693-709.

Buizza, R, A. Hollingsworth, F. Lalaurette, and A. Ghelli, 1999: Probabilistic predictions of precipitation using the ECMWF Ensemble Prediction System. *Wea. Forecasting*, **14**, 168-189.

Ferrier, B. S., Y. Jin, Y. Lin, T. Black, E. Rogers, and G. DiMego, 2002: Implementation of a new grid-scale cloud and rainfall scheme in the NCEP Eta model. Preprints, *15th Conf. On Numerical Weather Prediction*, San Antonio, TX, Amer. Meteor. Soc., 280-283.

Fritsch, J. M., and R. E. Carbone, 2004: Improving quantitative precipitation forecasts in the warm season. *Bull. Amer. Meteor. Soc.*, **85**, 955-965.

Gallus, W. A., Jr., 1999: Eta simulations of three extreme rainfall events: Impact of resolution and choice of convective scheme. *Wea. Forecasting*, **14**, 405-426.

Grimit, E. P., and C. F. Mass, 2002: Initial results of a mesoscale short-range ensemble forecasting system over the Pacific Northwest. *Wea. Forecasting*, **17**, 192-205.

Hamill, T. M., 1999: Hypothesis test for evaluating numerical precipitation forecasts. *Wea. Forecasting*, **14**, 155-167.

Hong, S.-Y., H.-M. H. Juang, and Q. Zhao,1998: Implementation of prognostic cloud scheme for a regional spectral model. *Mon. Wea. Rev.*, **126**, 2621-2639.

Janjic Z., 2001: Nonsingular Implementation of the Mellor-Yamada Level 2.5 Scheme in the NCEP Meso Model. NCEP Office Note No. 437, 61pp.

--------, 1994: The step-mountain Eta coordinate model: Further developments of the convection closure schemes. *Mon. Wea. Rev.*, **122**, 927-945.

Jankov, I., and W. A. Gallus Jr., 2004: Contrast between good and bad forecasts of warm season MCS rainfall. *J. Hydrol.*, **288**, 122-152.

-------, -------, M. Segal, B. Shaw, and S. E. Koch, 2005: The impact of different WRF model physical parameterizations and their interactions on warm season MCS rainfall. *Wea. Forecasting* (in press).

Jian, G.-J., S.-L. Shieh, and J.A. McGinley, 2003: Precipitation simulation associated with Typhoon Sinlaku (2002) in Taiwan area using the LAPS diabatic initialization for MM5. *Terrestrial, Atmospheric, and Oceanic Sciences,* **14**, 261-288.

Kain, J. S., and J. M. Fritsch, 1993: The role of the convective "trigger function" in numerical prediction of mesoscale convective systems. *Meteor. Atmos. Phys.,* **49**, 93-106.

Lin, Y.-L., R. D. Farley, and H. D. Orville, 1983: Bulk scheme of the snow field in a cloud model. *J. Climate Appl. Meteor.*, **22**, 1065-1092.

Mason, I., 1989: Dependence of the critical success index on sample climate and threshold probability. *Aust. Met. Mag.*, **37**, 75-81.

Mason, S. J., and N. E. Graham, 1999: Conditional probabilities, relative operating characteristics, and relative operating levels. *Wea. Forecasting*, **14**, 713-725.

Schaefer, J. T., 1990: The critical success index as an indicator of warning skill. *Wea. Forecasting*, **5**, 570-575.

Stein, U., and P. APSert, 1993: Factor separation in numerical simulations. *J. Atmos. Sci.*, **50**, 2107-2115.

Stensrud, and M.S. Wandishin, 2000: The correspondence ratio in forecast evaluation. *Wea. Forecasting*, **15**, 593-602.

--------, J.-W. Bao and T. T. Warner, 2000: Using initial condition and model physics perturbations in short-range ensemble simulations of mesoscale convective systems. *Mon. Wea. Rev.*, **128**, 2077-2107.

Tracton, M. S., and E. Kalnay, 1993: Operational ensemble prediction at the National Meteorological Center: Practical aspects. *Wea. Forecasting*, **8**, 379-398.

Troen, I., and L. Mahrt, 1986: A simple model of the atmospheric boundary layer: Sensitivity to surface evaporation. *Bound.-Layer Meteor.*, **47**, 129-148.

Weckwerth, T. M., D. B. Parsons, S. E. Koch, J. A. Moore, M. A. LeMone, B. B. Demoz, C. Flamant, B. Geerts, J. Wang, and W. F. Feltz, 2004: An overview of the International H_2O Project (IHOP_2002) and some preliminary highlights. *Bull. Amer. Meteor. Soc.*, **85**, 253-277.

List of Figures

Figure 7. The **BMJ-ETA-MPF** (solid lines) and **BMJ**-MRF-**MPF** (dashed lines) thermodynamic profiles from the model runs initialized with both Eta (left column) and LAPS (right column) analyses at the point indicated by '*' in Fig. 5a at; a) and b) 00 UTC; c) and d) 02 UTC; e) and f) 04 UTC; g) and h) 06 UTC.

Figure 8. Rank histograms for a) 18_full, b) 6_cu_pbl_**MPF**, c) 6_**BMJ**_pbl_mp and d) 9_cu_**ETA**_mp ensembles (see Table 4 caption for the notation legends), for the 00-06 h forecast period and using the Eta initial conditions.

Figure 9. As in Figure 8 except for the 12-18 h forecast period.

List of Tables

Table 1. Notation used for different physical schemes and initializations in the present study.

Table 2. Time series of percentage changes in system rain rate (averaged for all 8 cases) due to physics changes (f_1 represents rainfall in the run where PBL scheme is changed from MRF to **ETA**, f_2 represents rainfall in the run where microphysics is changed from MPN to **MPL**, f_3 represents rainfall in the run where microphysics is changed from MPN to **MPF**, f_4 represents rainfall in the run where convective treatment is changed from KF to **NC**, and f_5 represents rainfall in the run where convective treatment is changed from KF to **BMJ**) averaged over points where rainfall exceeded specified thresholds (0.01 in. and 0.5 in.) for two different initializations (LAPS and Eta). f_0 represents rainfall in the control run (KF-MRF-MPN). $\hat{f}_{13}$, $\hat{f}_{24}$, and $\hat{f}_{34}$ represent corresponding synergistic terms. Values presented in bold-italic, bold and italic face indicate results that are statistically significant at the 95%, 90%, and 80% confidence level, respectively.

Table 3. As in Table 2 except for domain total rain volume.

Table 4. Areas under ROC curves averaged for all 8 cases for 18_full ensemble (including all 18 model configurations); 9-member ensemble, 9_cu_**ETA**_mp, (including 3 different convective treatments-cu, **ETA** PBL, and 3 different microphysics-mp); two 6-member ensembles, 6_cu_pbl_**MPF** and 6_**BMJ**_pbl_mp (the first including 3 different convective treatments, 2 different PBL schemes-pbl and **MPF**, and the second including the **BMJ**

scheme, 2 different PBL schemes and 3 different microphysics), for the 0.01 in. and 0.5 in. thresholds, for the two different initializations, and the 4 specified 6-hourly forecast periods.

Table A1. ETS and bias (in parentheses) values averaged over the 8 IHOP cases for different physical scheme combinations for the 00-06 h forecast period for four different rainfall thresholds and for two different initializations. The notation presented in Table 1 is used to indicate different model configurations with physical schemes that are changed from the 'control run' (KF-MRF-MPN) presented in bold face. Runs initialized with LAPS analyses are presented in italic face.

Table A2. As in Table A1, except for the 12-18h period.

a)

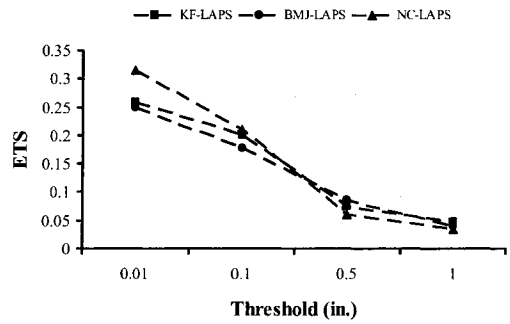

b)

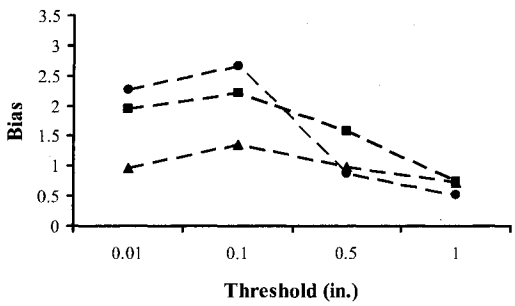

c)

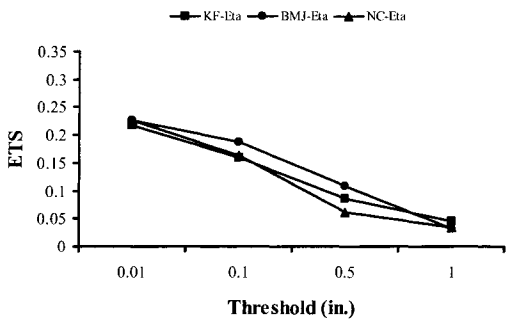

d)

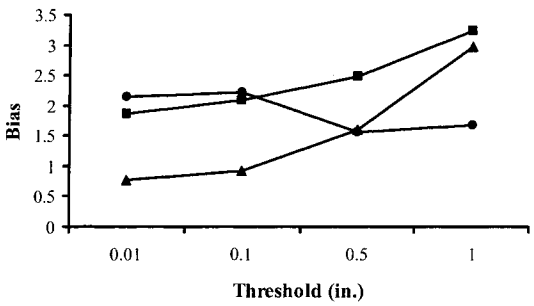

Figure 1. Average a) ETS, and b) Bias for the 6 configurations associated with the KF, BMJ and NC runs initialized with LAPS initialization and c) and d) as a) and b) respectively, except for Eta initialization.

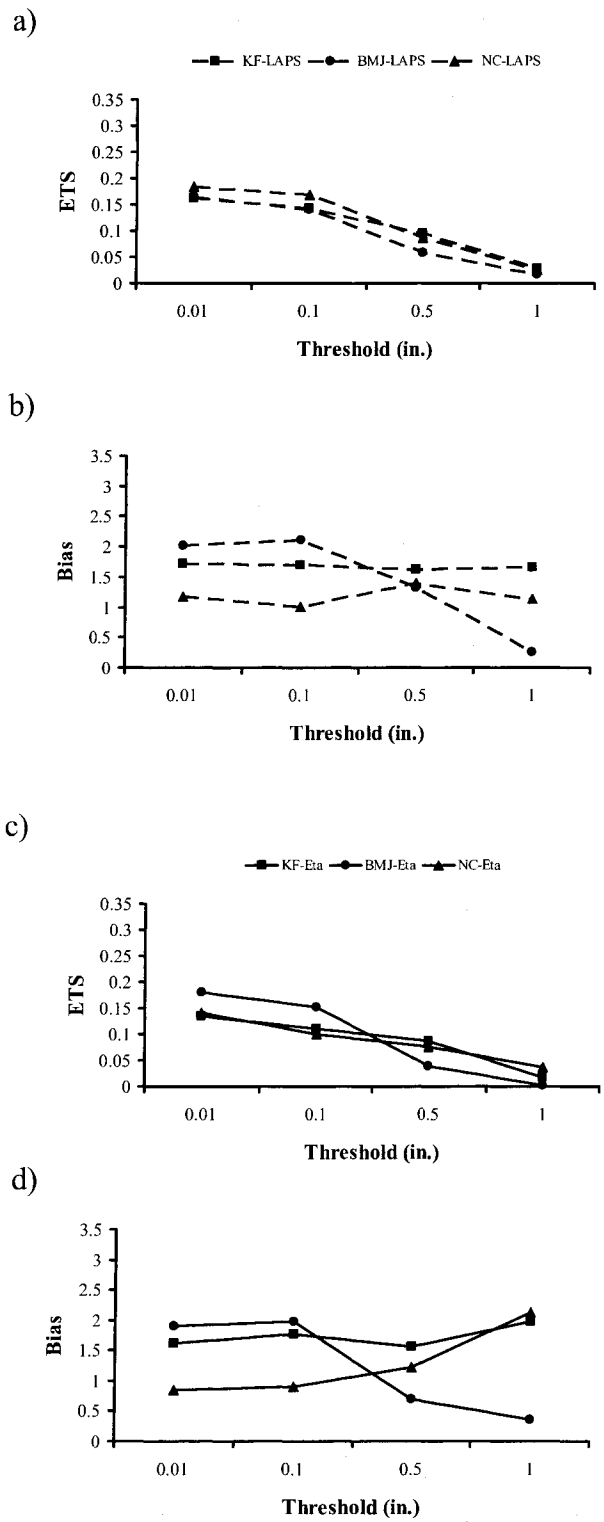

Figure 2. As in Figure 1 except for the 12-18 h forecast period.

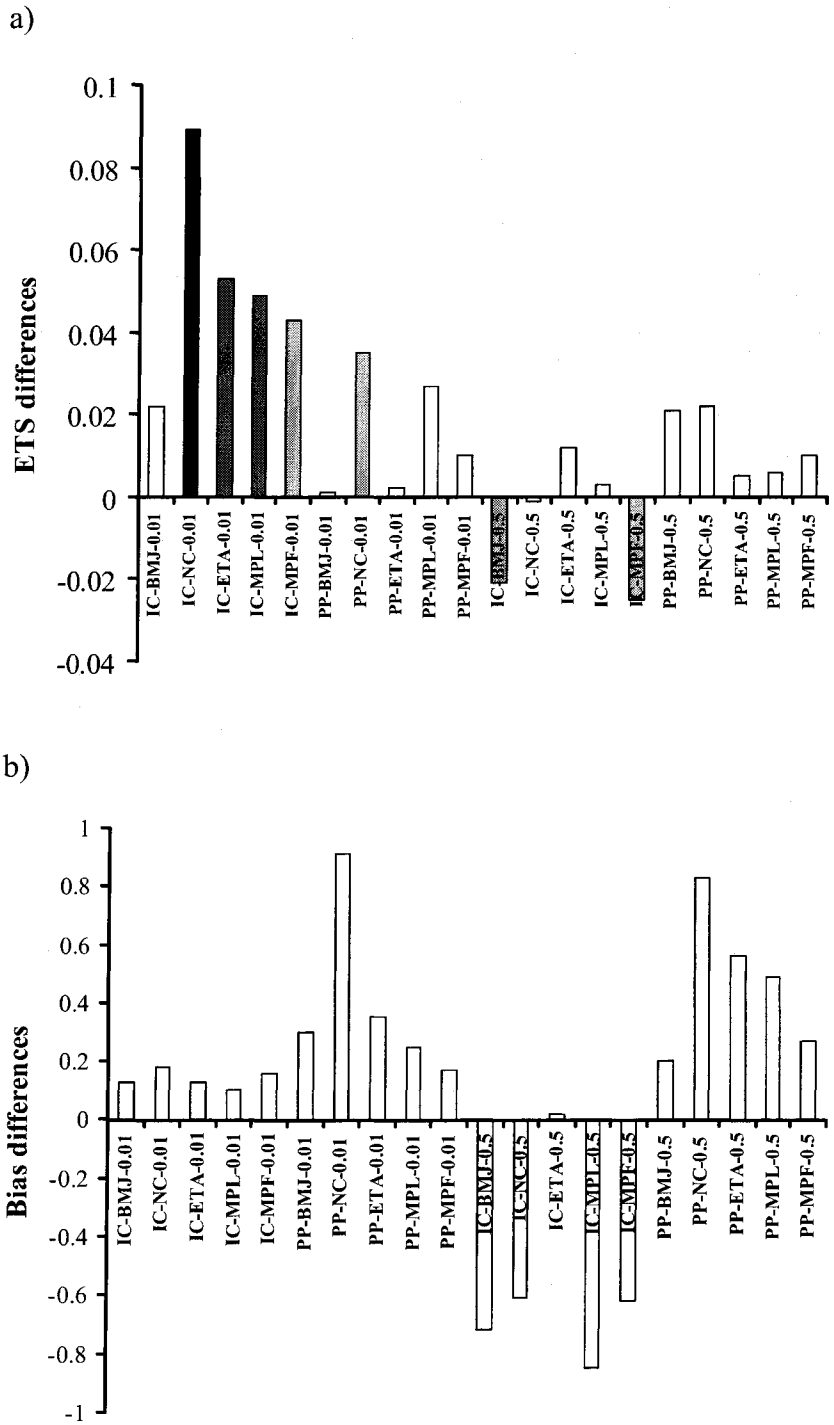

Figure 3. Differences in a) ETS and b) bias when the initial conditions were changed (LAPS runs minus ETA runs) while physical parameterizations kept the same (IC), and when physical parameterizations were changed (PP) and skill scores were averaged for the two different initial conditions, for the 0.01 and 0.5 in. thresholds, during the 00-06 h forecast period. Bars shaded in black, dark gray, and gray color indicate results that are statistically significant at the 95%, 90%, and 80% confidence level, respectively.

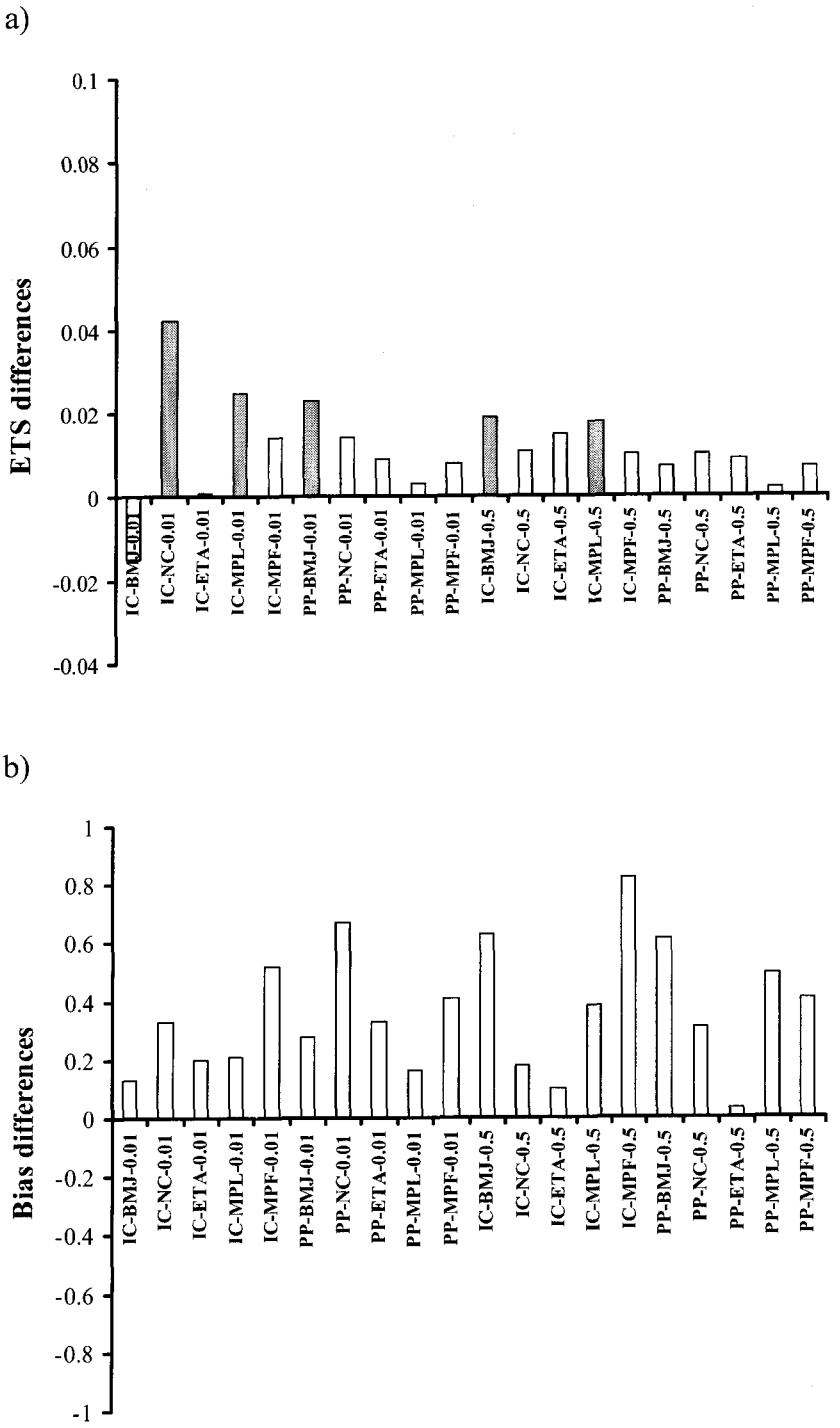

Figure 4. As in Figure 3, except for the 12-18 h forecast period.

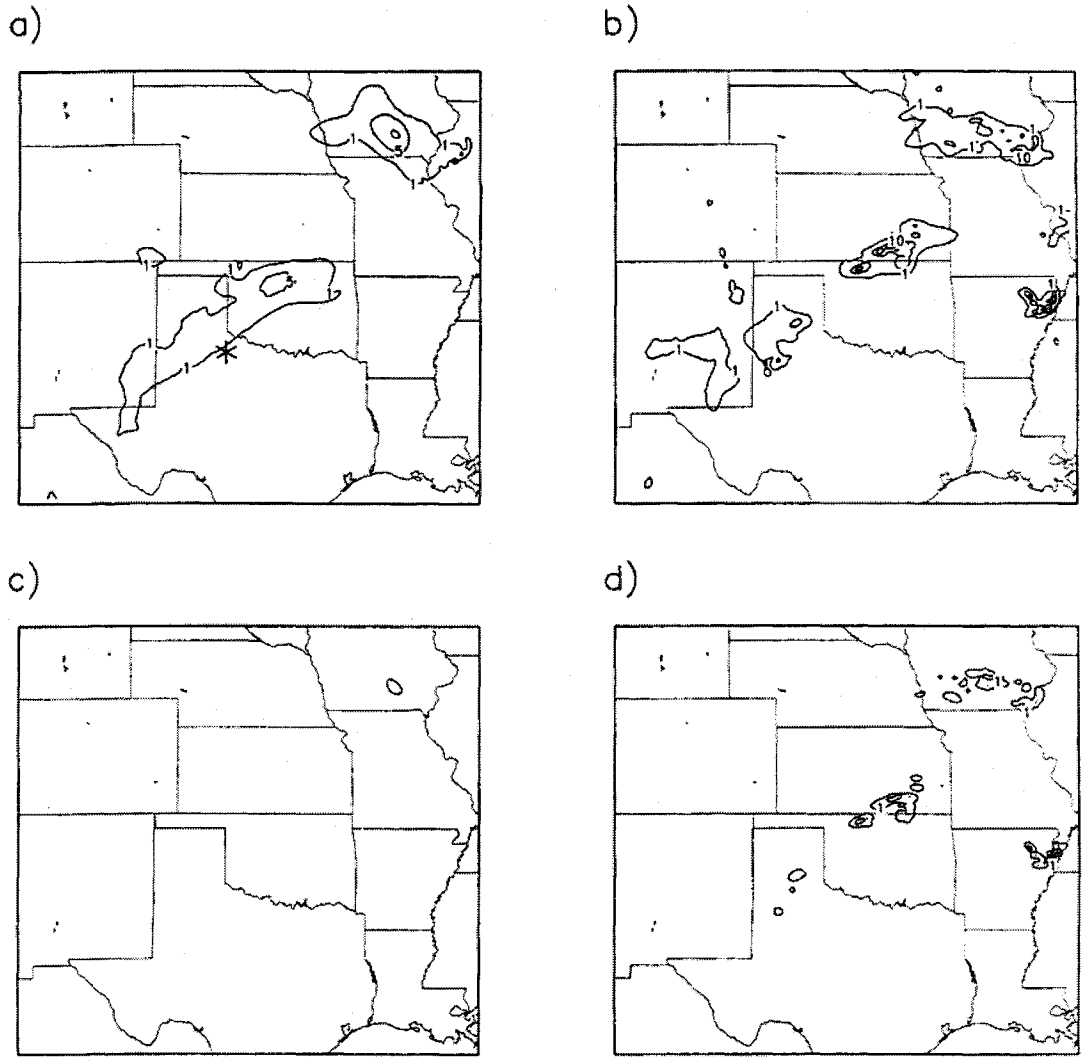

Figure 5. Total accumulated precipitation for the 00-01 h forecast period initialized with a) Eta, b) LAPS, and c) and d) as a) and b) respectively, except for grid-resolved precipitation component. Based on **BMJ-ETA-MPF** model simulation initialized at 00 UTC June 13, 2002. Contours are shown for 1 mm, 5 mm, 10 mm, 20 and 30 mm.

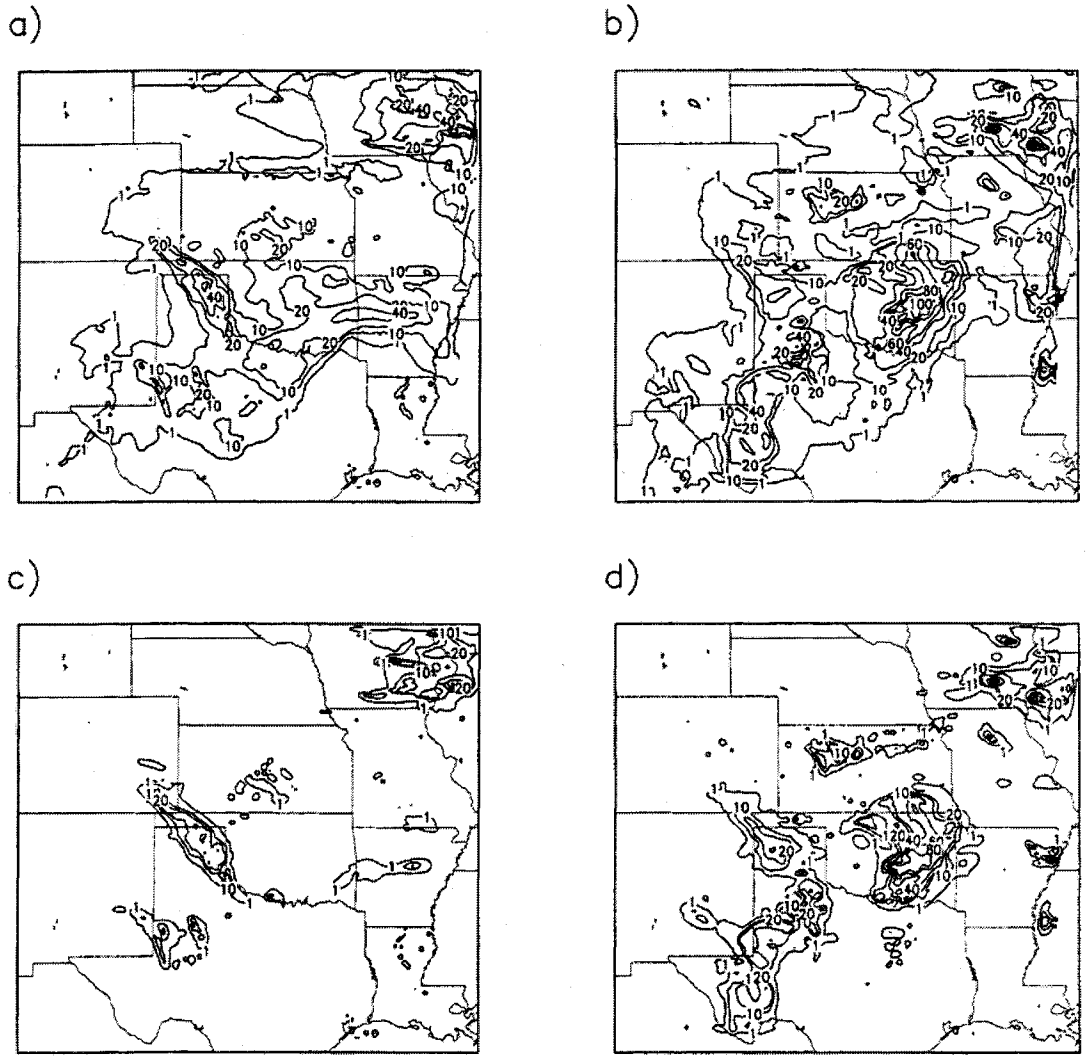

Figure 6. As in Figure 5, except for the 17-18 h forecast period. Contours are shown for 1 mm, 10 mm, 20 mm, and then every 20 mm up to 120 mm.

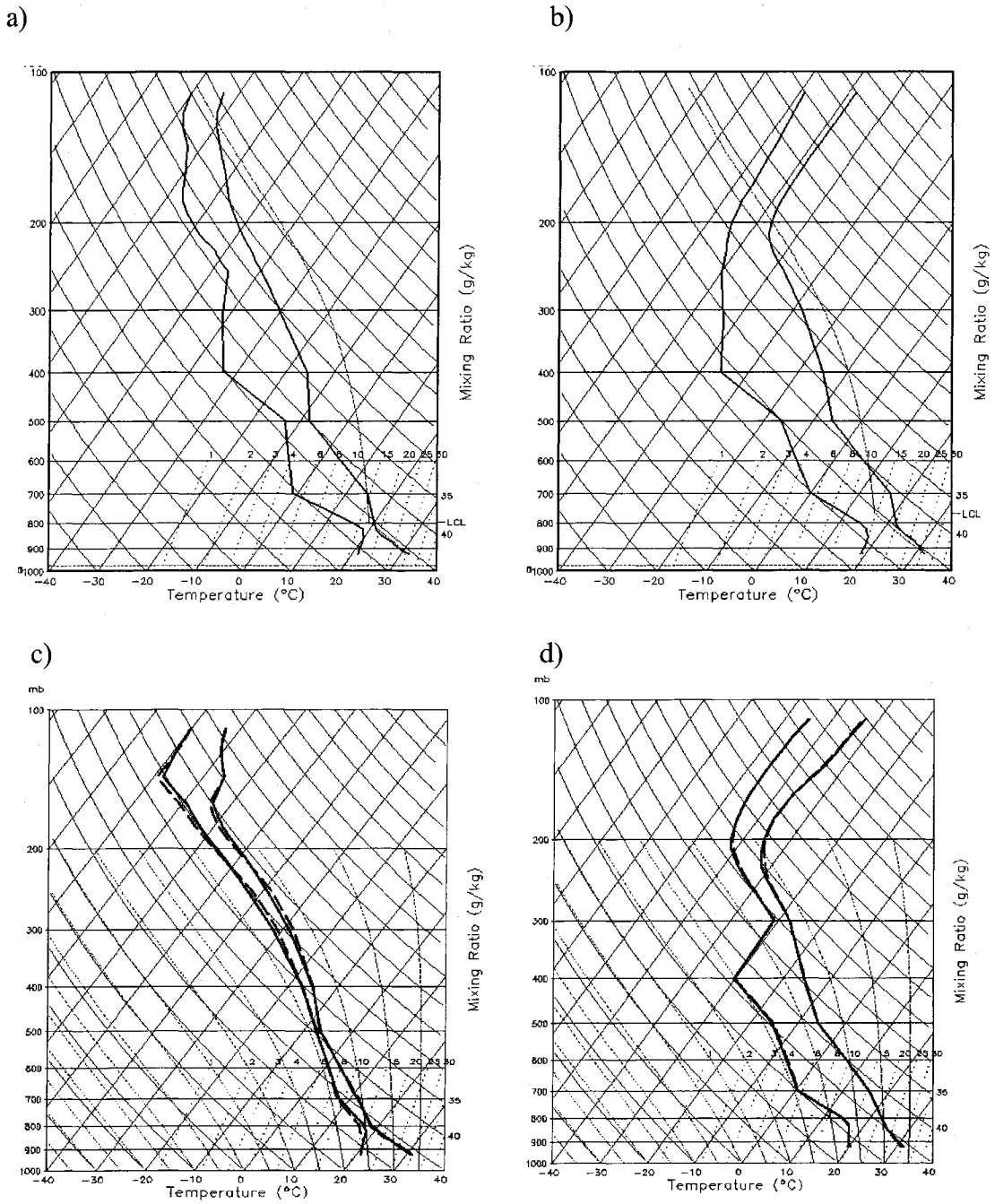

Figure 7. The **BMJ-ETA-MPF** (solid lines) and **BMJ**-MRF-**MPF** (dashed lines) thermodynamic profiles from the model runs initialized with both Eta (left column) and LAPS (right column) analyses at the point indicated by '*' in Fig. 5a at; a) and b) 00 UTC; c) and d) 02 UTC; e) and f) 04 UTC; g) and h) 06 UTC.

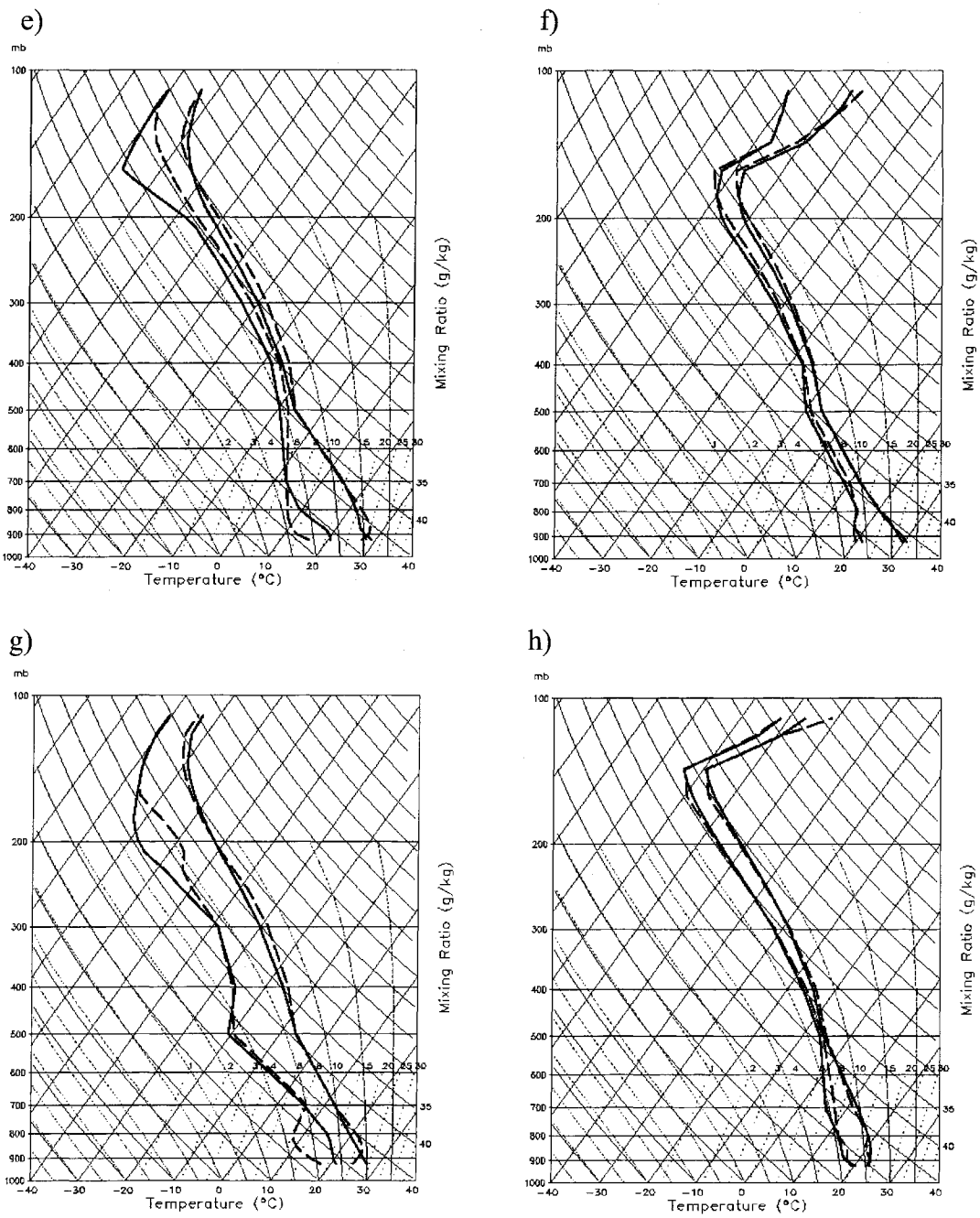

Figure 7; continued

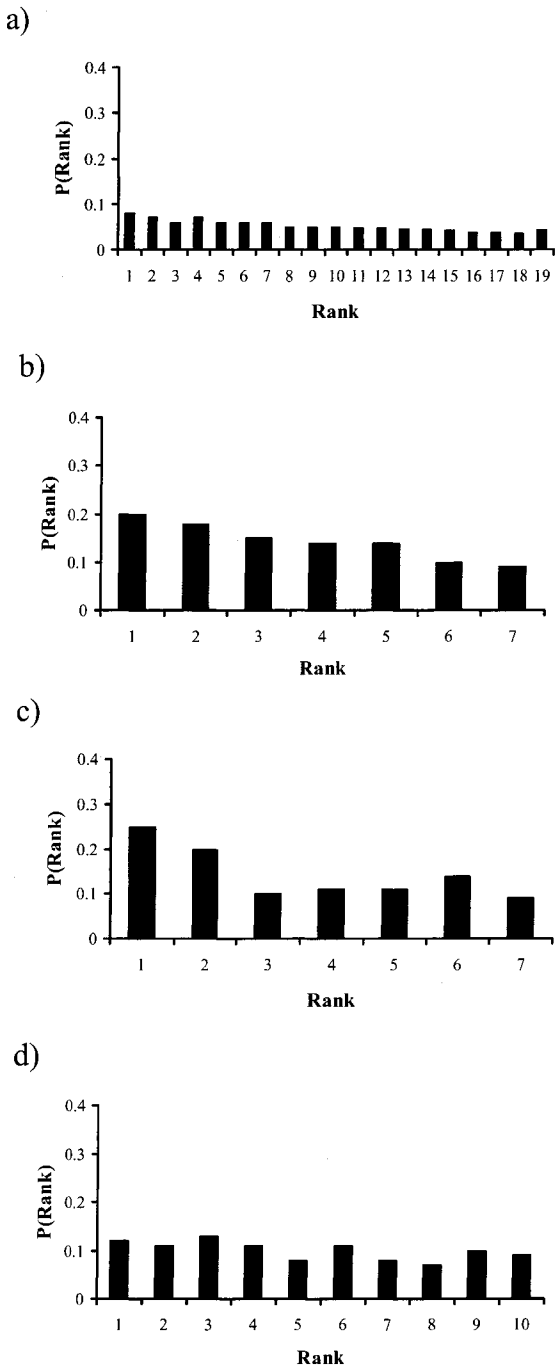

Figure 8. Rank histograms for a) 18_full, b) 6_cu_pbl_**MPF**, c) 6_**BMJ**_pbl_mp and d) 9_cu_**ETA**_mp ensembles (see Table 4 caption for the notation legends), for the 00-06 h forecast period and using the Eta initial conditions.

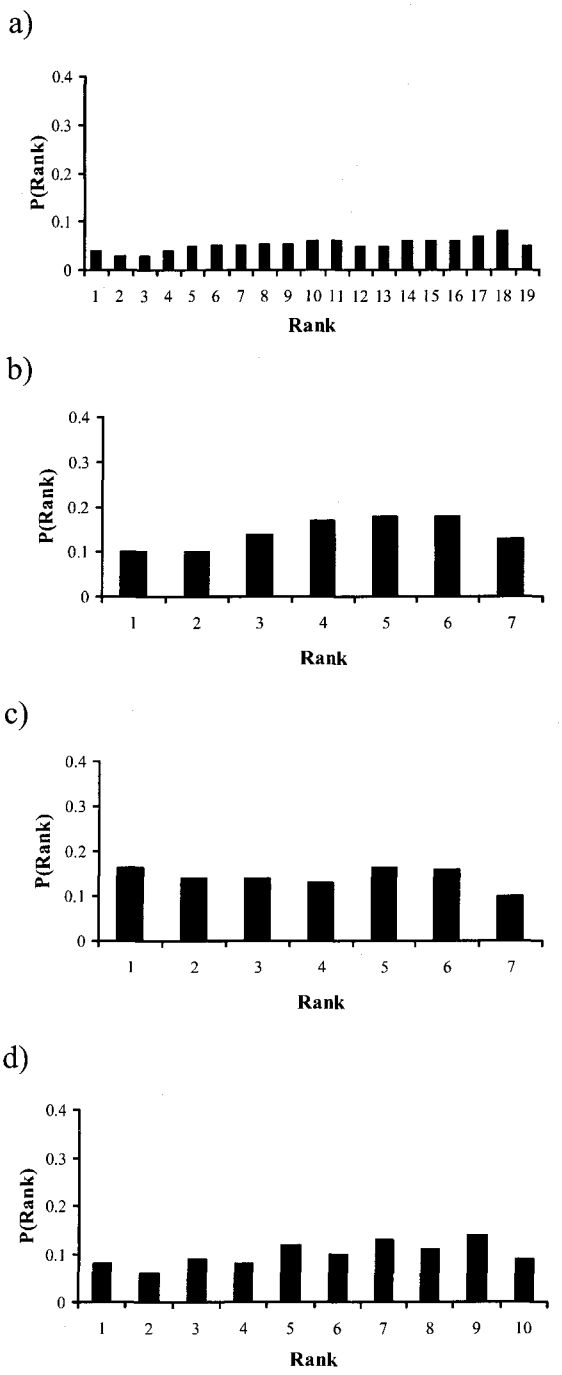

Figure 9. As in Figure 8 except for the 12-18 h forecast period.

Table 1. Notation used for different physical schemes and initializations in the present study.

Physical scheme/Initialization	Notation
Physical scheme	
Betts-Miller-Janjic convection	BMJ
Kain-Fritsch convection	KF
Run without a convection	NC
ETA PBL	ETA
MRF PBL	MRF
Lin et al. microphysics	MPL
NCEP-5 microphysics	MPN
Ferrier microphysics	MPF
Initialization	
40 km NCEP ETA	Eta
LAPS 'hot' start	LAPS

Table 2. Time series of percentage changes in system rain rate (averaged for all 8 cases) due to physics changes (f_1 represents rainfall in the run where PBL scheme is changed from MRF to **ETA**, f_2 represents rainfall in the run where microphysics is changed from MPN to **MPL**, f_3 represents rainfall in the run where microphysics is changed from MPN to **MPF**, f_4 represents rainfall in the run where convective treatment is changed from KF to **NC**, and f_5 represents rainfall in the run where convective treatment is changed from KF to **BMJ**) averaged over points where rainfall exceeded specified thresholds (0.01 in. and 0.5 in.) for two different initializations (LAPS and Eta). f_0 represents rainfall in the control run (KF-MRF-MPN). $\hat{f}_{13}$, $\hat{f}_{24}$, and $\hat{f}_{34}$ represent corresponding synergistic terms. Values presented in bold-italic, bold and italic face indicate results that are statistically significant at the 95%, 90%, and 80% confidence level, respectively.

Threshold (in.)	**Initialization**	**Forecast period (h)**			
		00-06	**06-12**	**12-18**	**18-24**
	LAPS analysis				
0.01	$(f_2 - f_0)/f_0$ (%)	*5*	*16*	*16*	*39*
	$(f_3 - f_0)/f_0$ (%)	**10**	**14**	**12**	**22**
	$(f_4 - f_0)/f_0$ (%)	***52***	***55***	***37***	***10***
0.5	$(f_2 - f_0)/f_0$ (%)	*2*	*0*	*8*	*25*
	Eta analysis				
0.01	$(f_2 - f_0)/f_0$ (%)	**9**	**5**	**6**	**26**
	$(f_3 - f_0)/f_0$ (%)	*6*	*1*	*7*	*5*
	$(f_4 - f_0)/f_0$ (%)	***31***	***24***	***4***	***21***
	$(f_5 - f_0)/f_0$ (%)	***-29***	***-45***	***-47***	***-48***
	$\hat{f}_{24}/f_0$ (%)	***28***	***100***	***85***	***80***
	$\hat{f}_{34}/f_0$ (%)	*-19*	*-9*	*-12*	*-32*
0.5	$(f_1 - f_0)/f_0$ (%)	**2**	**4**	**8**	**15**
	$(f_2 - f_0)/f_0$ (%)	**16**	**8**	**2**	**21**
	$(f_5 - f_0)/f_0$ (%)	***-15***	***-25***	***-44***	***-20***
	$\hat{f}_{13}/f_0$ (%)	**-1**	**-3**	**-1**	**-17**
	$\hat{f}_{24}/f_0$ (%)	***1***	***37***	***41***	***23***

Table 3. As in Table 2 except for domain total rain volume.

Threshold (in.)	Initialization	Forecast period (h)			
		00-06	06-12	12-18	18-24
	LAPS analysis				
0.01	$(f_2 - f_0)/f_0$ (%)	*37*	*32*	*53*	*94*
	$(f_3 - f_0)/f_0$ (%)	*26*	*22*	*22*	*46*
0.5	$(f_2 - f_0)/f_0$ (%)	*59*	*72*	*94*	*180*
	$(f_3 - f_0)/f_0$ (%)	*37*	*54*	*41*	*101*
	$(f_5 - f_0)/f_0$ (%)	**-50**	**-68**	**-69**	**-91**
	$\hat{f}_{12}/f_0$ (%)	*0*	*-25*	*-20*	*-83*
	$\hat{f}_{13}/f_0$ (%)	*14*	*-15*	*-39*	*-27*
	Eta analysis				
0.01	$(f_1 - f_0)/f_0$ (%)	*8*	*7*	*13*	*22*
	$\hat{f}_{14}/f_0$ (%)	*11*	*45*	*23*	*10*
	$\hat{f}_{24}/f_0$ (%)	*21*	*47*	*24*	*24*
0.5	$(f_1 - f_0)/f_0$ (%)	*3*	*8*	*6*	*18*
	$(f_2 - f_0)/f_0$ (%)	**29**	**27**	**27**	**95**
	$(f_4 - f_0)/f_0$ (%)	*-47*	*-10*	*-37*	*-23*
	$(f_5 - f_0)/f_0$ (%)	*-45*	*-76*	*-74*	*-82*
	$\hat{f}_{15}/f_0$ (%)	*3*	*12*	*11*	*2*
	$\hat{f}_{24}/f_0$ (%)	*39*	*88*	*52*	*57*
	$\hat{f}_{34}/f_0$ (%)	**15**	**33**	**11**	**32**

Table 4. Areas under ROC curves averaged for all 8 cases for 18_full ensemble (including all 18 model configurations); 9-member ensemble, 9_cu_**ETA**_mp, (including 3 different convective treatments-cu, **ETA** PBL, and 3 different microphysics-mp); two 6-member ensembles, 6_cu_pbl_**MPF** and 6_**BMJ**_pbl_mp (the first including 3 different convective treatments, 2 different PBL schemes-pbl and **MPF**, and the second including the **BMJ** scheme, 2 different PBL schemes and 3 different microphysics), for the 0.01 in. and 0.5 in. thresholds, for the two different initializations, and the 4 specified 6-hourly forecast periods.

Threshold (in.)	**Ensemble type**	**Area under ROC curve**			
		00-06h	**06-12h**	**12-18h**	**18-24 h**
	Runs initialized with LAPS analysis				
0.01	18_full	0.802	0.721	0.691	0.720
	9_cu_**ETA**_mp	0.805	0.752	0.708	0.712
	6_cu_pbl_**MPF**	0.791	0.731	0.682	0.684
	6_**BMJ**_pbl_mp	0.775	0.685	0.700	0.662
0.25	18_full	0.662	0.596	0.600	0.706
	9_cu_**ETA**_mp	0.674	0.643	0.641	0.704
	6_cu_pbl_**MPF**	0.652	0.606	0.607	0.661
	6_**BMJ**_pbl_mp	0.640	0.546	0.590	0.624
	Runs initialized with Eta analysis				
0.01	18_full	0.871	0.743	0.649	0.634
	9_cu_**ETA**_mp	0.882	0.835	0.743	0.719
	6_cu_pbl_**MPF**	0.851	0.797	0.711	0.703
	6_**BMJ**_pbl_mp	0.862	0.802	0.703	0.701
0.25	18_full	0.664	0.635	0.582	0.582
	9_cu_**ETA**_mp	0.674	0.694	0.619	0.602
	6_cu_pbl_**MPF**	0.644	0.638	0.591	0.600
	6_**BMJ**_pbl_mp	0.637	0.605	0.552	0.558

Table A1. ETS and bias (in parentheses) values averaged over the 8 IHOP cases for different physical scheme combinations for the 00-06 h forecast period for four different rainfall thresholds and for two different initializations. The notation presented in Table 1 is used to indicate different model configurations with physical schemes that are changed from the 'control run' (KF-MRF-MPN) presented in bold face. Runs initialized with LAPS analyses are presented in italic face.

Run	Threshold (in.)			
	0.01	**0.10**	**0.50**	**1.0**
KF-MRF-MPN-Eta	0.2 20(1.6)	0.165 (1.8)	0.095 (2.2)	**0.052** (2.7)
KF-MRF-MPN-LAPS	*0.265 (1.6)*	*0.211 (1.8)*	*0.067 (1.1)*	*0.041 (0.4)*
KF-**ETA**-**MPL**-Eta	0.207 (2.1)	0.154 (2.3)	0.081 (2.7)	0.040 (3.8)
*KF-**ETA**-**MPL**-LAPS*	*0.235 (2.4)*	*0.187 (2.6)*	*0.077 (1.8)*	*0.055 (0.8)*
KF-**ETA**-MPN-Eta	0.209 (1.9)	0.156 (2.0)	0.086 (2.2)	0.045 (2.7)
*KF-**ETA**-MPN-LAPS*	*0.242 (2.0)*	*0.201 (2.1)*	*0.066 (1.2)*	*0.033 (0.4)*
KF-**ETA**-**MPF**-Eta	0.216 (1.9)	0.156 (2.2)	0.085 (2.5)	0.039 (3.3)
*KF-**ETA**-**MPF**-LAPS*	*0.272 (1.8)*	*0.205 (2.1)*	*0.090 (2.2)*	***0.063** (1.2)*
KF-MRF-**MPL**-Eta	0.227 (1.9)	0.165 (2.1)	0.085 (2.7)	0.044 (3.7)
*KF-MRF-**MPL**-LAPS*	*0.255 (2.1)*	*0.196 (2.6)*	*0.073 (1.8)*	*0.059 (1.2)*
KF-MRF-**MPF**-Eta	0.225 (1.8)	0.164 (2.1)	0.083 (2.6)	0.049 (3.2)
*KF-MRF-**MPF**-LAPS*	*0.276 (1.8)*	*0.206 (2.1)*	*0.075 (1.4)*	*0.038 (0.5)*
NC-ETA-MPL-Eta	**0.233** (0.9)	0.167 (1.1)	0.064 (2.3)	0.035 (4.8)
*NC-**ETA**-**MPL**-LAPS*	***0.349** (1.0)*	***0.247** (1.3)*	*0.086 (1.9)*	*0.044 (1.2)*
NC-ETA-MPN-Eta	0.211 (0.7)	0.161 (0.8)	0.051 (1.2)	0.027 (2.4)
*NC-**ETA**-MPN-LAPS*	*0.327 (0.8)*	*0.215 (1.8)*	*0.048 (0.9)*	*0.022 (0.5)*
NC-ETA-MPF-Eta	0.224 (0.9)	0.169 (1.1)	0.081 (1.8)	0.044 (2.8)
NC-ETA-MPF-LAPS	*0.298 (1.1)*	*0.203 (1.4)*	*0.055 (0.8)*	*0.041 (0.5)*
NC-MRF-**MPL**-Eta	**0.236** (0.8)	0.161 (0.9)	0.058 (1.8)	0.035 (3.6)
*NC-MRF-**MPL**-LAPS*	*0.308 (1.1)*	*0.201 (1.5)*	*0.066 (1.0)*	*0.039 (0.8)*
NC-MRF-MPN-Eta	0.200 (0.5)	0.142 (0.5)	0.034 (0.8)	0.017 (1.6)
NC-MRF-MPN-LAPS	*0.304 (0.7)*	*0.191 (0.7)*	*0.057 (0.3)*	*0.029 (0.4)*
NC-MRF-**MPF**-Eta	**0.258** (0.9)	**0.181 (1.1)**	0.085 (1.7)	0.048 (2.6)
*NC-MRF-**MPF**-LAPS*	*0.311 (1.1)*	*0.208 (1.4)*	*0.057 (1.0)*	*0.032 (1.0)*
BMJ-ETA-MPL-Eta	0.223 (2.2)	**0.185 (2.4)**	0.096 (1.9)	0.034 (2.4)
BMJ-ETA-MPL-LAPS	*0.246 (2.1)*	*0.167 (2.6)*	***0.100** (1.0)*	*0.053 (0.6)*
BMJ-ETA-MPN-Eta	0.217 (2.1)	**0.180 (2.2)**	**0.107 (1.5)**	0.017 (1.5)
BMJ-ETA-MPN-LAPS	*0.249 (2.2)*	*0.182 (2.6)*	*0.070 (0.8)*	*0.026 (0.5)*
BMJ-ETA-MPF-Eta	**0.254** (2.0)	**0.215 (1.9)**	**0.152 (0.9)**	0.042 (0.6)
BMJ-ETA-MPF-LAPS	*0.249 (2.4)*	*0.177 (2.8)*	*0.079 (1.1)*	*0.029 (0.8)*
BMJ-MRF-**MPL**-Eta	0.225 (2.3)	**0.180 (2.4)**	**0.094 (1.9)**	0.037 (2.3)
*BMJ-MRF-**MPL**-LAPS*	*0.249 (2.4)*	*0.179 (2.8)*	*0.099 (0.7)*	*0.054 (0.5)*
BMJ-MRF-**MPN**-Eta	0.219 (2.1)	**0.175 (2.2)**	**0.104 (1.5)**	0.021 (1.1)
BMJ-MRF-MPN-LAPS	*0.249 (2.1)*	*0.178 (2.5)*	***0.100** (0.7)*	*0.046 (0.3)*
BMJ-MRF-**MPF**-Eta	0.223 (2.2)	**0.187 (2.2)**	**0.095 (1.7)**	0.035 (2.2)
BMJ-MRF-MPF-LAPS	*0.252 (2.5)*	*0.180 (2.7)*	*0.074 (1.0)*	*0.038 (0.4)*

Table A2. As in Table A1, except for the 12-18h period.

Run	Threshold (in.)			
	0.01	**0.10**	**0.50**	**1.0**
KF-MRF-MPN-Eta	0.138 (1.2)	0.115 (1.3)	**0.100** (1.3)	0.015 (1.9)
KF-MRF-MPN-LAPS	*0.169 (1.3)*	*0.155 (1.7)*	*0.091 (1.0)*	*0.027 (0.8)*
KF-**ETA-MPL**-Eta	0.134 (2.1)	0.100 (2.3)	0.086 (1.9)	0.027 (2.4)
*KF-**ETA-MPL**-LAPS*	*0.160 (2.1)*	*0.145 (1.9)*	*0.102 (1.4)*	*0.029 (1.4)*
KF-**ETA**-MPN-Eta	0.146 (1.7)	0.129 (1.7)	0.085 (1.5)	0.022 (1.8)
*KF-**ETA**-MPN-LAPS*	*0.168 (1.8)*	*0.157 (1.6)*	*0.089 (1.3)*	*0.018 (0.9)*
KF-**ETA-MPF**-Eta	0.117 (1.8)	0.100 (2.0)	0.068 (1.6)	0.009 (1.8)
*KF-**ETA-MPF**-LAPS*	*0.133 (2.0)*	*0.122 (1.8)*	*0.105 (1.0)*	*0.027 (1.0)*
KF-MRF-**MPL**-Eta	0.148 (1.5)	0.111 (1.7)	0.089 (1.7)	0.017 (2.3)
*KF-MRF-**MPL**-LAPS*	*0.177 (1.7)*	*0.146 (1.7)*	*0.103 (2.5)*	***0.047** (1.6)*
KF-MRF-**MPF**-Eta	0.130 (1.4)	0.104 (1.6)	0.089 (1.4)	0.018 (1.6)
*KF-MRF-**MPF**-LAPS*	*0.172 (1.5)*	*0.141 (1.5)*	*0.085 (2.6)*	*0.023 (1.3)*
NC-ETA-MPL-Eta	0.154 (1.0)	0.098 (1.1)	0.061 (1.6)	0.015 (3.1)
***NC-ETA-MPL**-LAPS*	*0.156 (1.4)*	*0.152 (1.0)*	*0.079 (1.9)*	*0.016 (1.4)*
NC-ETA-MPN-Eta	0.164 (1.0)	0.121 (0.9)	**0.101** (1.1)	**0.045** (2.2)
***NC-ETA**-MPN-LAPS*	*0.156 (1.3)*	*0.152 (1.0)*	*0.079 (0.9)*	*0.016 (1.1)*
NC-ETA-MPF-Eta	0.137 (1.1)	0.092 (1.2)	0.052 (1.5)	0.034 (2.0)
***NC-ETA-MPF**-LAPS*	*0.164 (1.4)*	*0.151 (1.1)*	*0.057 (2.3)*	*0.014 (1.5)*
NC-MRF-**MPL**-Eta	0.148 (0.6)	0.110 (0.7)	0.083 (1.2)	0.026 (2.6)
***NC**-MRF-**MPL**-LAPS*	***0.239 (1.1)***	***0.213 (1.0)***	*0.113 (1.5)*	*0.043 (1.4)*
NC-MRF-MPN-Eta	0.107 (0.6)	0.070 (0.6)	0.067 (0.8)	0.037 (1.3)
***NC**-MRF-MPN-LAPS*	*0.211 (0.8)*	*0.195 (0.8)*	***0.118 (0.7)***	*0.040 (0.5)*
NC-MRF-**MPF**-Eta	0.145 (0.8)	0.111 (0.9)	**0.092** (1.1)	**0.062** (1.6)
***NC**-MRF-**MPF**-LAPS*	*0.181 (1.1)*	*0.159 (1.2)*	*0.077 (1.1)*	*0.034 (0.9)*
BMJ-ETA-MPL-Eta	**0.169 (2.0)**	**0.150 (2.1)**	0.041 (0.8)	0.005 (0.5)
***BMJ-ETA-MPL**-LAPS*	*0.167 (2.1)*	*0.141 (2.8)*	*0.064 (1.4)*	*0.020 (0.5)*
BMJ-ETA-MPN-Eta	**0.187 (1.9)**	**0.166 (1.9)**	0.038 (0.6)	0.000 (0.2)
***BMJ-ETA**-MPN-LAPS*	*0.162 (2.2)*	*0.148 (2.7)*	*0.065 (1.2)*	*0.014 (0.4)*
BMJ-ETA-MPF-Eta	**0.202 (2.0)**	**0.164 (2.1)**	0.026 (0.9)	0.001 (0.6)
***BMJ-ETA-MPF**-LAPS*	*0.160 (2.1)*	*0.145 (2.6)*	*0.053 (1.0)*	*0.020 (0.3)*
BMJ-MRF-**MPL**-Eta	**0.172 (1.9)**	**0.149 (2.1)**	0.041 (0.6)	0.001 (0.3)
***BMJ**-MRF-**MPL**-LAPS*	*0.176 (2.0)*	*0.148 (1.6)*	*0.065 (1.4)*	*0.022 (0.6)*
BMJ-MRF-**MPN**-Eta	**0.190 (1.7)**	**0.164 (1.8)**	0.037 (0.6)	0.006 (0.1)
***BMJ**-MRF-MPN-LAPS*	*0.168 (1.8)*	*0.145 (1.5)*	*0.043 (1.4)*	*0.009 (0.2)*
BMJ-MRF-**MPF**-Eta	0.159 (1.9)	**0.125 (1.9)**	0.050 (0.7)	0.000 (0.4)
***BMJ**-MRF-**MPF**-LAPS*	*0.160 (2.0)*	*0.126 (1.5)*	*0.061 (1.6)*	*0.015 (0.5)*

4. FURTHER ANALYSIS OF PBL SCHEME SENSITIVITY

4. 1 Introduction

As an addition to the previously discussed research more detailed analysis of the differences in performance of two PBL schemes [local mixing Eta PBL scheme (often referred to as Mellor-Yamada-Janjic 2.5; Janjic 2001) and non-local mixing YSU PBL scheme (Noh et al. 2002) as an improved version of MRF PBL scheme (Troen and Mahrt 1986)] has been performed. For this purpose a 13-km grid spacing WRF-ARW model, initialized with Rapid Update Cycle (RUC) model analyses (Benjamin et al. 2002) was used for simulation of several cases during June of 2005. The cases were purposely selected to explore regions with clear sky over parts of the central United States during the first 24 hours of the integration. The integration domain covered the whole continental United States. Observations used for verification of simulated sensible heat flux, latent heat flux, and PBL height were obtained from the AmeriFlux website (http://public.oml.gov/ameriflux).

4.2 Local versus non-local mixing PBL schemes

In numerical models the PBL is usually classified into four categories based on stability (stable, wind shear driven turbulence, forced convection and free convection), where the first two categories are in stable regime while the second two are in the unstable regime. The stability categories are often defined based on the values of the bulk Richardson number of the surface layer and the ratio between the PBL height and Monin-Obukhov length (|h/L|).

Based on the way that the PBL scheme deals with vertical exchange processes it can be classified as having local or non-local mixing. In this extended analysis the YSU scheme (an improved version of the MRF PBL scheme) was considered as an example of a non-local mixing scheme and the Eta as an example of a local mixing PBL scheme.

The PBL height in the non-local mixing MRF and YSU schemes is given by (Troen and Mahrt 1986):

$$h = Rib_{cr} \frac{\theta_{va} |U(h)|^2}{g(\theta_v(h) - \theta_s)} \qquad (1)$$

where Rib_{cr} is the critical bulk Richardson number, U(h) is the horizontal wind speed at h, θ_{va} is the virtual potential temperature at the lowest model level, $\theta_v(h)$ is the virtual potential temperature at h and θ_s is the appropriate temperature near the surface. θ_s is given by:

$$\theta_s = \theta_{va} + \theta_T (= b \frac{\overline{(w'\theta_v')_0}}{w_s}) \qquad (2)$$

where θ_T is the scaled virtual temperature excess near the surface, w_s is the mixed layer velocity scale $(= u_* \phi_m^{-1})$, with u_* the surface frictional velocity scale, ϕ_m the wind profile function evaluated at the top of the surface layer (function of h/L), $\overline{(w'\theta_v')_0}$ the virtual heat flux from the surface, and b a factor set to 7.8 . Vertical mixing in the MRF scheme relies on so-called K-theory.

With regard to the MRF scheme performance, it has been documented that the scheme simulates too much mixing (Persson et al. 2001). As a possible way to improve the

scheme performance, a decrease in Rib_{cr} was considered. In that way the turbulent intensity would be reduced by weakening the entrainment. However, based on an evaluation of precipitation forecasts the scheme performance degraded when the entrainment was decreased. This problem was addressed in the YSU scheme by adding a term in the turbulence diffusion equations for prognostic variables which treat the entrainment explicitly (Noh et al. 2002). Also, the entrainment has been implicitly parameterized by raising the height of the PBL above the minimum flux level.

Regarding the local-mixing Eta PBL scheme (hereafter ETA), it computes K (eddy diffusivity) from the local gradients in turbulent kinetic energy (TKE), vertical wind shear and stability, and Blackadar length scale (Janjic 1994) regardless of stability regime. For the local-mixing scheme the height of the PBL is defined at the levels where the TKE decreases under certain values, depending on the regime. During the night (stable regime) the PBL height is usually set to the lowest model level.

4.3 Differences in performance between YSU and ETA schemes

It has been documented that ETA tends to produce a PBL that is too shallow, too moist and consequently too cold in daylight (Bright and Mullen 2002, Jankov et al. 2006). Results from the present analysis for the clear sky conditions were consistent with this finding. For all simulated cases during the day time, area averaged values of sensible heat flux, latent heat flux, PBL height, 2-m temperature and 2-meter specific humidity indicated that simulations using the ETA scheme were characterized by lower sensible heat flux, lower PBL height, and a cooler and more moist lower atmosphere compared to simulations using

YSU. Lower sensible heat flux values and a lack of entrainment at the top of the Convective Boundary Layer (CBL) might support the fact that the ETA scheme often produces shallower and cooler CBLs. Shallower CBLs produced by the ETA scheme were more moist consistent with higher values of the latent heat flux. Thus, a different partition between sensible and latent heat (i. e. Bowen ratio) and the fact that the schemes handle mixing differently might explain the causes of differences in performance between the schemes. In order to evaluate the impact of the partitioning between the sensible and latent heat and mixing, scaling based on CBL moisture and temperature differences was performed.

4.3.1 Scaling based on CBL moisture and temperature differences

By performing scaling based on typical differences in specific humidity and potential temperature in the lower atmosphere it was possible to evaluate if these differences were forced by the difference in partitioning between sensible and latent heat only. The difference in specific humidity (dq) between the two BL schemes due to the differences in latent heat flux (dHL) was scaled as:

$$dq = \frac{dHL * t}{L * h * \rho} . \qquad (3)$$

By assuming an average dHL of 50 W/m^2 for the day time duration of t=40000 s with L=2.5x10^6 J/kg, CBL depth of approximately h=1000 m and ρ=1.2 kg/m^3 the late afternoon value of dq would be about 0.66 g/kg, and by assuming h=1500 m, the dq value would be

0.44 g/kg. Assuming dHL< 50W/m^2, which was on average more typical for the simulations used in the present study, dq should be less than 0.44 g/kg.

Scaling of differences in q between the two schemes due to differences in CBL depth (dh) and thus occurrence of additional drying (dq_i) in the case of the deeper CBL (deeper CBL penetrates deeper into a drier layer) can be performed by using:

$$dq_i = \frac{dh * \Delta q}{h} \tag{4}$$

where Δq is the averaged initial (i.e morning) decrease of q within the layer dh. For dh of 300 m, Δq of approximately 3 g/kg and h=1000 m, the scaled value for dq_i is about 1g/kg. For the cases used in the present analysis, dq_i appeared to be larger than dq in the afternoon. This might imply that drying of the YSU is rather due to its deeper CBL and thus additional elevated dry air mixing, than due to its lower latent heat.

With regard to differences in potential temperature between the two schemes ($d\theta$); in analogy to (3):

$$d\theta = \frac{dHS * t}{h * C_p * \rho} \tag{5}$$

where dHS is a difference in sensible heat flux and C_p is specific heat capacity at constant pressure (C_p= 1004 J/kg K). For simulations used in the present analysis it was reasonable to use dHS of 100 W/m^2, which resulted in a $d\theta$ of about 3.3 K.

If the changes in the CBL θ and q are only due to surface fluxes, then:

$$\frac{d\theta}{dq} \approx \frac{L}{C_p} \approx 2.5 \frac{K}{\frac{g_w}{kg_a}} \qquad (6)$$

However, in the present analysis the scaling above indicated a value of dθ/dq larger than 2.5, suggesting that as the CBL deepens the mixing effect of q should have an important role in generating the differences in q between the two schemes.

4.3.2 Sensitivity testing

4.3.2a Entrainment sensitivity simulation

By assuming a lack of an entrainment effect in the ETA scheme, and based on the fact that the entrainment thermal flux at the top of the CBL is typically considered to be ~-.2*Hs, the first experiment used 1.2*Hs for the sensible heat flux at the surface while solving the vertical eddy diffusion for θ (scaling approach used in a simple convective mixed layer, less popular for multi-level models). Resulting areally averaged values indicated a slight CBL warming of ~1 K and an increase in the CBL depth of about 120 m compared to the original ETA simulations.

4.3.2b Surface roughness length sensitivity simulations

Further tests were based on the fact that the two schemes within their surface layer formulations use different surface roughness lengths for z_{0t} and z_{0q}, which may have a large

impact on the surface flux partitioning. Typically it is assumed that z_{0q} is equal to z_{0t}, with z_0 larger than both z_{0t} and z_{0q}. This is the way roughness lengths are defined in the ETA surface layer. In reality z_{0q} is somewhat smaller than z_{0t}. By modifying the ETA scheme code to have $z_{0q}<z_{0t}$ it was expected to change the Bowen ratio toward drying.

First, a test run was performed by setting $z_0=z_{0t}=z_{0q}$ in the ETA surface scheme. It resulted in an increase of latent heat, a slight warming of the CBL (verified by both areally averaged 2-meter temperature and by using Iowa Environmental Mesocale archived surface temperature data) and an increase in CBL height of 50 m on average. This suggests that by modifying the ETA scheme code to have $z_{0q}< z_{0t}$ the Bowen ratio would possibly change toward further drying and warming of the CBL. This should be the subject of future work.

On the other hand, in the surface layer subroutine used by the YSU scheme, the effective z_{0q} is significantly lower than z_0, while $z_{0t}=z_0$. This relation between the roughness lengths is likely to yield overpredicted sensible heat flux and underpredicted latent heat flux. In this case, the test was to examine the Bowen ratio response to a 'reasonable' prescription of $z_{0q}=z_{0t}$ or $z_{0q}<z_{0t}$, where $z_0>z_{0t}$, z_{0q}. The first sensitivity test with z_{0t} and z_{0q} equalized to z_0 resulted in a decrease in sensible heat flux of about ~70 W/m^2 and an increase in latent heat flux of about ~80 W/m^2 on average which resulted in a lower and more moist CBL. The same test was repeated but with a more realistic prescription for z_{0t} and z_{0q}. z_{0t} and z_{0q} were set to be ~ $0.1*z_0$. The results showed the same trends in latent heat flux, sensible heat flux, CBL height and moisture but with lower magnitudes. Generally, these tests imply a large sensitivity of Bowen ratio to the roughness lengths definition.

4.3.3 Vegetation type impact on the PBL schemes performance

As earlier mentioned, the above results and speculations relied on areally averaged values of simulated parameters of interest (sensible heat flux, latent heat flux, and PBL height). However, in order to verify these results the comparison to the observed values had to be at a single point. The choice of verification points depended on the availability of observed data on a relatively coarse observational grid and the number of verifying points that satisfied the 'clear sky' condition. Observations were obtained from the AmeriFlux web site. The 'clear sky' requirement in a point with available observations was satisfied if the analyzed/simulated relative humidity profile indicated values less than 70% and 30% in the lower and upper atmosphere , respectively.

By analyzing the behavior of the two different schemes at a point and comparing it to the actual values it turned out that the conclusions derived from the areally averaged sensible and latent heat fluxes do not necessarily agree with a point to point analysis. More precisely, the surface flux simulations from different schemes were dependent on the vegetation type. For sites in the corn belt tendencies in simulated surface fluxes agreed well with the areally averaged results. ETA simulations tended to have lower sensible heat fluxes and higher latent heat fluxes, while opposite was the case for wooded areas. Interestingly, regardless of surface fluxes the PBL simulated with YSU was always higher to various degrees, and the 2-meter specific humidity was always lower compared to the ETA PBL. This once again may indicate the importance of the way in which different schemes handle vertical mixing.

4.4 Summary

In order to investigate differences in performance between the two PBL schemes (ETA and YSU) in more details additional (albeit preliminary) tests were performed. In general, the preliminary results agreed well with the previously documented finding that the YSU scheme tends to simulate higher and drier PBLs compared to the ETA scheme. On the other hand, simulated surface fluxes analyses pointed toward an important issue, the impact of vegetation type on differences in the PBL schemes' performance. In addition, preliminary results highlighted the importance of vertical exchange processes for the differences in performance between the two schemes. The main focus of future investigation will be on the PBL schemes' performance dependence on vegetation type.

5. GENERAL CONCLUSSIONS

Knowledge of how different physical schemes or their combinations influence rainfall forecasts may be of major importance in designing and interpreting experiments as well as mixed physics ensembles. The main goal of the dissertation was to note and quantify general trends in the impact of various physical schemes and their interactions on warm season MCS rainfall forecasts and to examine if and how these impacts change under different initial conditions. For this purpose, a matrix of 18 WRF model configurations, with 12–km grid spacing, was created using different physical scheme combinations for 8 IHOP MCS cases. For each case, three different treatments of convection were used (KF, **BMJ** and the use of no convective scheme), with 3 different microphysical schemes (MPN, **MPL**, and **MPF**) and two different PBL schemes (MRF and **ETA**). The runs were initialized with a diabatic LAPS 'hot' start initialization (Jian et al. 2003) and 40 km Eta GRIB files.

For an investigation of the impact that various physical schemes and their interactions have on simulated rainfall runs initialized with LAPS 'hot' start initialization were used. An analysis of objective skill measures (ETS and bias) indicated that no single model configuration was clearly better than the rest. The best configuration varied both with time and rainfall threshold. The highest sensitivity of the simulated rainfall was to the choice of convective treatment, with less sensitivity to the PBL scheme, and the least to microphysics.

By using the factor separation method (Stein and Alpert 1993) additional testing of sensitivity of rain rate and rain volume to physics changes was performed. This method was used to quantify the impacts of the variation of two different physical schemes as compared

to a 'control run' and their interaction (synergy) on the simulated rainfall. Statistical significance of the obtained results was tested by following a resampling method suggested by Hamill (1999). A change from KF to **NC** significantly increased system rain rate. A change from KF to **BMJ** significantly increased areal coverage of lighter rainfall while lowering system rain rates (though not significantly) compared to KF runs. In general, changes in convective treatment were found to have the largest impact on rain rate when KF was replaced with **NC** no matter what microphysical and PBL schemes were used. Regarding rain volume, the microphysical scheme choice exerted the largest impact in **NC** runs and least impact in **BMJ** runs, as would be expected by the amount of grid-resolved precipitation likely to occur in each.

The impact of interactions (synergy) of different physical schemes, though occasionally of comparable magnitude to that occurring from a change in one scheme alone, was found to vary greatly and typically not to be statistically significant (in our limited sample of 8 cases). One exception was for the interaction of **ETA** with **MPL** or **MPF** which did significantly reduce the rain volume increase that had been noted for the heavier threshold when the microphysics were switched from MPN. These results suggest that most of the significant trends noted for a switch in one physical process scheme (e.g., increase in rain rate when KF is switched to **NC**) remain consistent even when other physical process schemes are changed. A switch from MPN to either **MPL** or **MPF** increased rain volume markedly no matter what convective and PBL schemes were used. A switch from KF to **BMJ** decreased rain volume, especially for heavier amounts, regardless of what microphysics and PBL schemes were used.

In order to investigate if and how the impact of various physical schemes and their interactions on warm season MCS rainfall forecasts alters under different initial conditions runs initialized with both a diabatic LAPS 'hot' start initialization and 40 km Eta GRIB files were used. Differences in objective skill measures for runs initialized with different initial conditions but using the same model configuration, as well as for runs initialized with the two different initial conditions but with changes in model configuration were occasionally statistically significant implying that both variations in physics and initial conditions may be used in order to increase the spread of an ensemble used for MCS rainfall forecasting.

The results from the factor separation methodology indicated that for both initializations, changes in convective treatment affected the rain rate the most. For runs initialized with LAPS analyses, rain volume was affected the most by changes in microphysics, while for runs initialized with 40 km Eta analyses, rain volume was influenced most by choice of convective treatment. In addition, it was found that information about the interactions among different physical schemes obtained through the synergistic term analysis might be useful in an ensemble calibration procedure.

An analysis of rank histograms and areas under ROC curves for ensembles using various model configurations and different initial conditions supported results from the factor separation methodology which identified convective and microphysical treatments as those with the largest impact on simulated MCS rainfall.

In conclusion, the results indicate that sensitivity of the WRF-ARW model rainfall forecasts to the use of varied physical schemes and their interactions depends on the model initialization. Regardless of the model initialization it appears that if an ensemble designed for MCS rainfall prediction lacks sufficient spread model runs with different convective

schemes should be included,. If rain volume is a desired quantity (e. g., hydrological purposes), and initialization uses the LAPS analyses, runs with **MPL** and **MPF** microphysical schemes may require different bias correction or weighting in an ensemble compared to runs using MPN. In contrast, when the Eta analysis is used for initialization, runs with these different microphysical schemes may not need such different weighting, but runs with **NC** and **BMJ** would require different weighting as compared to KF runs. Knowledge of which physical schemes exert the greatest impact on rainfall forecasts can allow for a design of ensembles, used for MCS rainfall forecasting, that maximize skill while lowering the number of members required.

Finally, to investigate in more detail differences in performance of the two different PBL schemes (ETA and YSU) some additional tests were performed. Generally, the preliminary results agreed well with previous findings, regarding the height and moistness of the simulated PBLs, but also pointed toward a different important issue. Simulated surface flux analyses indicated the sensitivity of differences in the PBL schemes' performance to the vegetation type. Also, preliminary results highlighted the role of mixing in creating differences in performance between the two schemes. The preliminary analyses will be extended and the results further investigated.

Acknowledgements

First, I would like to thank all committee members (William A. Gallus Jr., Raymond W. Arritt, William J. Gutowski, Mike T.-C. Chen, Xiaoqing Wu, and Steven E. Koch) for their valuable assistance. I would also like to thank Moti Segal, Gene Takle and John Brown for their help with my research, and to all members of Iowa State University Graduate Meteorology Club for their support. Finally, I would like to thank to my family for all help, understanding and support they provided me with.

References

Benjamin, S. G., J. M. Brown, K. J. Brundage, D. Devenyi, G. A. Grell, D. Kim, B. E. Schwartz, T. G. Smirnova , T. L. Smith, S. S. Weygandt, and G. S. Manikin, 2002: RUC20 – The 20-km version of the Rapid Update Cycle. *NWS Technical Procedures Bulletin No. 490.*

Bright, D. R., and S. L. Mullen, 2002: The sensitivity of the numerical simulation of the southwest monsoon boundary layer to the choice of PBL turbulence scheme in MM5. *Wea. Forecasting*, **17**, 99-114.

Hamill, T. M., 1999: Hypothesis test for evaluating numerical precipitation forecasts. *Wea. Forecasting*, **14**, 155-167.

Janjic, I. Z., 1990: The Step-Mountain Coordinate: Physical Package. *Monthly Weather Review*: Vol. 118, No. 7, pp. 1429–1443.

--------, Z., 2001: Nonsingular Implementation of the Mellor-Yamada Level 2.5 Scheme in the NCEP Meso Model. NCEP Office Note No. 437, 61pp.

--------, 1994: The step-mountain Eta coordinate model: Further developments of the convection closure schemes. *Mon. Wea. Rev.*, **122**, 927-945.

Jian, G.-J., S.-L. Shieh, and J.A. McGinley, 2003: Precipitation simulation associated with Typhoon Sinlaku (2002) in Taiwan area using the LAPS diabatic initialization for MM5. *Terrestrial, Atmospheric, and Oceanic Sciences,* **14**, 261-288.

Noh, Y., W.-G. Cheon, and S.-Y. Hong, 2003: Improvement of the K-profile model for the planetary boundary layer based on large eddy simulation data. *Bound.-Layer Meteor.*, **107**, 401-427.

Persson, P., B. Walter, J-W Bao, and S. Michelson, 2001: Validation of boundary-layer parameterizations in maritime storm using aircraft data. The ninth conference on mesoscale processes, Ft. Lauderdale, FL, July 30-Aug. 2.

Stein, U., and P. Alpert, 1993: Factor separation in numerical simulations. *J. Atmos. Sci.*, **50**, 2107-2115.

Troen, I., and L. Mahrt, 1986: A simple model of the atmospheric boundary layer: Sensitivity to surface evaporation. *Bound.-Layer Meteor.*, **47**, 129-148.